

Les éléments du processus s dans la Voie Lactée



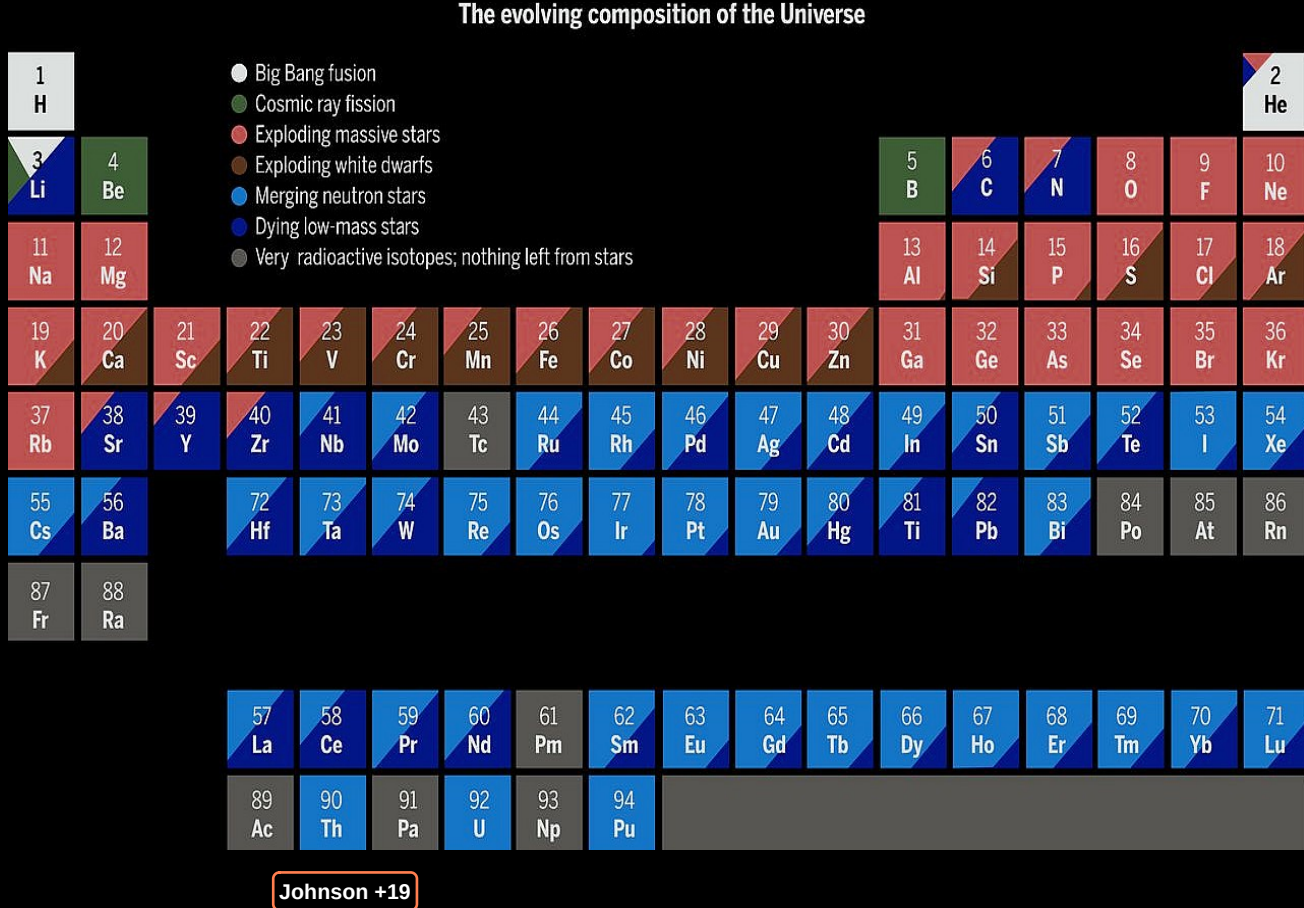
Gabriele Contursi

Prix de Thèse SF2A 2024

I. Nucleosynthèse et éléments lourds

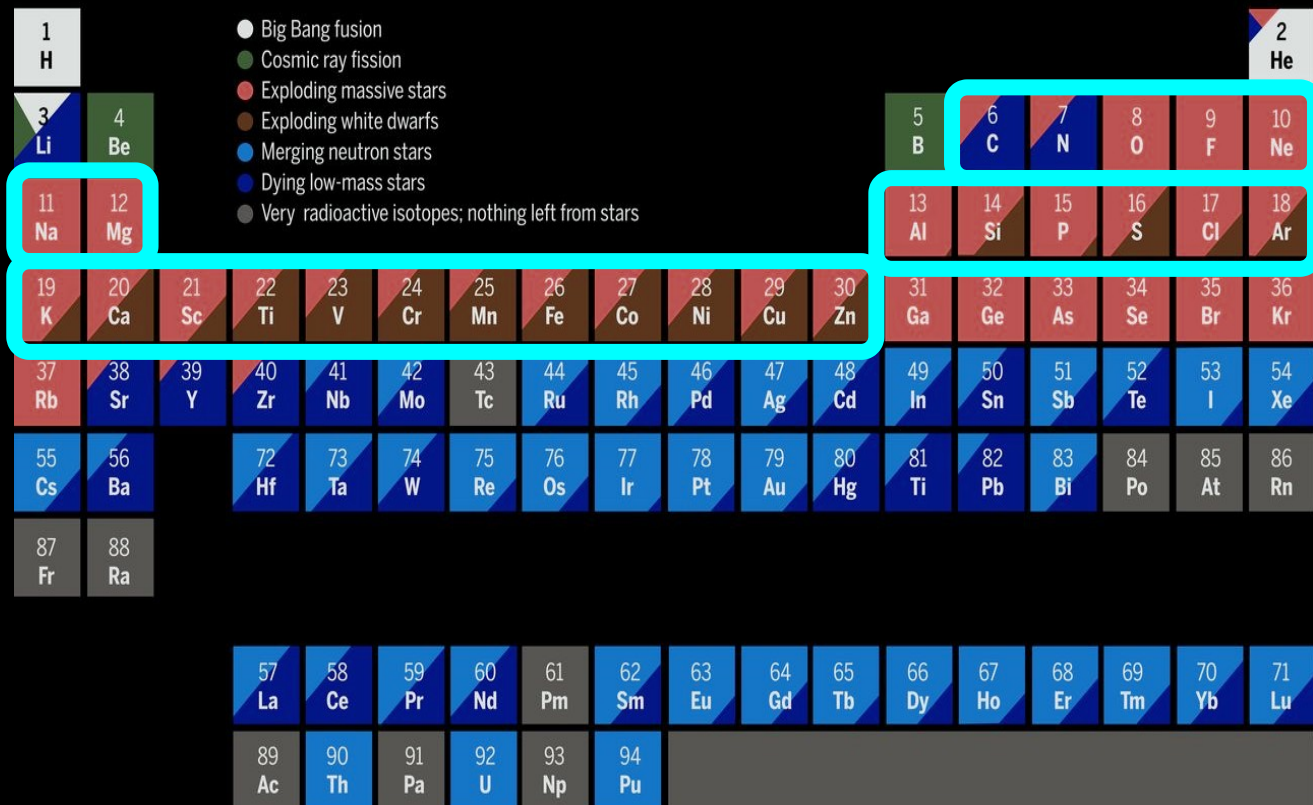
Presque tous les éléments sont synthétisés dans les étoiles.

Les éléments ne sont pas formés par les mêmes sources et processus.



I. Nucleosynthèse et éléments lourds

The evolving composition of the Universe

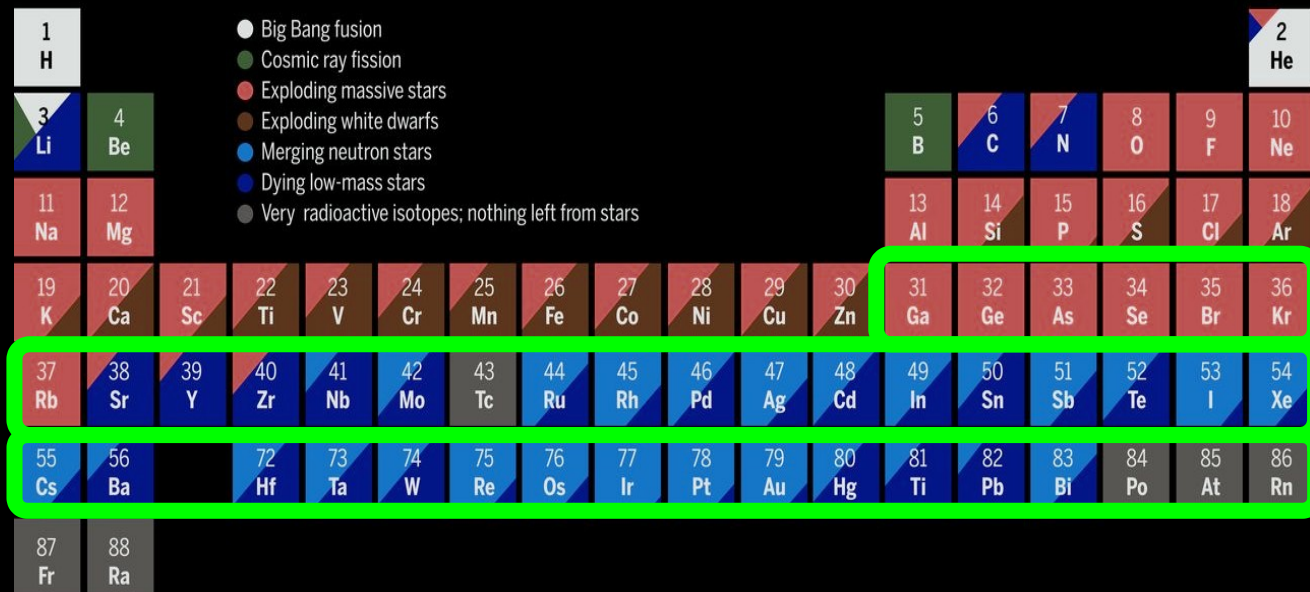


Les Atomes plus
légers que le fer sont
formés par fusion
nucléaire

Johnson +19

I. Nucleosynthèse et éléments lourds

The evolving composition of the Universe

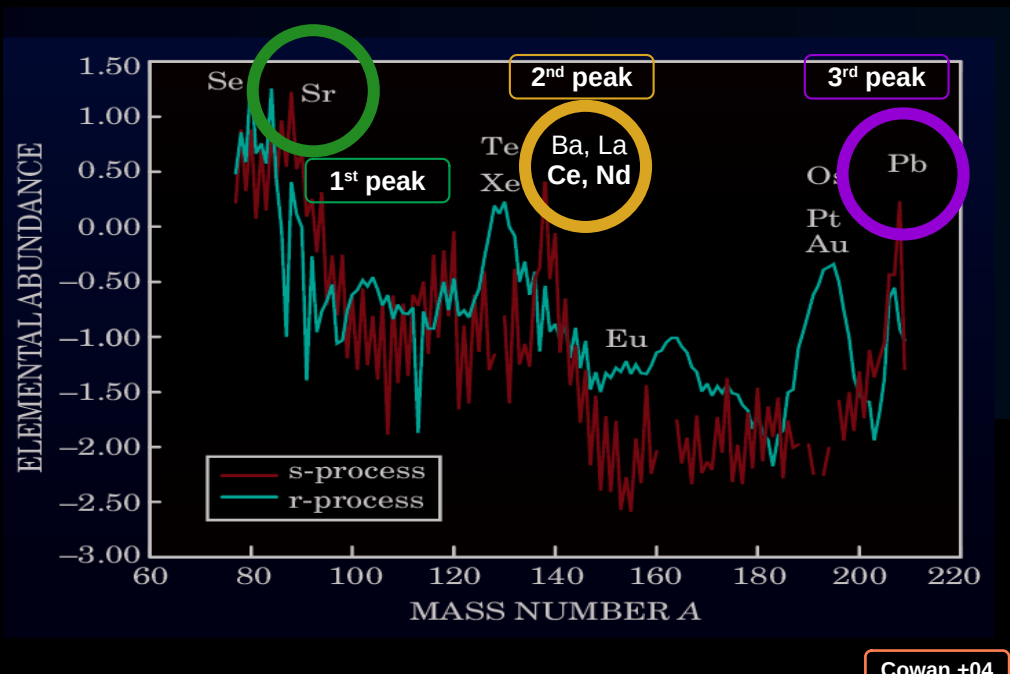


Les atomes plus lourds que Fe principalement formés par captures de neutrons via 2 processus : slow (s-) et rapid (r-)
[Burbridge & al. 57, Cameron 57]

57 La	58 Ce	59 Pr	60 Nd	61 Pm	62 Sm	63 Eu	64 Gd	65 Tb	66 Dy	67 Ho	68 Er	69 Tm	70 Yb	71 Lu
89 Ac	90 Th	91 Pa	92 U	93 Np	94 Pu									

Johnson +19

I. Elements du s- processus



Les éléments du processus s sont principalement répartis autour de 3 pics:

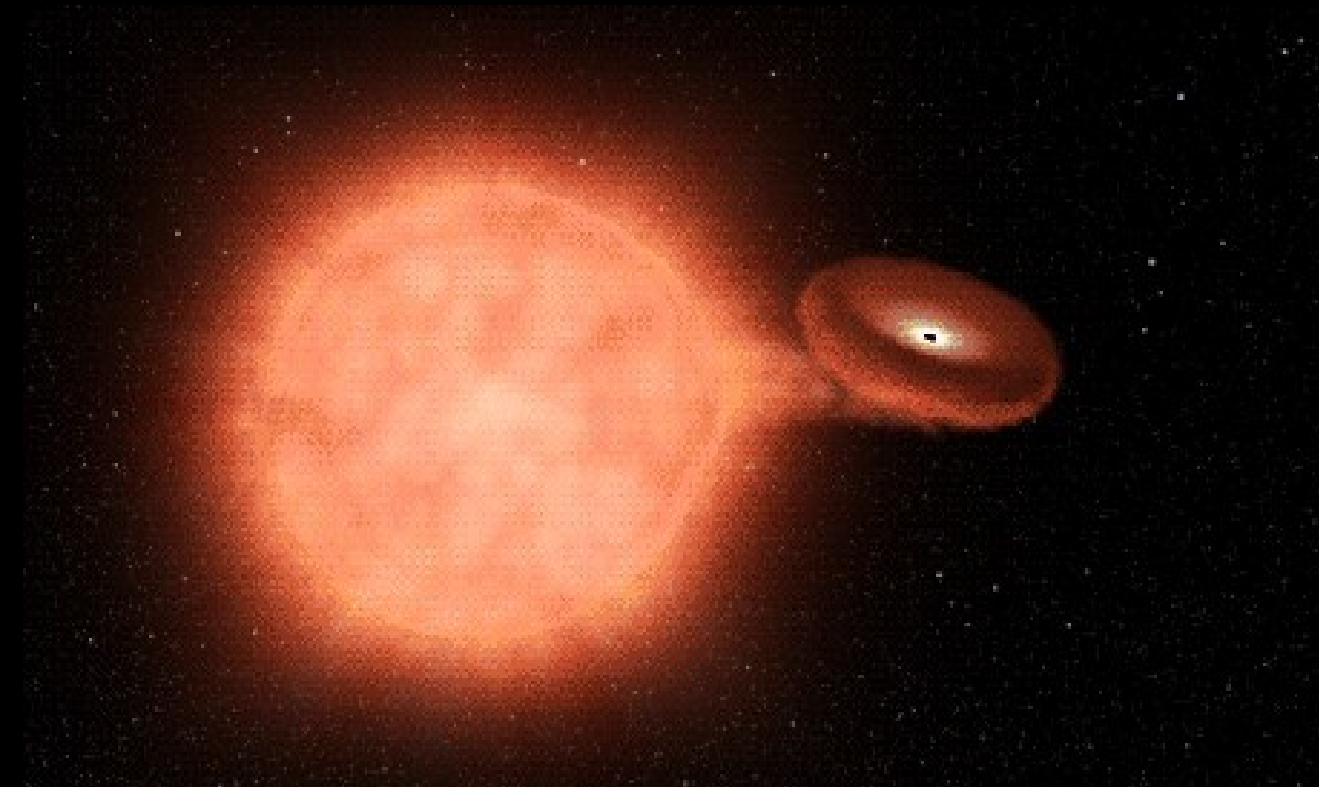
Sr-Y-Zr, Ba-La-Ce-Nd et Pb

Les elements s permettent de :

→ Comprendre leur production dans les étoiles

→ Etudier l'évolution chimique de la Voie Lactée

I. Supernovae de type Ia



SN Ia responsable de la production d'éléments du pic de fer (Fe, Cu, ...)
Echelle de temps: > 1 Gyr

I. Etoiles massives et Supernovae de type II



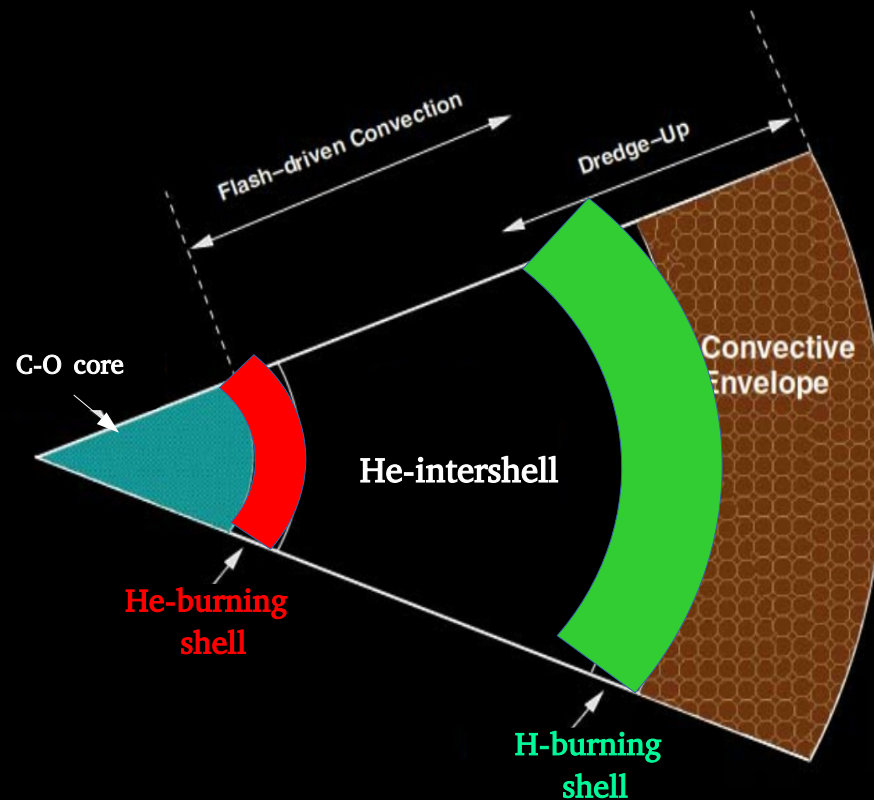
SN II responsable de la production d'éléments:

α- (O, Si, S, Ca, ...)

r-process (Eu, Gd, Au, Pb ?)

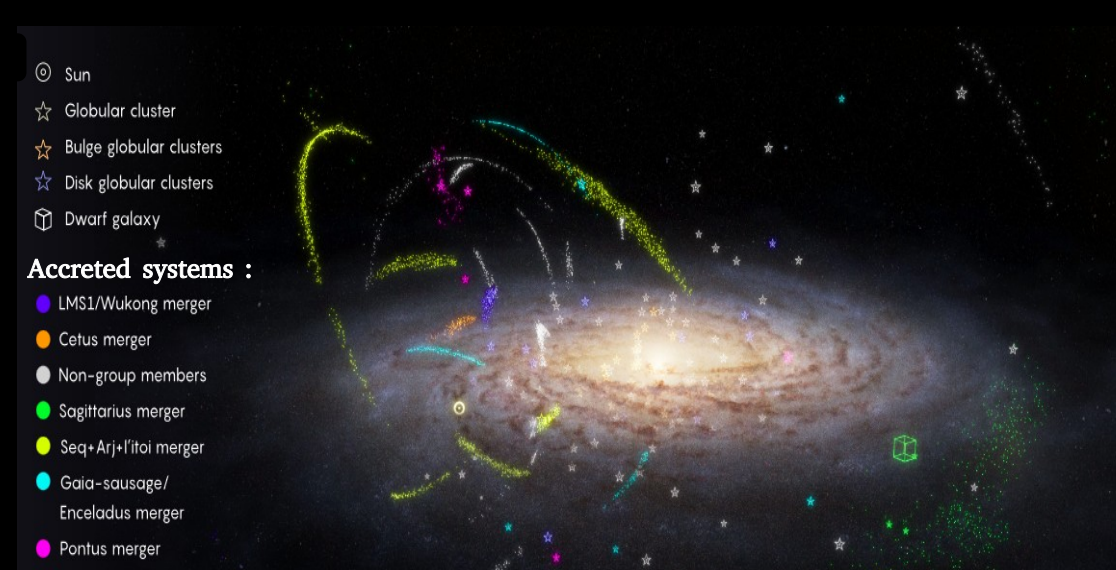
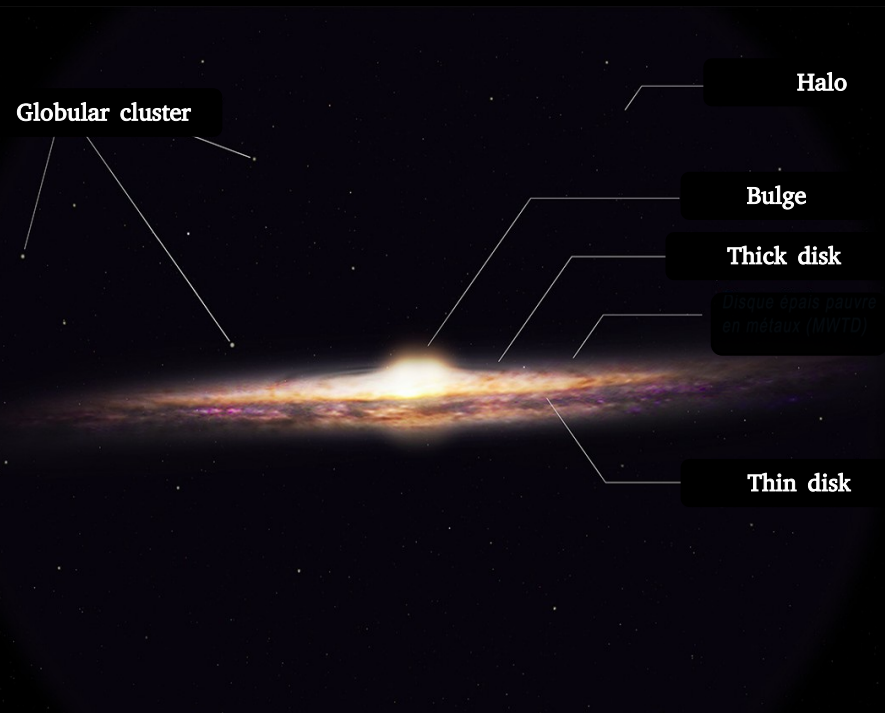
Echelle de temps : ~ 10 Myr

II. Etoiles de type AGB



Adapted from Karakas +14

I. Archéologie Galactique



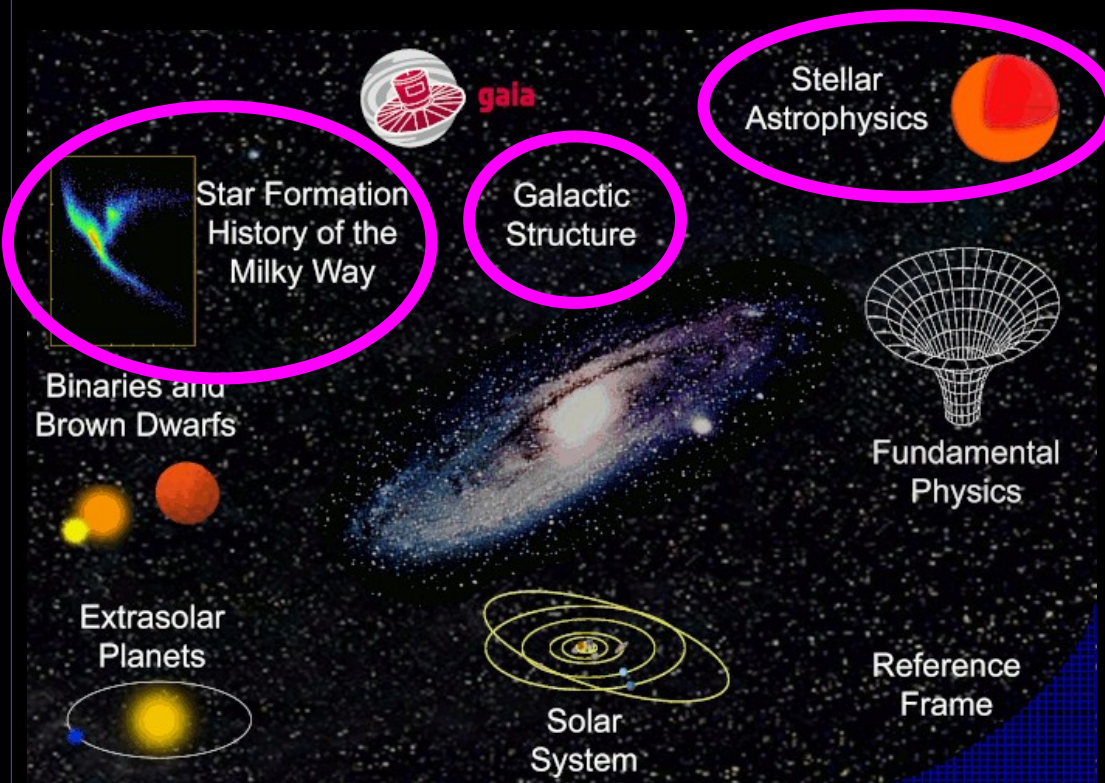
@S. Payne-Wardenaar / K. Malhan, MPIA

Differentes propriétés cinématiques, dynamiques et chimiques des étoiles du disque/halo/bulbe/systèmes accrétés

Archéologie Galactique = Reconstruire l'histoire de la Voie Lactée

I. Gaia/RVS: LE relevé spectroscopique spatial

- Lancé the 19 December 2013
- Situé au point L_2
- Données analysées par le Data Processing and Analysis Consortium
- Plusieurs groupes parmi lequel le module **GSP-Spec** [PI : Recio-Blanco]
 - Dernière Data Release (DR3): 13 Juin 2022. (34 mois d'observation)



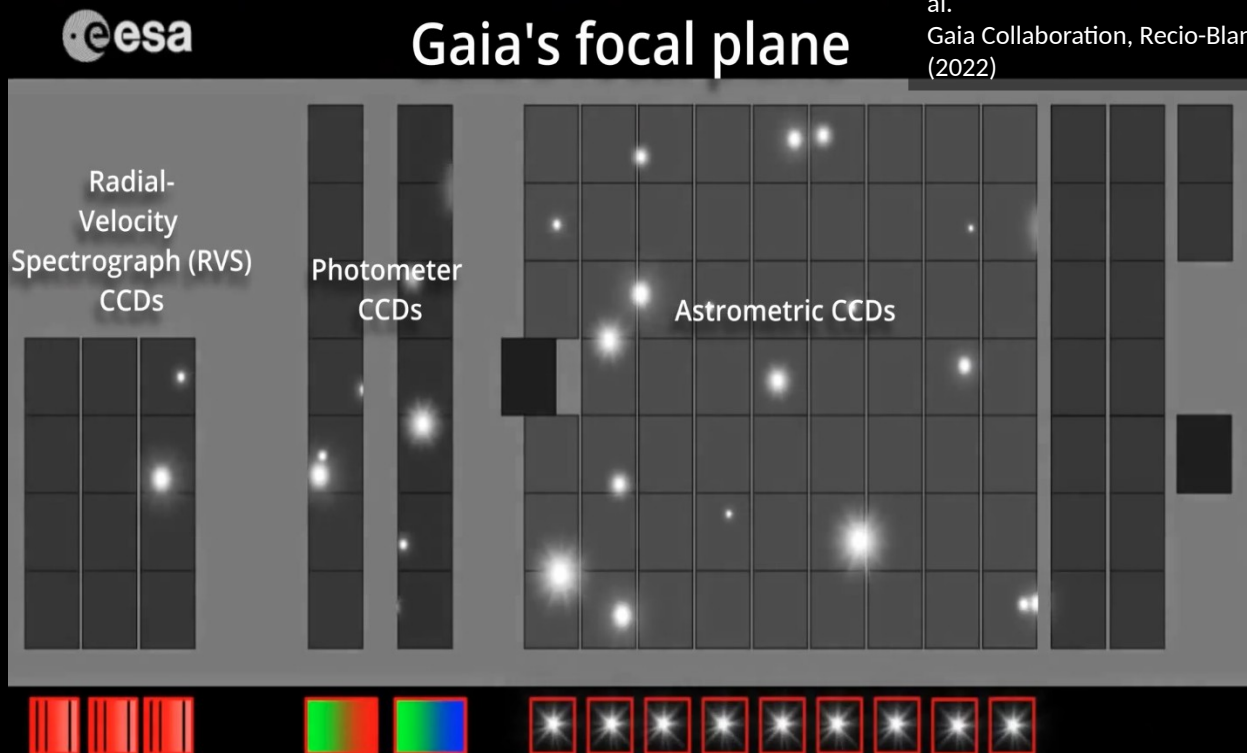
I. Gaia/RVS: LE relevé spectroscopique spatial

Crédits: ESA/Gaia/DPAC, S. Jordan et al.

Gaia Collaboration, Recio-Blanco et al. (2022)

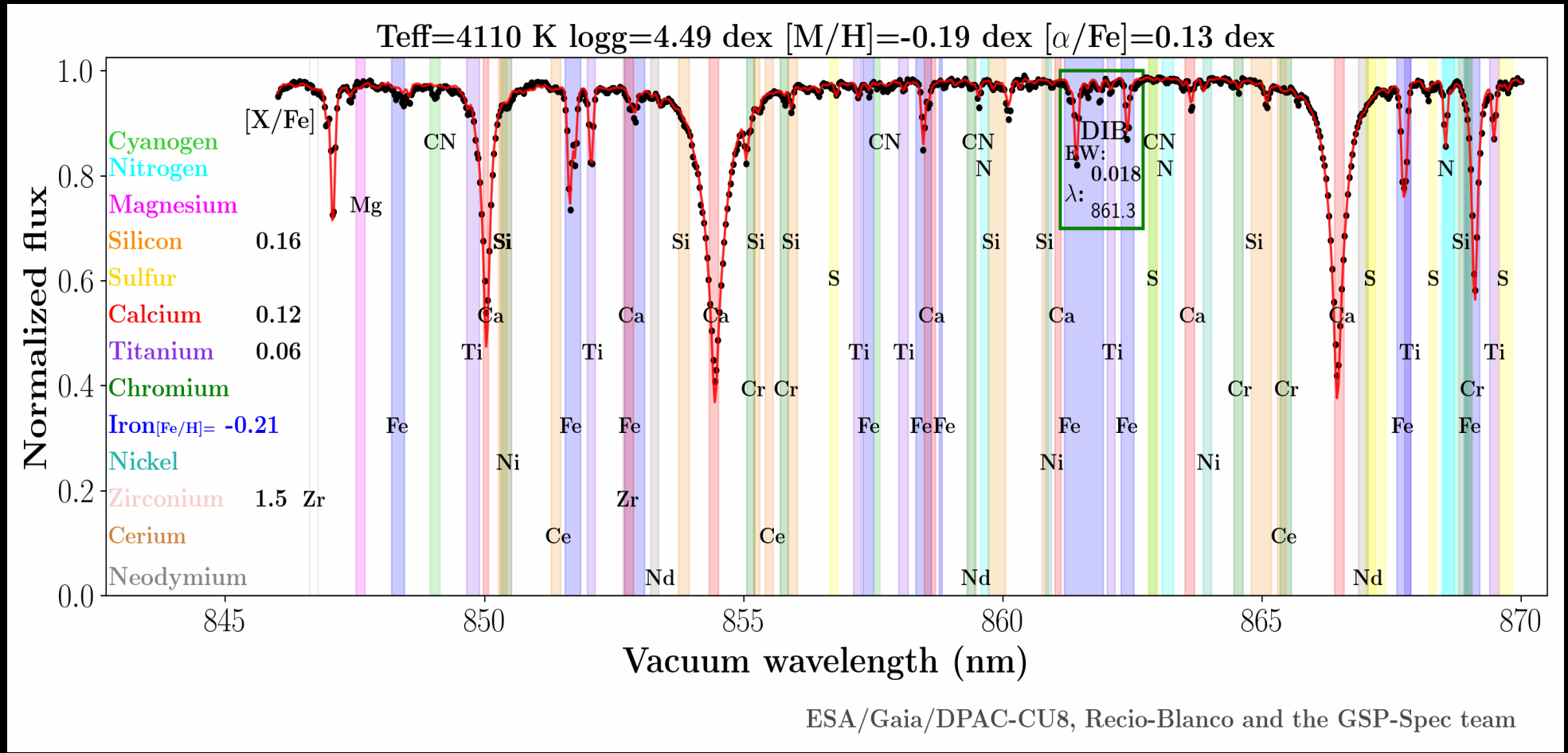
**Radial Velocity
Spectrometer
(RVS) :**
Resolution
11 500

*Domaine de longueur
d'onde:*
846 - 870 nm



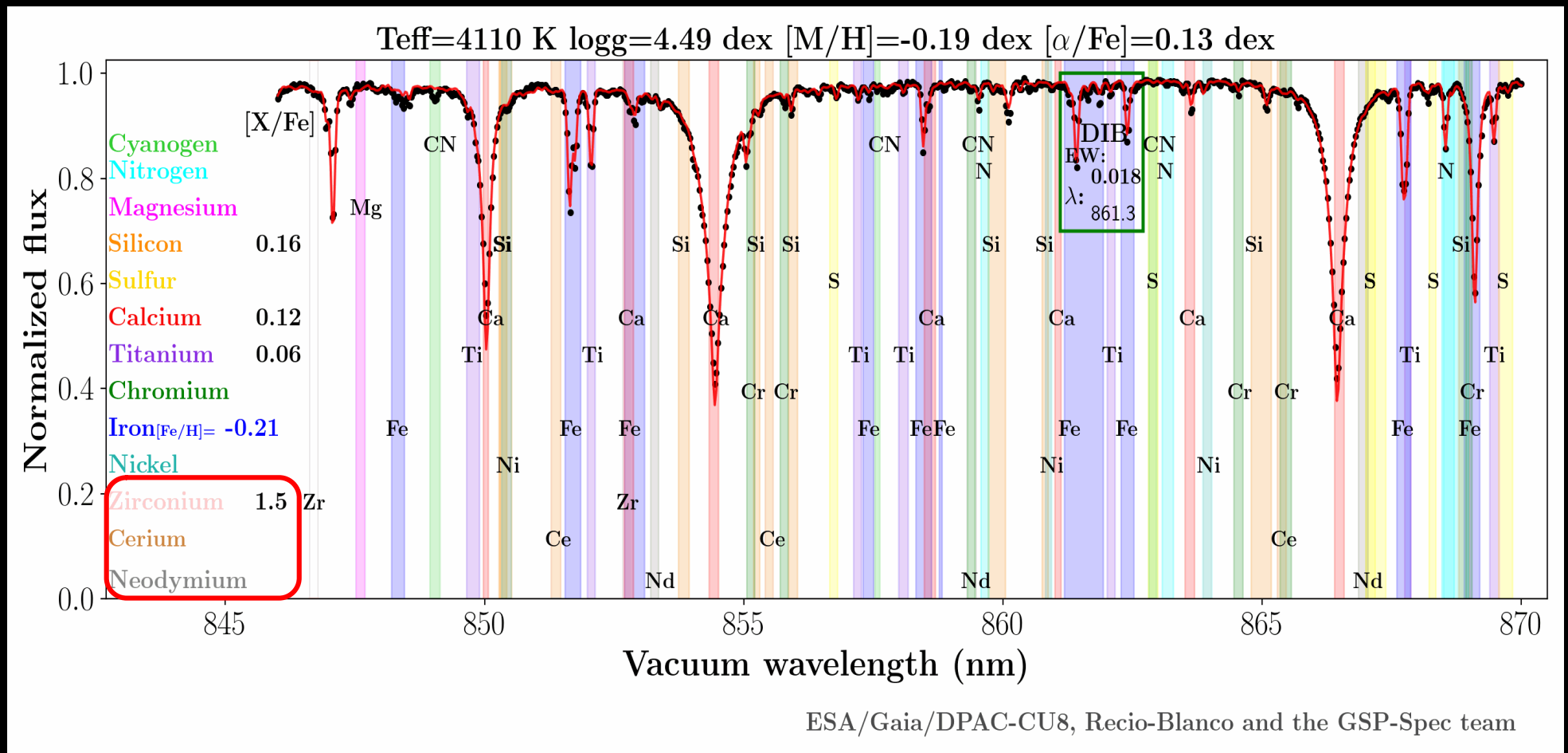
I. Abondances chimique de Gaia

Jusqu'à 13 abondances chimiques (avec les flags associés)



I. Abondances chimique de Gaia

Jusqu'à 13 abondances chimiques (avec les flags associés)
Trois éléments formés par capture des neutrons: Zr, **Ce**, Nd

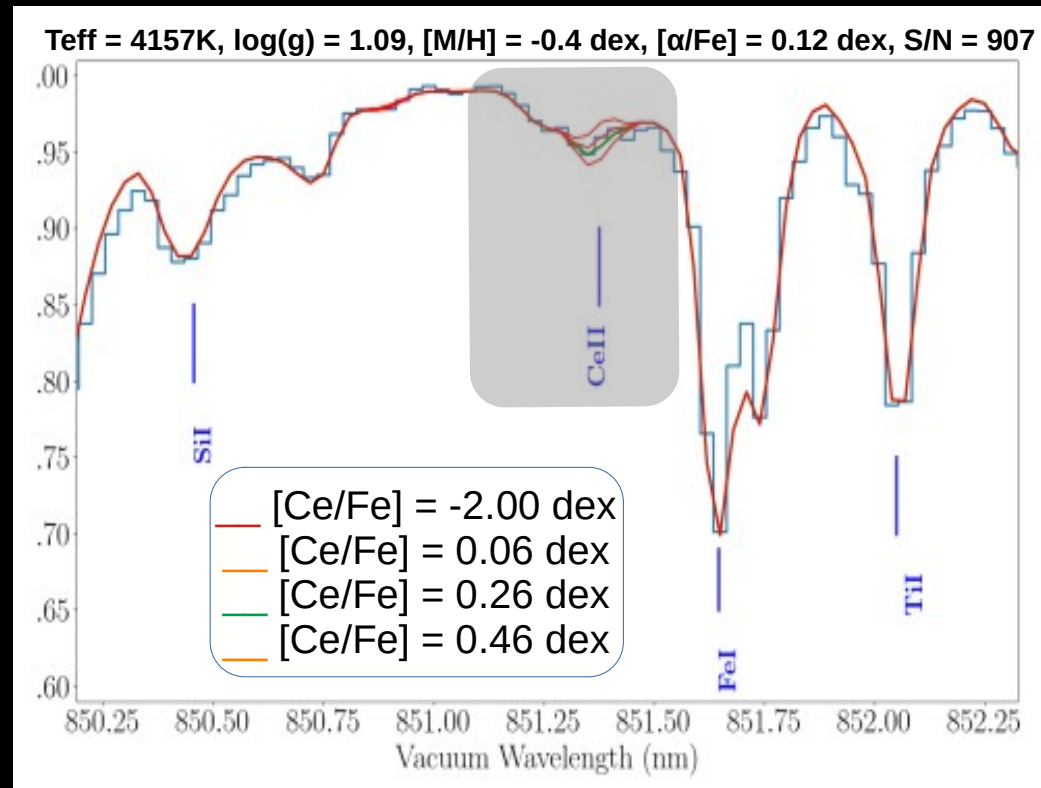


ESA/Gaia/DPAC-CU8, Recio-Blanco and the GSP-Spec team

I. Abondances Chimiques de Gaia

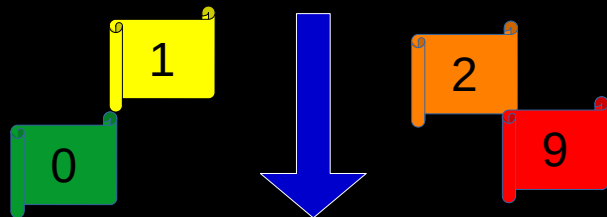
Jusqu'à 13 abondances chimiques (avec les flags de qualité associés)

Trois éléments formés par capture des neutrons, dont le
Cerium ($Z = 58$), $\sim 80\%$ *s-process* [Prantzos+18]



II. Ce dans la Voie Lactée

103 948 abondances de cerium



Echantillon pour l'archéologie Galactique: 7397 stars

A&A 670, A106 (2023)
<https://doi.org/10.1051/0004-6361/202244469>
© The Authors 2023

Astronomy & Astrophysics

The cerium content of the Milky Way as revealed by *Gaia* DR3 GSP-Spec abundances

G. Contursi¹✉, P. de Laverny¹, A. Recio-Blanco¹, E. Spitoni¹, P. A. Palicio¹, E. Poggio¹, V. Grisoni^{2,3}, G. Cescutti^{4,5,6}, F. Matteucci^{4,5,6}, L. Spina⁷, M. A. Alvarez⁸, G. Kordopatis¹, C. Ordenovic¹, I. Oreshina-Slezak¹, and H. Zhao^{1,9}

¹ Université Côte d'Azur, Observatoire de la Côte d'Azur, CNRS, Laboratoire Lagrange, Bd de l'Observatoire, CS 34229, 06304 Nice cedex 4, France
e-mail: gabriele.contursi@oca.eu

² Dipartimento di Fisica e Astronomia, Università degli Studi di Bologna, Via Gobetti 93/2, 40129 Bologna, Italy

³ INAF, Osservatorio di Astrofisica e Scienza dello Spazio, Via Gobetti 93/3, 40129 Bologna, Italy

⁴ Dipartimento di Fisica, Sezione di Astronomia, Università di Trieste, via G.B. Tiepolo 11, 34131 Trieste, Italy

⁵ INAF Osservatorio Astronomico di Trieste, via G.B. Tiepolo 11, 34131 Trieste, Italy

⁶ INFN Sezione di Trieste, via Valerio 2, 34134 Trieste, Italy

⁷ INAF - Osservatorio astronomico di Padova, Vicolo Osservatorio 5, 35122 Padova, Italy

⁸ CIGUS CITIC – Department of Computer Science and Information Technologies, University of A Coruña, Campus of Elviña s/n, A Coruña 15071, Spain

⁹ Purple Mountain Observatory, Chinese Academy of Sciences, Nanjing 210023, PR China

Received 11 July 2022 / Accepted 16 November 2022

ABSTRACT

Context. The recent *Gaia* third data release contains a homogeneous analysis of millions of high-quality Radial Velocity Spectrometer (RVS) stellar spectra by the GSP-Spec module. This led to the estimation of millions of individual chemical abundances and allows us to chemically map the Milky Way. The published GSP-Spec abundances include three heavy elements produced by neutron-captures in stellar interiors: Ce, Zr, and Nd.

Aims. We study the Galactic content in cerium based on these *Gaia*/RVS data and discuss the chemical evolution of this element.

Methods. We used a sample of about 30 000 local thermal equilibrium Ce abundances, selected after applying different combinations of GSP-Spec flags. Based on the *Gaia* DR3 astrometric data and radial velocities, we explore the cerium content in the Milky Way and, in particular, its halo and disc components.

Results. The high quality of the Ce GSP-Spec abundances is quantified through literature comparisons. We found a rather flat [Ce/Fe] versus [M/H] trend. We also found a flat radial gradient in the disc derived from field stars and, independently, from 50 open clusters. This agrees with previous studies. The [Ce/Fe] vertical gradient was also estimated. We also report an increasing [Ce/Ca] versus [Ca/H] in the disc, illustrating the late contribution of asymptotic giant branch stars with respect to supernovae of type II. Our cerium abundances in the disc, including the young massive population, are well reproduced by a new three-infall chemical evolution model. In the halo population, the M 4 globular cluster is found to be enriched in cerium. Moreover, 11 stars with cerium abundances belonging to the Thamnos, Helmi Stream, and Gaia-Sausage-Enceladus accreted systems were identified from chemo-dynamical diagnostics. We found that the Helmi Stream might be slightly underabundant in cerium compared to the two other systems.

Conclusions. This work illustrates the high quality of the GSP-Spec chemical abundances, which significantly contribute to unveiling the heavy-element evolution history of the Milky Way.

Key words. Galaxy: abundances – stars: abundances – Galaxy: disk – Galaxy: halo – Galaxy: evolution

1. Introduction

Our understanding of the Milky Way has made a great leap forwards through the different data releases of the *Gaia* mission. The third release (Gaia Collaboration 2023b) consists of a major and unique step because it includes a large variety of new data products, including, in particular, an extensive characterisation of the *Gaia* sources. In this context, the module called general stellar parametrizer from spectroscopy (GSP-Spec hereafter; see Gaia Collaboration 2023a) has estimated atmospheric parameters (effective temperature T_{eff} , surface gravity $\log(g)$, global metallicity [M/H], and abundances of α -elements with respect

to iron $[\alpha/\text{Fe}]$) as well as individual chemical abundances of up to a dozen elements¹ for about 5.6 million stars that have been observed by the Radial Velocity Spectrometer (RVS hereafter; Cropper et al. 2018; Katz et al. 2023).

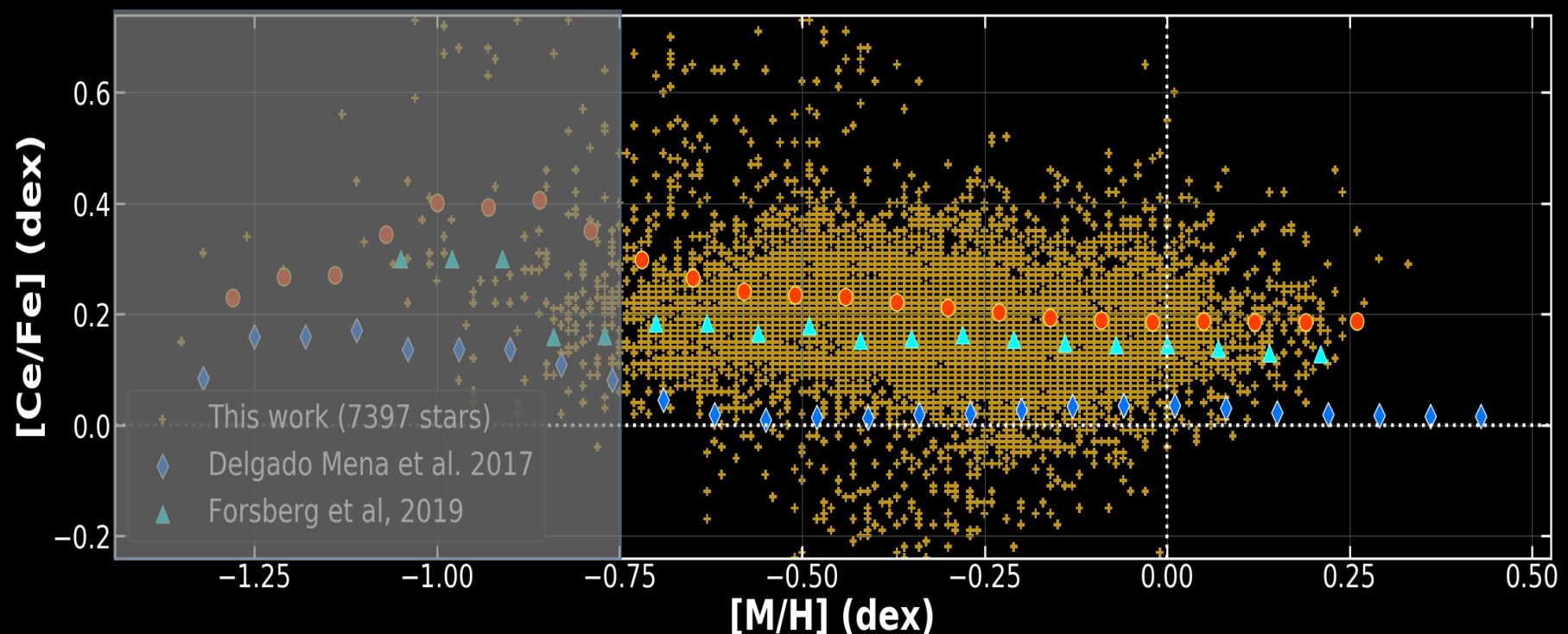
Three of these 13 chemical elements are produced by neutron capture in the inner layers of some specific stages of stellar evolution: zirconium ($Z = 40$), cerium ($Z = 58$), and neodymium ($Z = 60$). According to the seminal work of Burbidge et al.

¹ See https://www.cosmos.esa.int/web/gaia/iow_20210709. These elements are N, Mg, Si, S, Ca, Ti, Fe I, Fe II, Ni, Zr, Ce, and Nd.

II. Tendance plate de [Ce/Fe] vs [M/H]

[Ce/Fe] vs [M/H] au niveau moyen ~ 0.2 dex comme dans
[Forsberg +19, 277 stars].

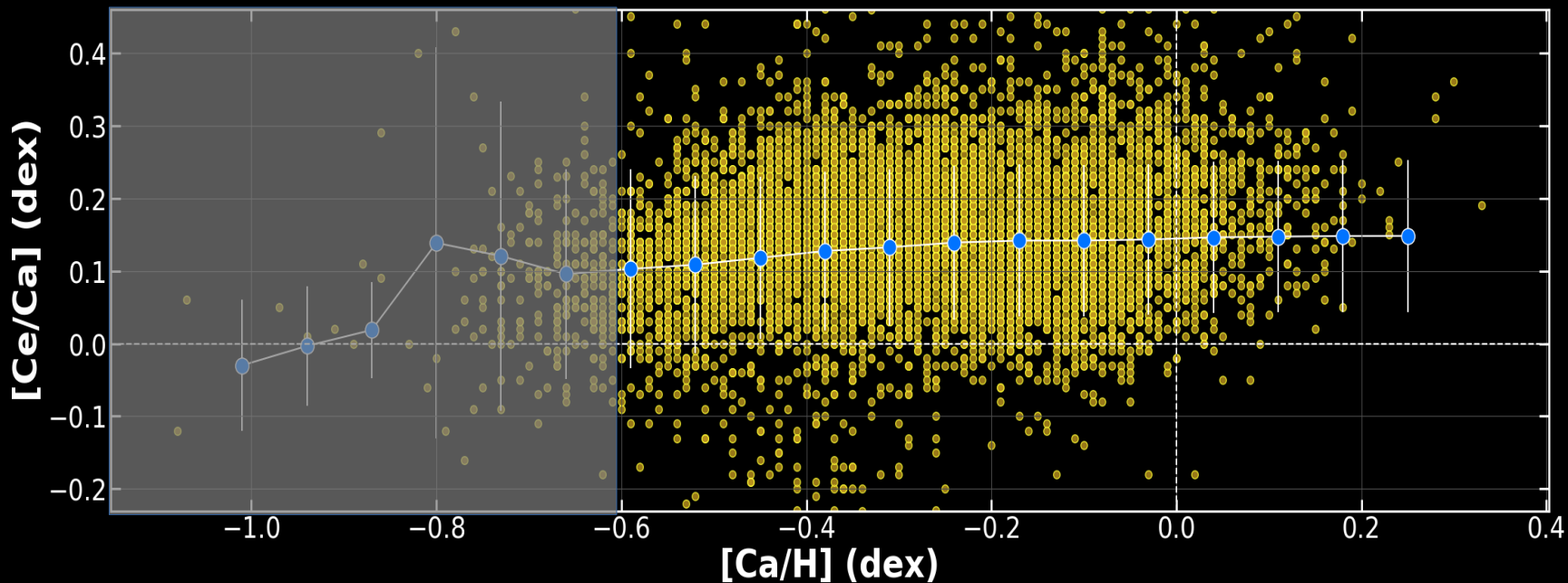
Même tendance plate mais avec un décalage de ~ 0.2 dex en
comparaison avec *[Delgado Mena +17, 653 stars]*.



II. Cerium vs Calcium

[Ce/Ca] augmente si [Ca/H] augmente également

Cela peut montrer la contribution plus tardive de l'AGB dans l'histoire de l'évolution chimique de la galaxie par rapport à la SN-II.

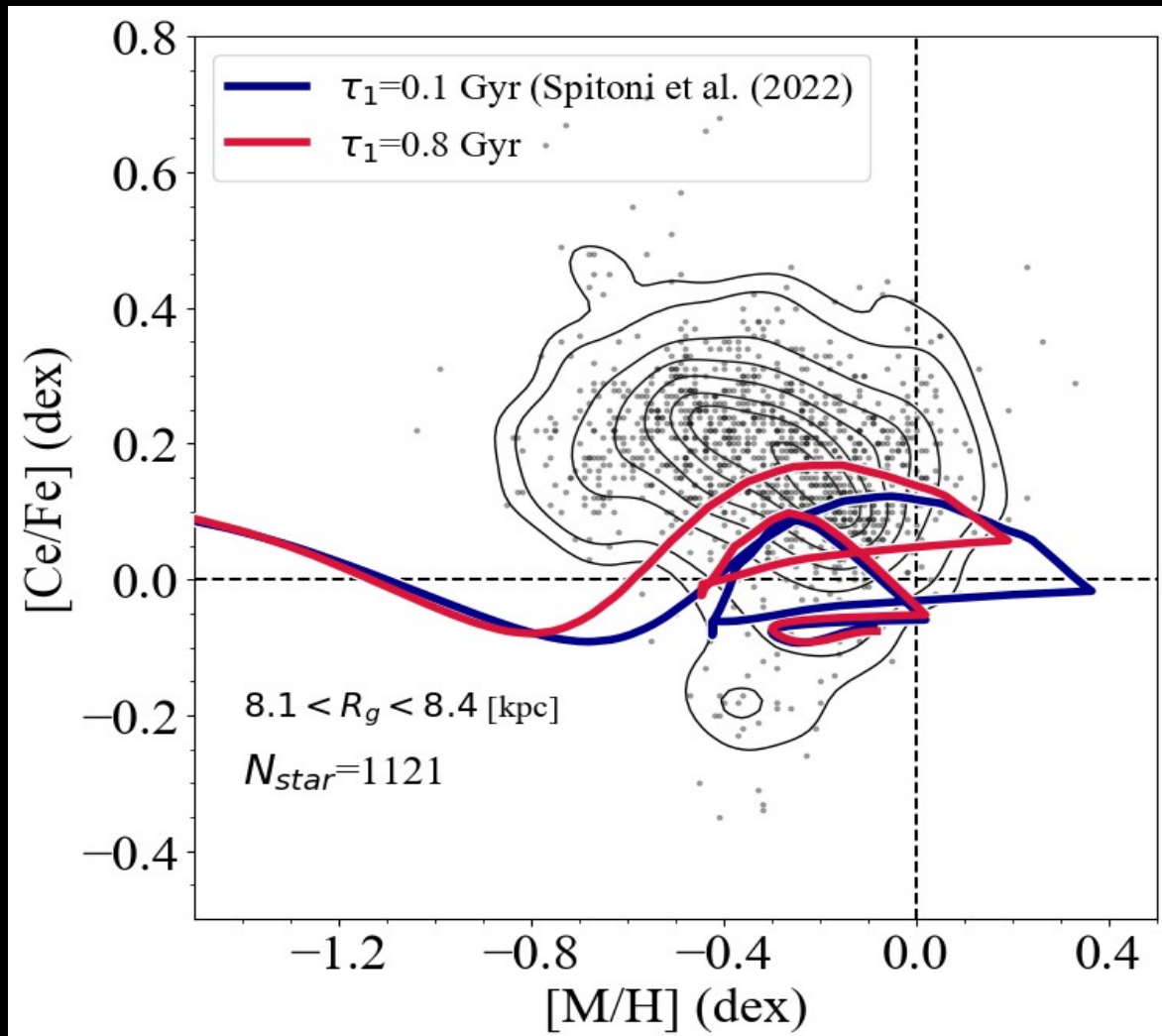


II. Comparaison avec le three-infall modèle

Contursi et al. (2023)

Prédiction du three-infall modèle de
Spitoni +23

→ *Test de différents « time-scale of gas accretion »*

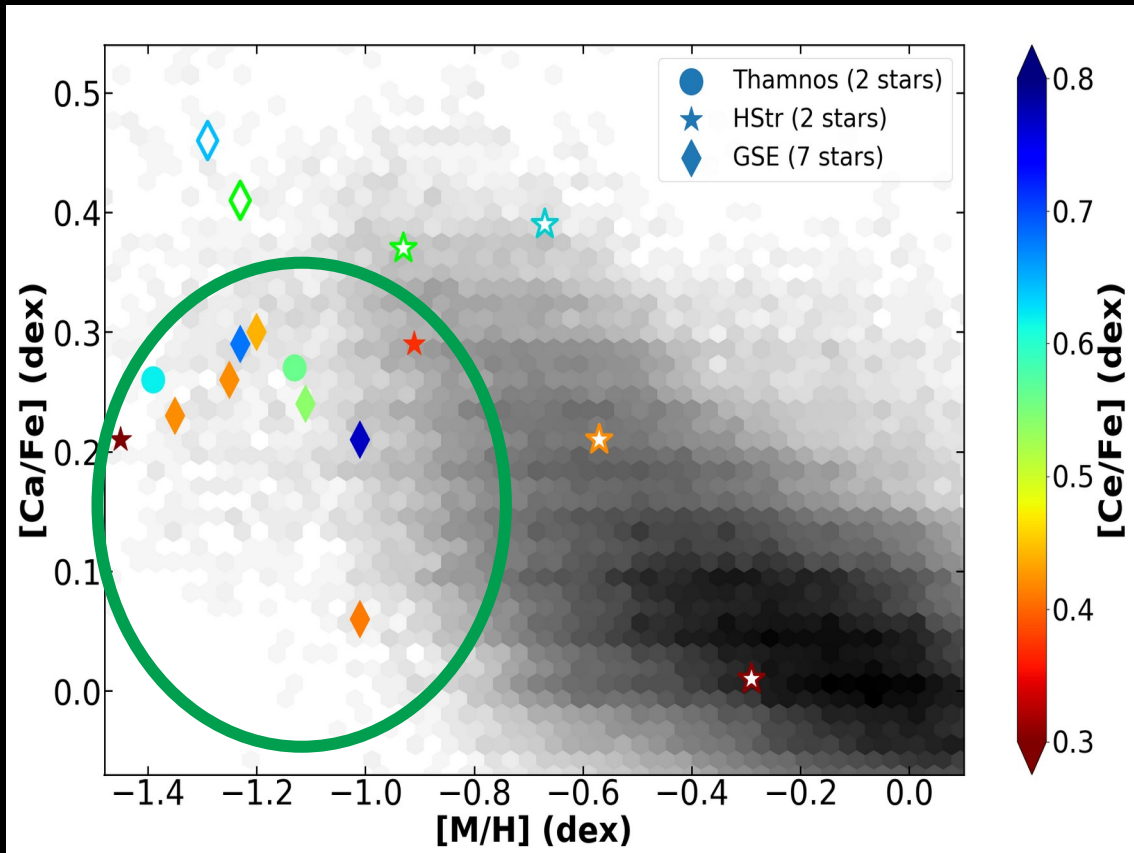


II. Cerium dans le Halo: Systèmes accrétés

Contursi et al. (2023)

11 étoiles (avec [Ce/Fe]) candidates à Thamnos, Helmi streams et GSE, trouvées.

Investigation de leur nature accrétée en regardant [Ca/Fe] en fonction de [M/H]



Thamnos
Helmi Stream
Gaia-Sausage-Enceladus

[M/H] (dex)	[Ca/Fe] (dex)	[Ce/Fe] (dex)
-1.26 ± 0.13	0.26 ± 0.01	0.59 ± 0.03
-1.18 ± 0.27	0.25 ± 0.04	0.32 ± 0.05
-1.16 ± 0.12	0.28 ± 0.08	0.53 ± 0.13

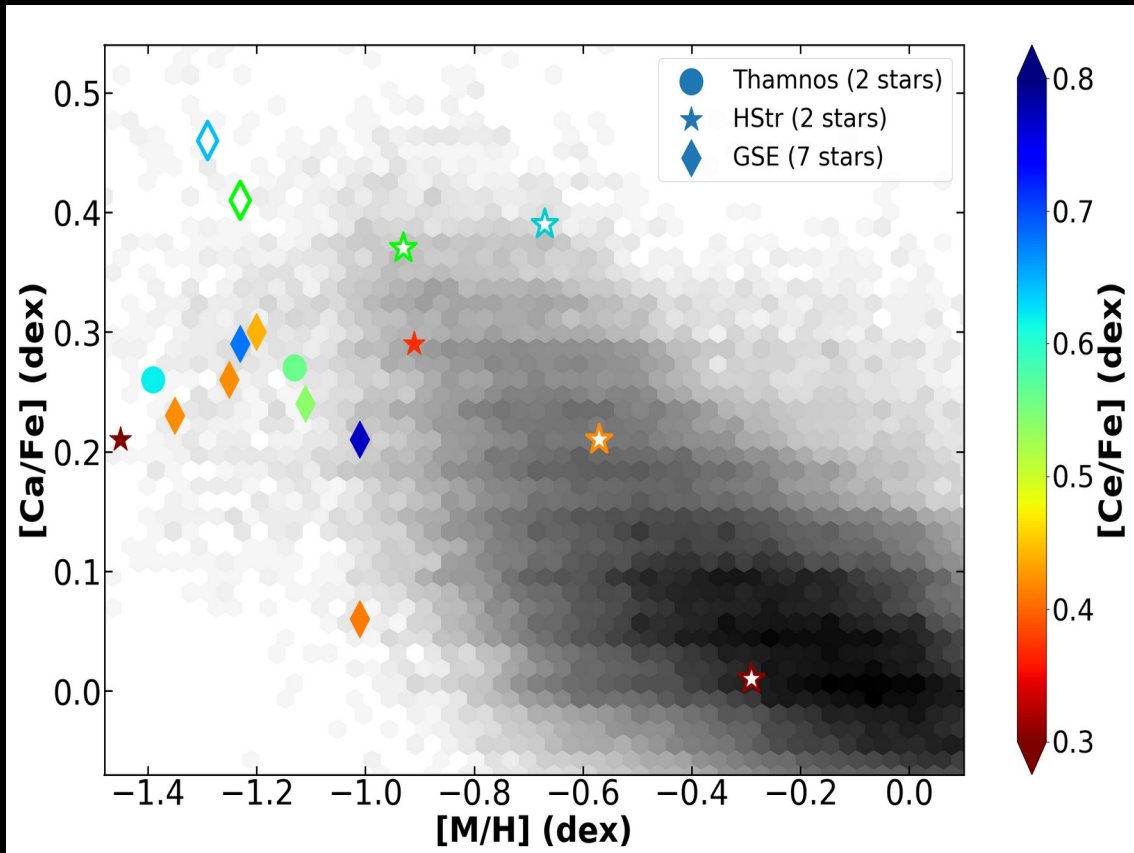
II. Cerium dans le Halo: Systèmes accrétés

Contursi et al. (2023)

[M/H] et [Ca/Fe] compatibles avec la littérature

[Y/Fe] peut être plus faible dans les satellites de faible masse
(*Recio-Blanco+21*, *Y étant un autre élément s*).

Notre [Ce/Fe] peut suggérer une masse plus faible du progéniteur Helmi que celui de GSE.
(*cf. Koppelman +19, Helmi +20*)



Thamnos
Helmi Stream
Gaia-Sausage-Enceladus

[M/H] (dex)	[Ca/Fe] (dex)	[Ce/Fe] (dex)
-1.26 ± 0.13	0.26 ± 0.01	0.59 ± 0.03
-1.18 ± 0.27	0.25 ± 0.04	0.32 ± 0.05
-1.16 ± 0.12	0.28 ± 0.08	0.53 ± 0.13

Sommaire

- I. Introduction : Éléments lourds et Gaia
- II. Contenu en cérium de la Voie Lactée
- III. Production d'éléments s dans les étoiles AGB**
- IV. Abondances de Plomb dans la Voie Lactée

III. Abondances d'éléments s dans les AGB de Gaia

Astronomy & Astrophysics manuscript no. output
September 21, 2023

©ESO 2023

Production of *s*-process elements in AGB stars as revealed by *Gaia/GSP-Spec* abundances

G. Contursi¹, P. de Lavemy¹, A. Recio-Blanco¹, P. A. Palicio¹, and C. Abia²

¹ Université Côte d'Azur, Observatoire de la Côte d'Azur, CNRS, Laboratoire Lagrange, Bd de l'Observatoire, CS 34229, 06304 Nice cedex 4, France

² Departamento de Física Teórica y del Cosmos, Universidad de Granada, E-18071 Granada, Spain

Received ?? ; accepted ??

ABSTRACT

Context. The recent parameterisation by the *GSP-Spec* module of *Gaia*/Radial Velocity Spectrometer stellar spectra has produced an homogeneous catalogue of about 174,000 Asymptotic Giant Branch (AGB) stars. Among the 13 chemical elements presented in this *Gaia* third data release, the abundance of two of them (cerium and neodymium) have been estimated in most of these AGB. These two species are formed by slow neutron captures (*s*-process) in the interior of low- and intermediate-mass stars. They belong to the family of second peak *s*-process elements.

Aims. We study the content and production rate of Ce and Nd in AGB stars, using the atmospheric parameters and chemical abundances derived by the *GSP-Spec* module.

Methods. We define a working sample of 19,544 AGB stars having high-quality Ce and/or Nd abundances, selected by applying a specific combination of the *GSP-Spec* quality flags. We compare these abundances with the yield production predicted by AGB evolutionary models.

Results. We first confirmed that the majority of the working sample is composed of AGB stars by estimating their absolute magnitude in the *K*-band and their properties in a *Gaia*-2MASS diagram. We also checked that these stars are oxygen-rich AGBs, as assumed during the *GSP-Spec* parameterisation. A good correlation between the Ce and Nd abundances is found, confirming the high quality of the derived abundances and that these species indeed belong to the same *s*-process family. We also found higher Ce and Nd abundances for more evolved AGB stars of similar metallicity, illustrating the successive mixing episodes enriching the AGB surface in *s*-process elements formed deeper in their stellar interior. We then compared the observed Ce and Nd abundances with FRUITY and Monash AGB yields and found that the higher Ce and Nd abundances can not be explained by AGBs of mass higher than $5 M_{\odot}$. On the contrary, the yields predicted by both models for AGB with an initial mass between ~ 1.5 and $\sim 2.5 M_{\odot}$ and metallicities between ~ -0.5 and ~ -0.0 dex are fully compatible with the observed *GSP-Spec* abundances.

Conclusions. This work, based on the largest catalogue of high-quality second-peak *s*-elements abundances in oxygen-rich AGB, allows to constrain evolutionary models and confirms the fundamental role played by low- and intermediate-mass stars in the enrichment of the Universe in these chemical species.

Key words. Galaxy: abundances, disc, halo, Stars: abundances, evolution, AGB and post-AGB

1. Introduction

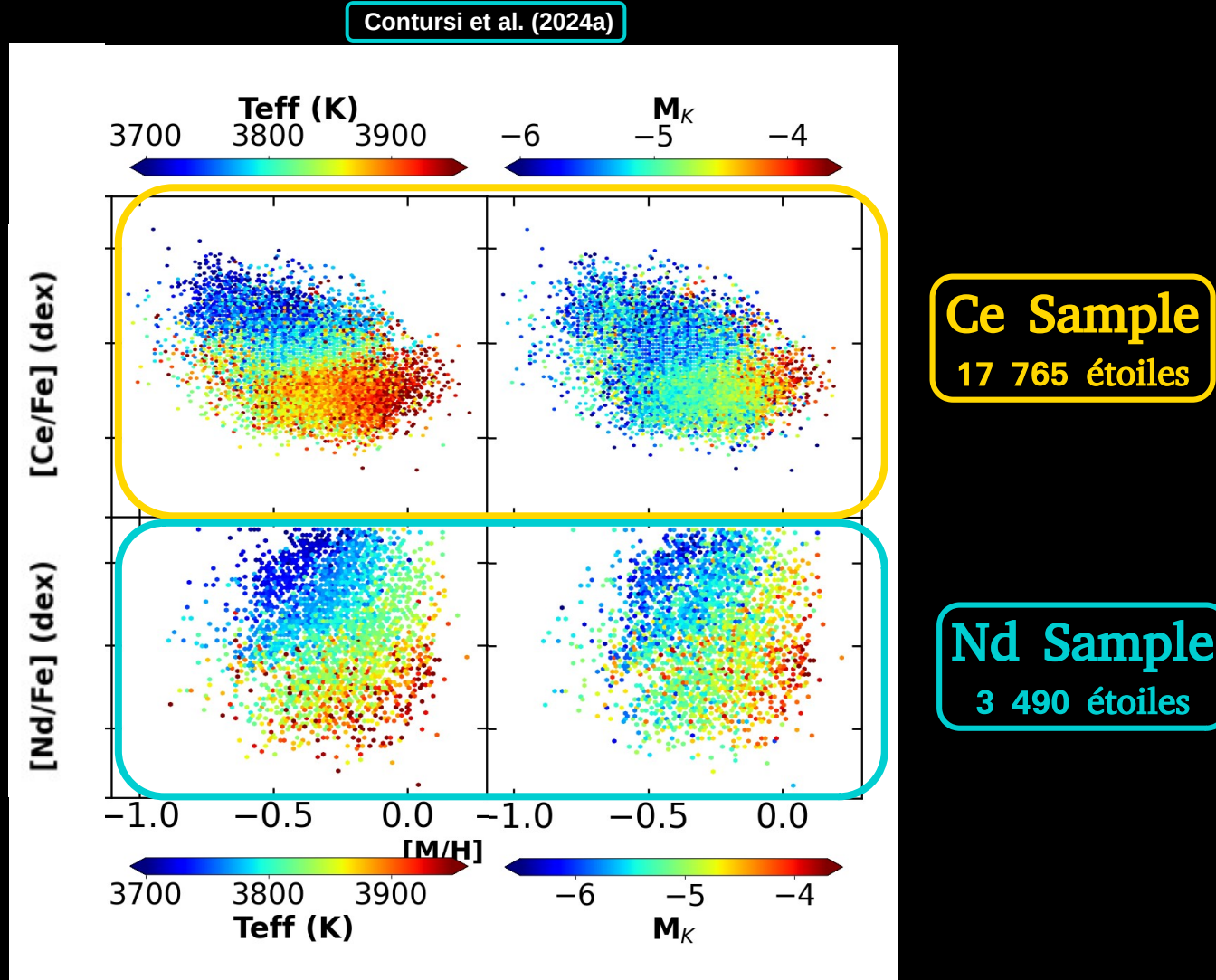
Asymptotic Giant Branch stars (AGB, hereafter) correspond to the late evolutionary stages of low (masses smaller than $\sim 3 M_{\odot}$) and intermediate-mass (between ~ 4 and $\sim 8 M_{\odot}$) stars. Due to their specific internal structure, efficient mixing events and high-mass loss rates, AGBs are among the main contributors to the interstellar medium enrichment in several species. They hence play a fundamental role in the chemical evolution of the Universe

$^{13}\text{C}(\alpha, n)^{16}\text{O}$ reaction [Arlandini et al. 1999] [Busso et al. 1999] [Karakas & Lattanzio 2014a] [Bisterzo et al. 2011] [2015]. Finally, third peak *s*-process elements such as Pb are thought to be predominantly formed within low-mass and low-metallicity AGBs [Gallino et al. 1998] [Choplin et al. 2022].

We remind that the internal structure of an AGB stars (mass $\leq 8 M_{\odot}$) is made by a compact and degenerated C-O core, a thin He-burning shell and an H-burning shell separated by a He-intershell (composed of about 75% of He and 22% of C ac-

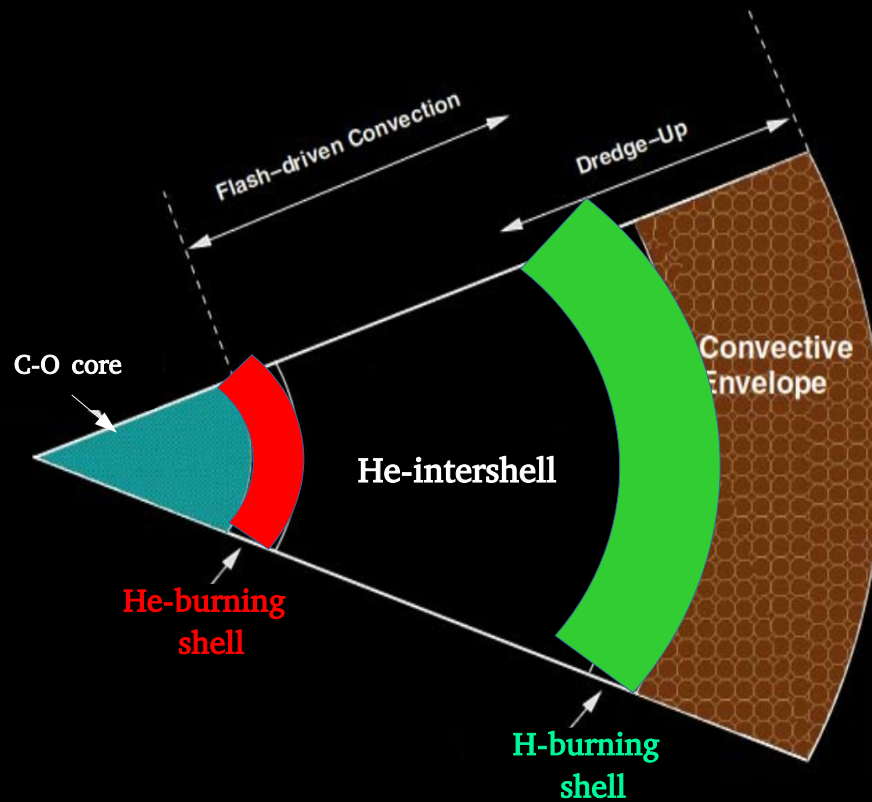
Publié dans A&A

III. Abondances de Ce et Nd plus élevées pour des étoiles plus froides



Les abondances de Nd et de Ce sont plus élevées pour les étoiles plus froides (à une métallicité donnée)

II. AGB Structure



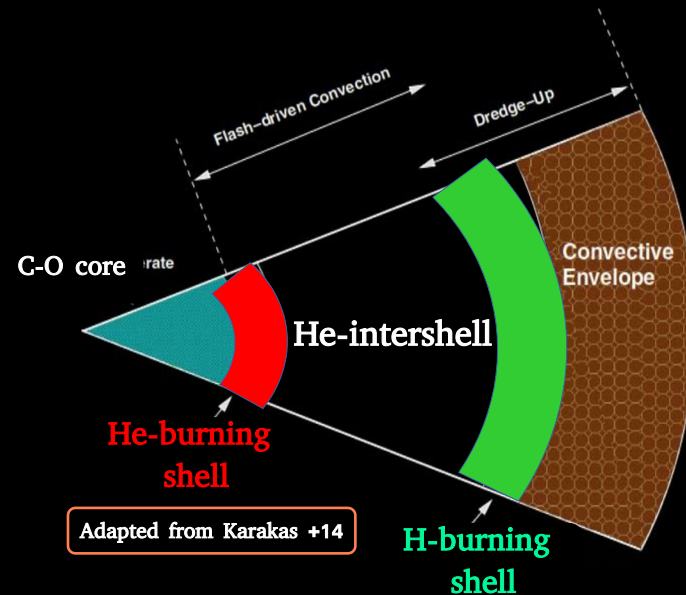
Adapted from Karakas +14

II. AGB Structure

He-burning shell inactive.

It Increases due to **H-burning shell**

When **He-burning shell** activates,
Thermal Pulses occur



II. AGB Structure

He-burning shell inactive.

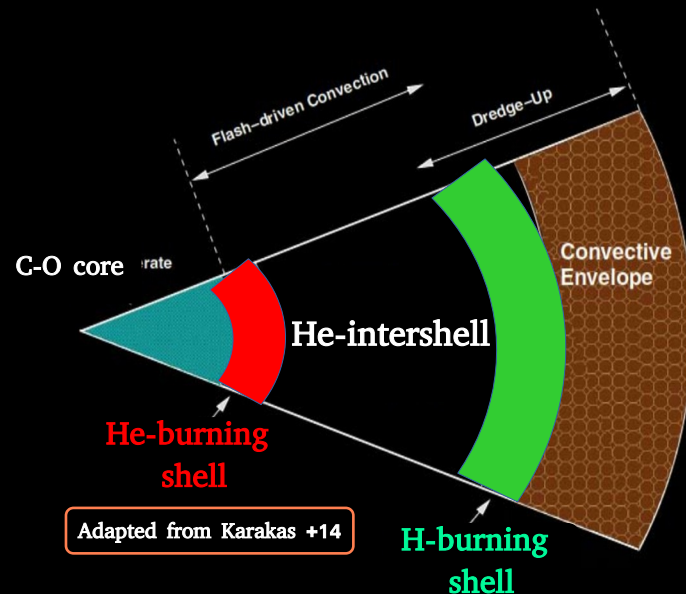
It Increases due to **H-burning shell**

When **He-burning shell** activates,
Thermal Pulses occur

Convection penetrates the **He-intershell**:
Third Dredge Up (TDU).

Increase of Carbon and s-process
elements in the **Envelope**

Opacity increases,
decrease of the effective temperature.



II. AGB Structure

He-burning shell inactive.

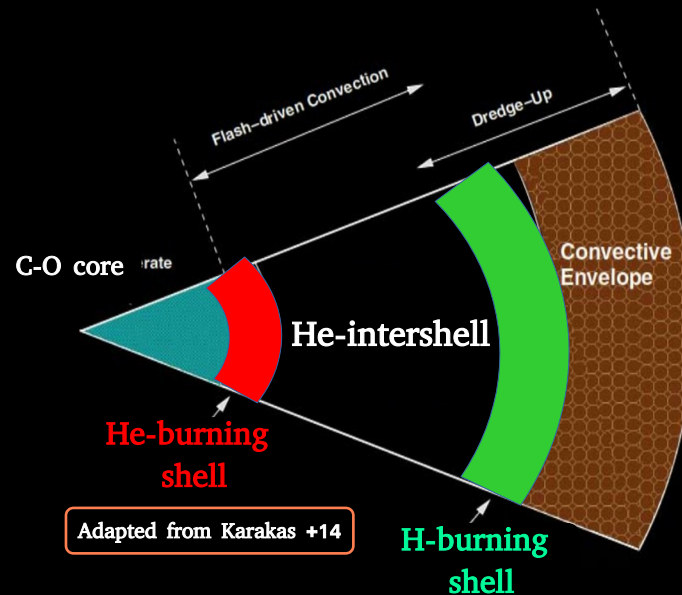
It Increases due to **H-burning shell**

When **He-burning shell** activates,
Thermal Pulses occur

Convection penetrates the **He-intershell**:
Third Dredge Up (TDU).

Increase of Carbon and s-process
elements in the **Envelope**

Opacity increases,
decrease of the effective temperature.



He-burning shell inactive

II. AGB Structure

He-burning shell inactive.

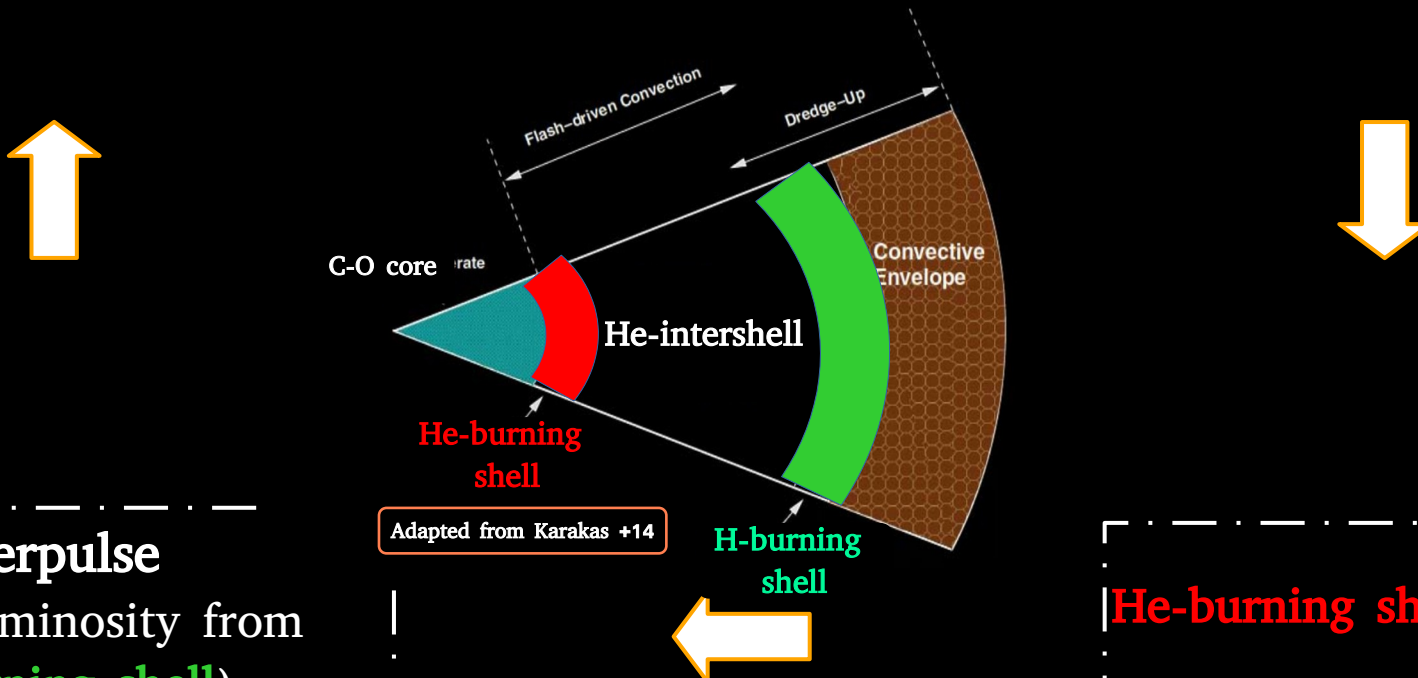
It Increases due to **H-burning shell**

When **He-burning shell** activates,
Thermal Pulses occur

Convection penetrates the **He-intershell**:
Third Dredge Up (TDU).

Increase of Carbon and s-process
elements in the **Envelope**

Opacity increases,
decrease of the effective temperature.

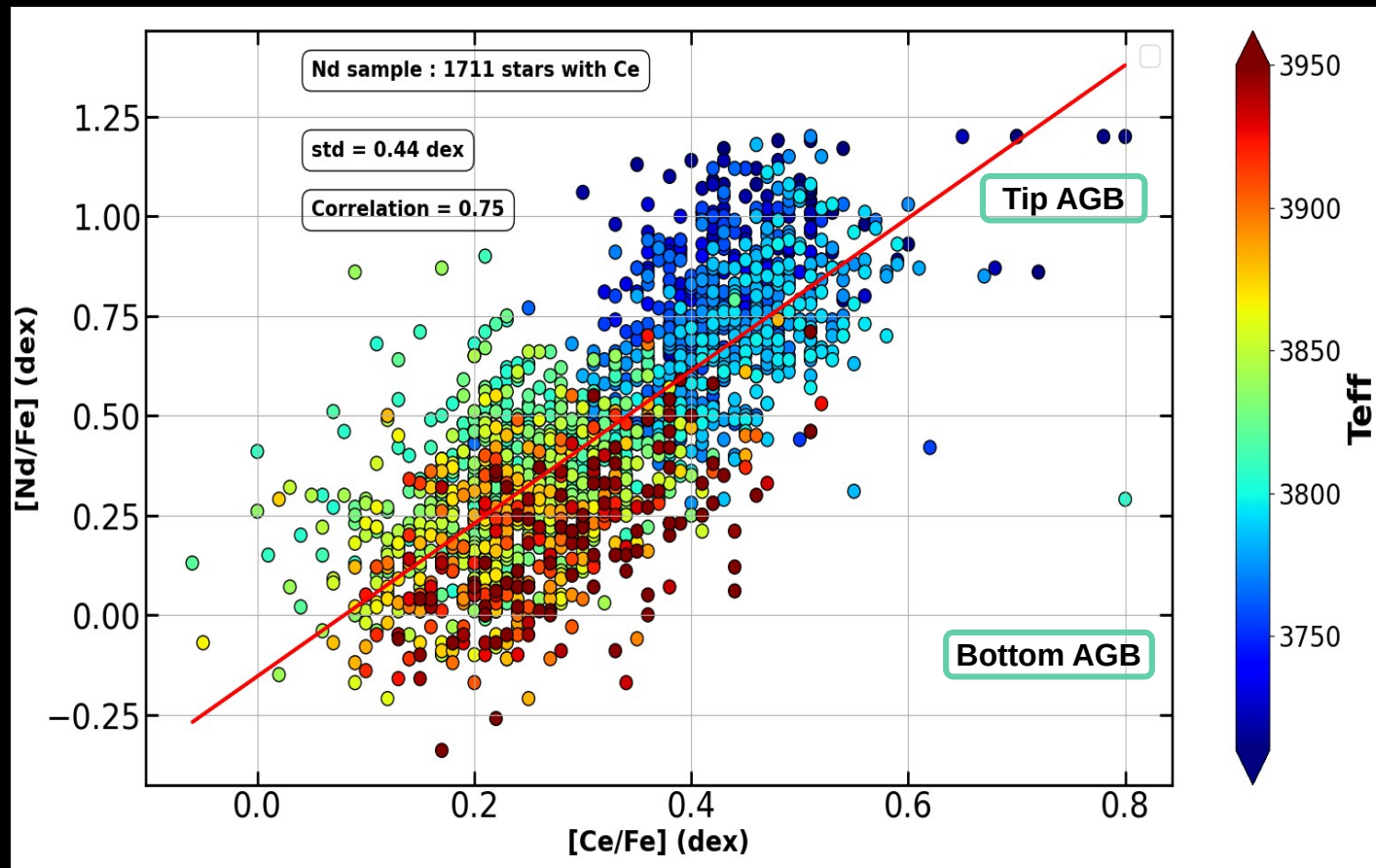


Interpulse
(Stellar luminosity from
H-burning shell)

He-burning shell inactive

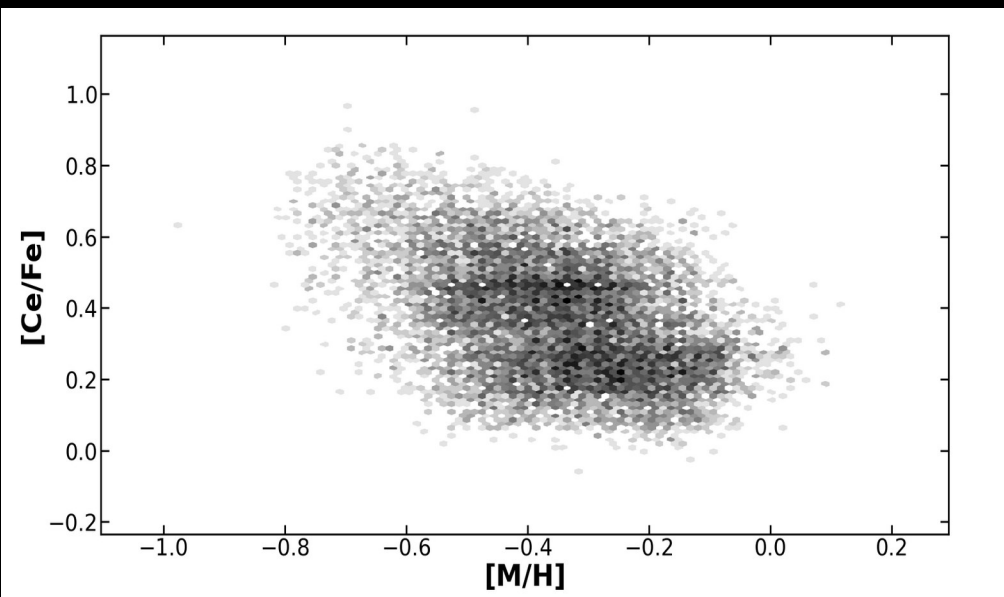
III. Corrélation entre Ce et Nd

Bonne corrélation (coefficient de corrélation de Pearson = 0,75) entre Ce et Nd (deux éléments du processus s du même pic)



Contursi et al. (2024a)

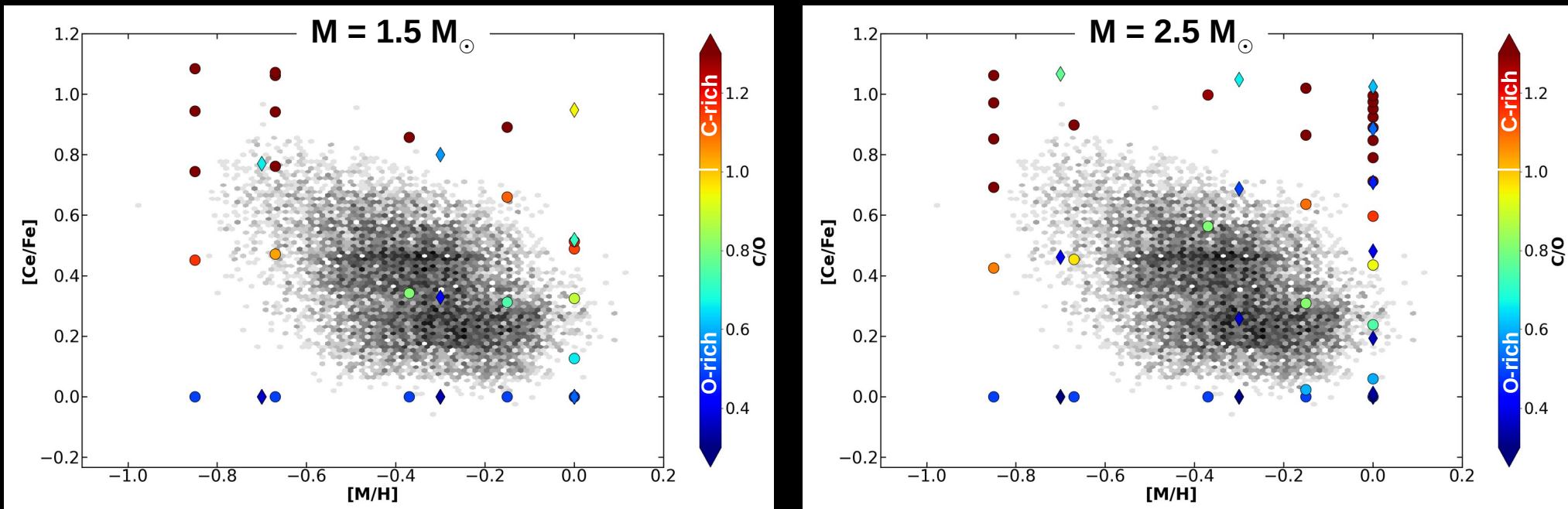
III. Comparaison avec les modèles d'AGB



→ Abondances GSP-Spec calculées en supposant une atmosphère riche en O : (C/O < 1)

→ Nd donne des résultats similaires à ceux de Ce

III. Comparaison avec les modèles d'AGB



Cercles : FRUITY models
Diamants : Monash models

Contursi et al. (2024a)

- Les étoiles AGB entre 1,5 et 2,5 M_{\odot} contribuent aux abondances de Ce les plus élevées.
- Modèles FRUITY plus proches des abondances de Ce

Sommaire

- I. Introduction : Éléments lourds et Gaia
- II. Contenu en cérium de la Voie Lactée
- III. Production d'éléments s dans les étoiles AGB
- IV. Abondances de Plomb dans la Voie Lactée**

IV. Abondances de Plomb dans la Voie Lactée

Astronomy & Astrophysics manuscript no. output
May 20, 2024

©ESO 2024

The AMBRE Project : Lead abundance in Galactic stars

G. Contursi¹*, P. de Laverny¹, A. Recio-Blanco¹, M. Molero², E. Spitoni³, and F. Matteucci^{3,4,5}

¹ Université Côte d'Azur, Observatoire de la Côte d'Azur, CNRS, Laboratoire Lagrange, Bd de l'Observatoire, CS 34229, 06304 Nice cedex 4, France

² Institut für Kemphysik, Technische Universität Darmstadt, Schlossgartenstr. 2, Darmstadt 64289, Germany

³ I.N.A.F. Osservatorio Astronomico di Trieste, via G.B. Tiepolo 11, 34131, Trieste, Italy

⁴ Dipartimento di Fisica, Sezione di Astronomia, Università di Trieste, Via G. B. Tiepolo 11, I-34143 Trieste, Italy

⁵ I.N.F.N. Sezione di Trieste, via Valerio 2, 34134 Trieste, Italy

Received ??; accepted ??

ABSTRACT

Context. The chemical evolution of neutron capture elements in the Milky Way is still a matter of debate. Although more and more studies investigate their chemical behaviour, there is still a lack of significant large sample of abundances of a key heavy element: lead.

Aims. Lead is the final product of the *s*-process nucleosynthesis channel and is one of the most stable heavy elements. The goal of this article is to present the largest catalogue of homogeneous Pb abundances, in particular for metallicities higher than -1.0 dex, and then to study the lead content of the Milky Way.

Methods. We analyse high-resolution spectra from the ESO UVES and FEROS archives. Atmospheric parameters are taken from the AMBRE parametrisation. We use the automated abundance method GAUGUIN to derive lead abundances in 653 slow-rotating FGK-type stars from the 368.346 nm Pb I line.

Results. We present the largest catalogue (~650 stars) of LTE and non-LTE lead abundances ever published with metallicities ranging from -2.9 to 0.6 dex and [Pb/Fe] from -0.7 to 3.3 dex. Within this sample, no lead-enhanced AGB stars are found but nine lead-enhanced metal-poor stars ($\text{[Pb/Fe]} > 1.5$) are detected. Most of them were already identified as carbon-enhanced metal-poor stars with enrichments in other *s*-process species. The lead abundance of 14 Gaia Benchmark stars are also provided. We then investigate the Pb content of the Milky Way disc by computing vertical and radial gradients and found a slightly decreasing [Pb/Fe] radial trend with metallicity. This trend together with other related ratios ([Pb/Eu] and [Pb/o]) are interpreted thanks to chemical evolution models. The two-infall model well reproduces the observed trends with respect to the metallicity. It is also found that the AGB contribution to the Pb Galactic enrichment has to be strongly reduced. Moreover, the contribution of massive stars with rather high rotational velocities could be favoured in the low-metallicity regime.

Key words. stars : abundances – surveys – stars: fundamental parameters

1. Introduction

Nucleosynthesis of elements heavier than iron cannot occur by stellar fusion and is mainly carried out via neutron captures. According to the seminal work of [Burbidge et al. \(1957\)](#), neutron captures occur through two processes: the slow (*s*-) process and the rapid (*r*-) process. The latter takes place at high neutron densities and short time scales (compared to β^- decay). Several neutrons are added before multiple α and β^- decays allowing the isotope to find stability.

The different sites of *r*-element production are still not clearly identified: among the different scenarios, one can find mergers of compact objects (neutron stars and/or neutron stars-black hole, e.g. [Freiburghaus et al. \(1996\)](#); [Surman et al. \(2008\)](#),

their actual production rates are still debated.

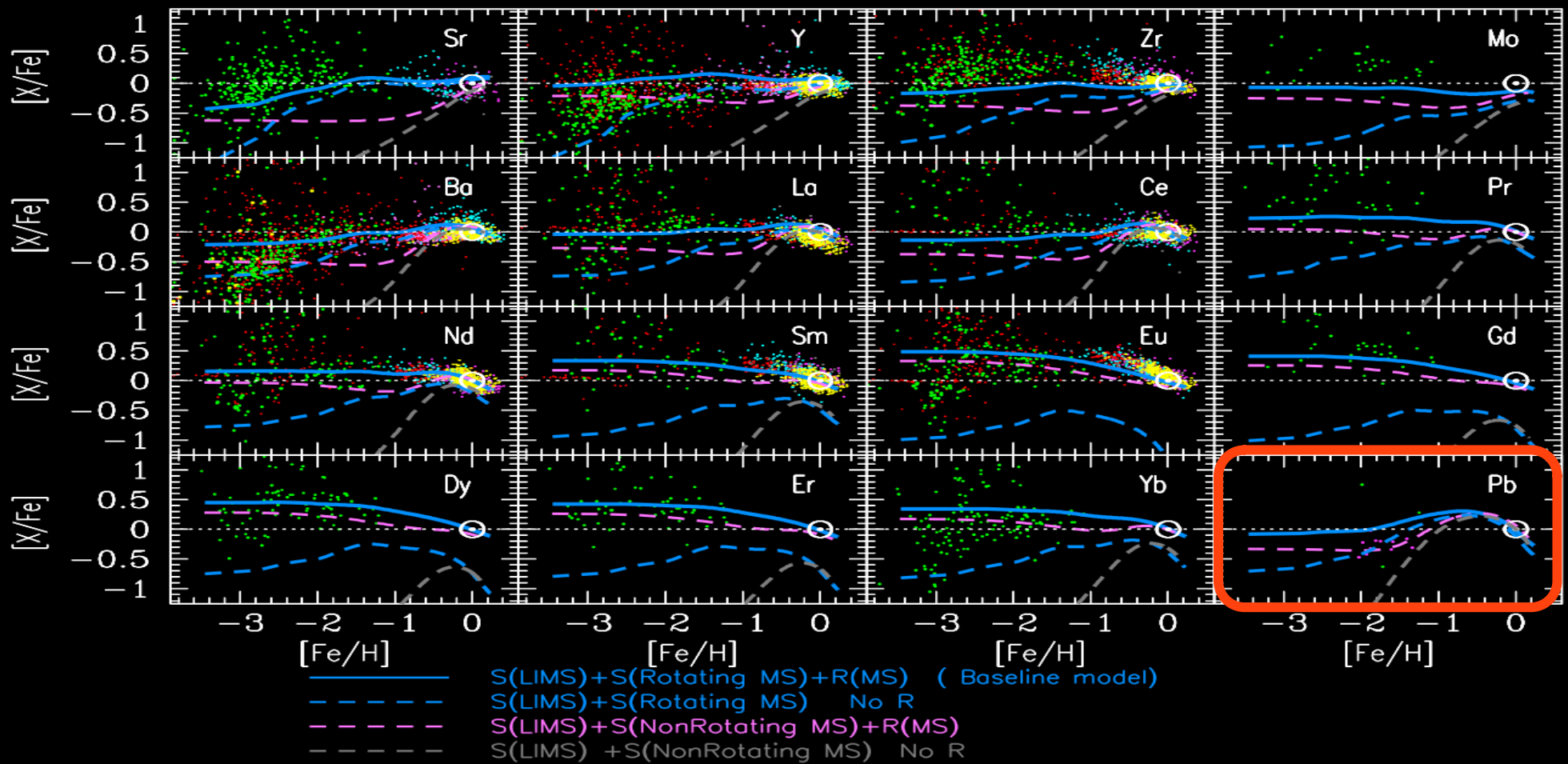
The abundances distribution of elements formed by the *s*-process as a function of atomic number shows three peaks: one around Sr-Y-Zr (weak component), one around Ba-La-Ce (main component) and one around Pb-Bi (strong component). The isotopes of lead and bismuth are the most stable ones formed by the *s*-process. For instance, one of the most stable Pb isotopes is ^{208}Pb ($Z = 82$, $N = 126$) because the neutron and proton shells are closed, reducing the cross-section to the next neutron capture.

In this context, each *s*-process peak is associated with a different source. The main sources are rotating massive stars and

Soumis à A&A

IV. Pourquoi le Pb ?

Manque important de données d'observation

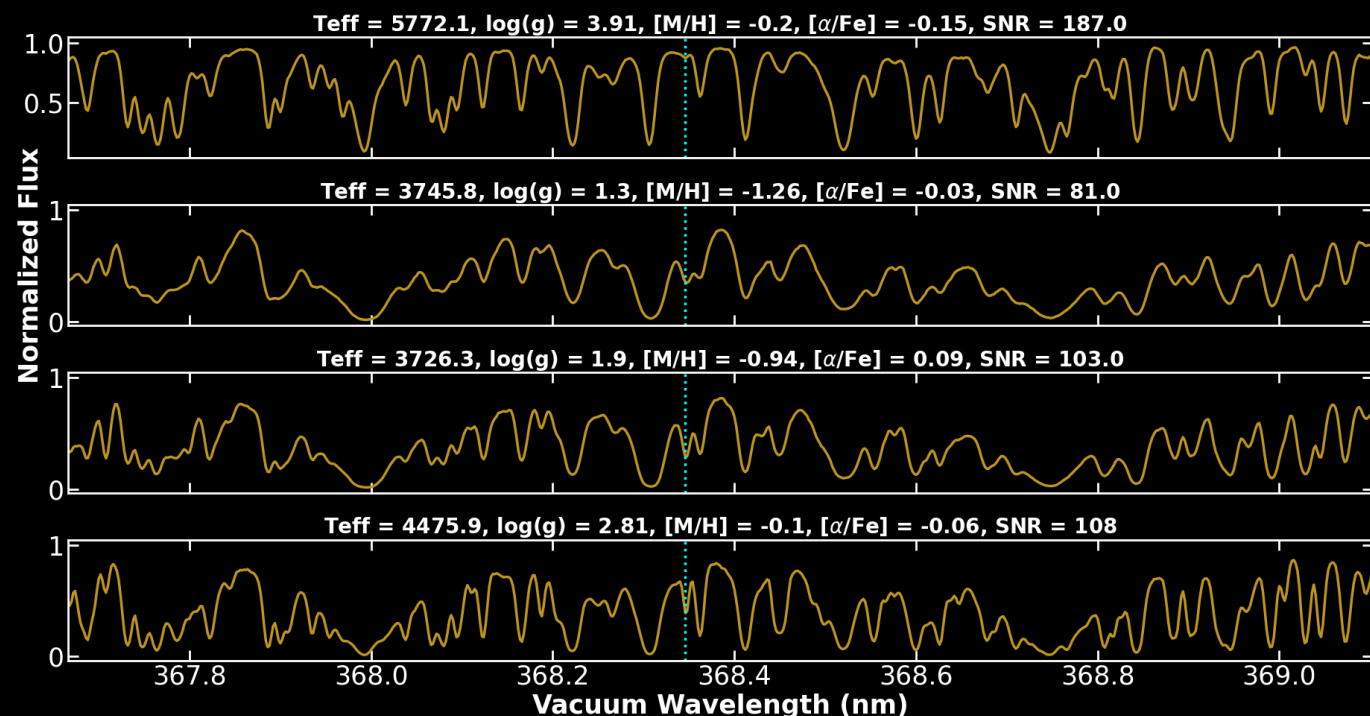




IV. Observations

Projet AMBRE:
Paramétrisation de 326 000
spectres archivés de l'ESO

8708 spectres des
spectrographes
UVES et FEROS

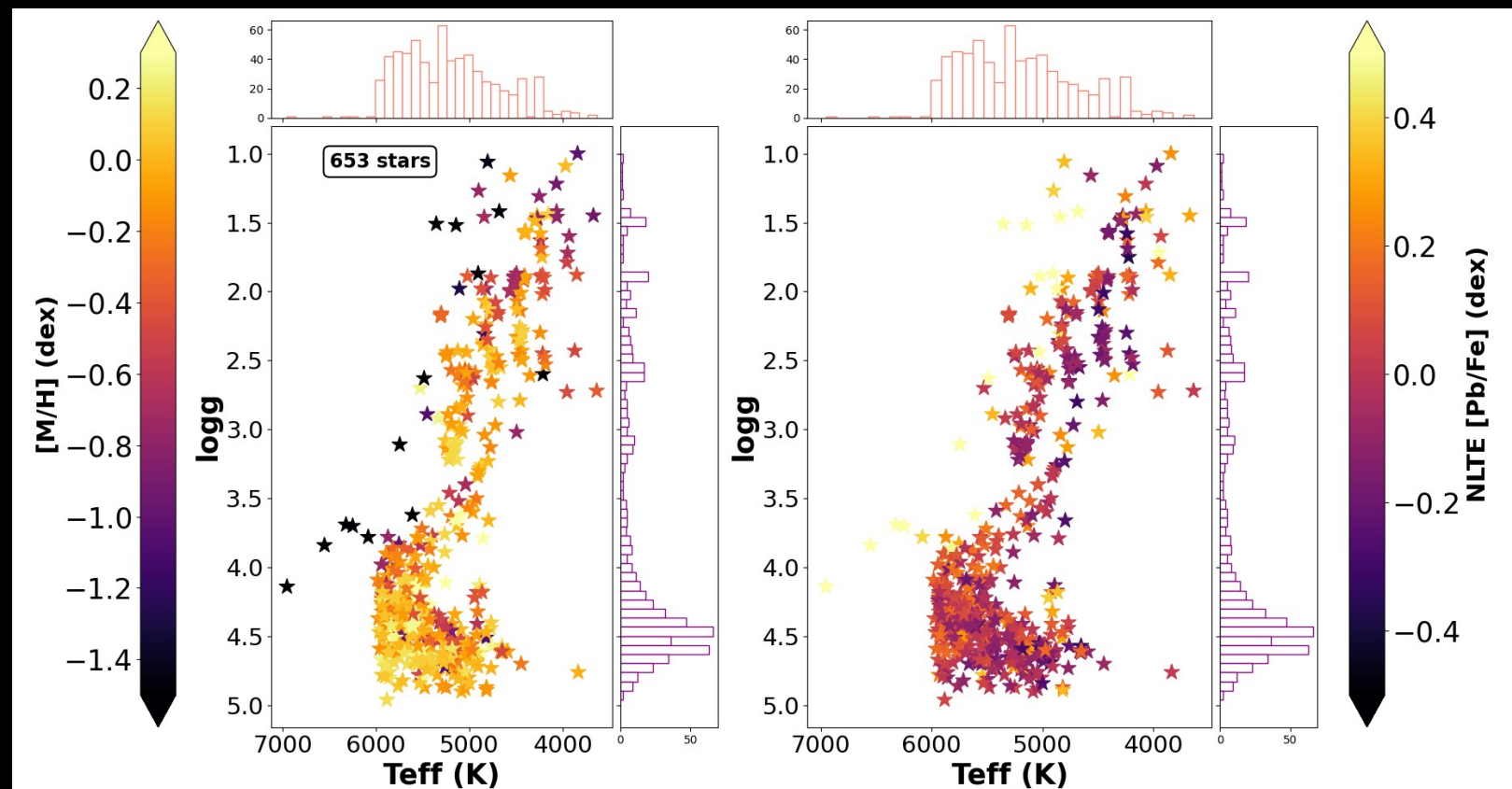


IV. Diagramme de Kiel

Parmi les 8708 spectres analysés, 1341 ont des abondances de Pb soit
698 étoiles = le plus grand échantillon de Pb jamais publié

- 13 Gaia Benchmark Stars avec abondances de Pb
- 32% de géantes ($\log(g) < 3.5$)
- 10 AGB ($T_{\text{eff}} < 4000\text{K}$ et $\log(g) < 2.0$) non enrichies en Pb

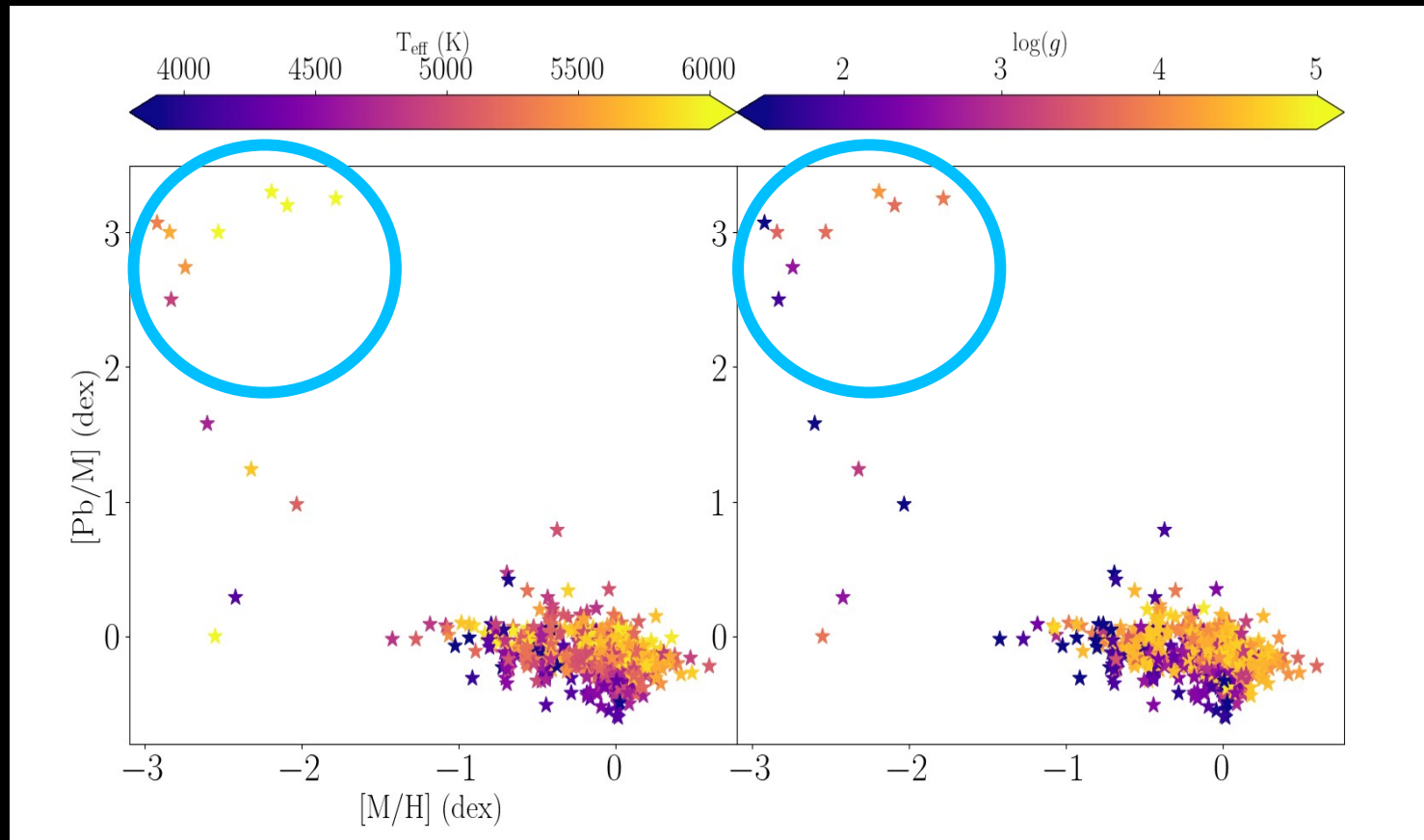
Contursi et al. (2024b)



IV. Etoiles enrichies en Pb

Parmi les 8708 spectres analysés, 1341 ont des abondances de Pb soit
698 étoiles = le plus grand échantillon de Pb jamais publié

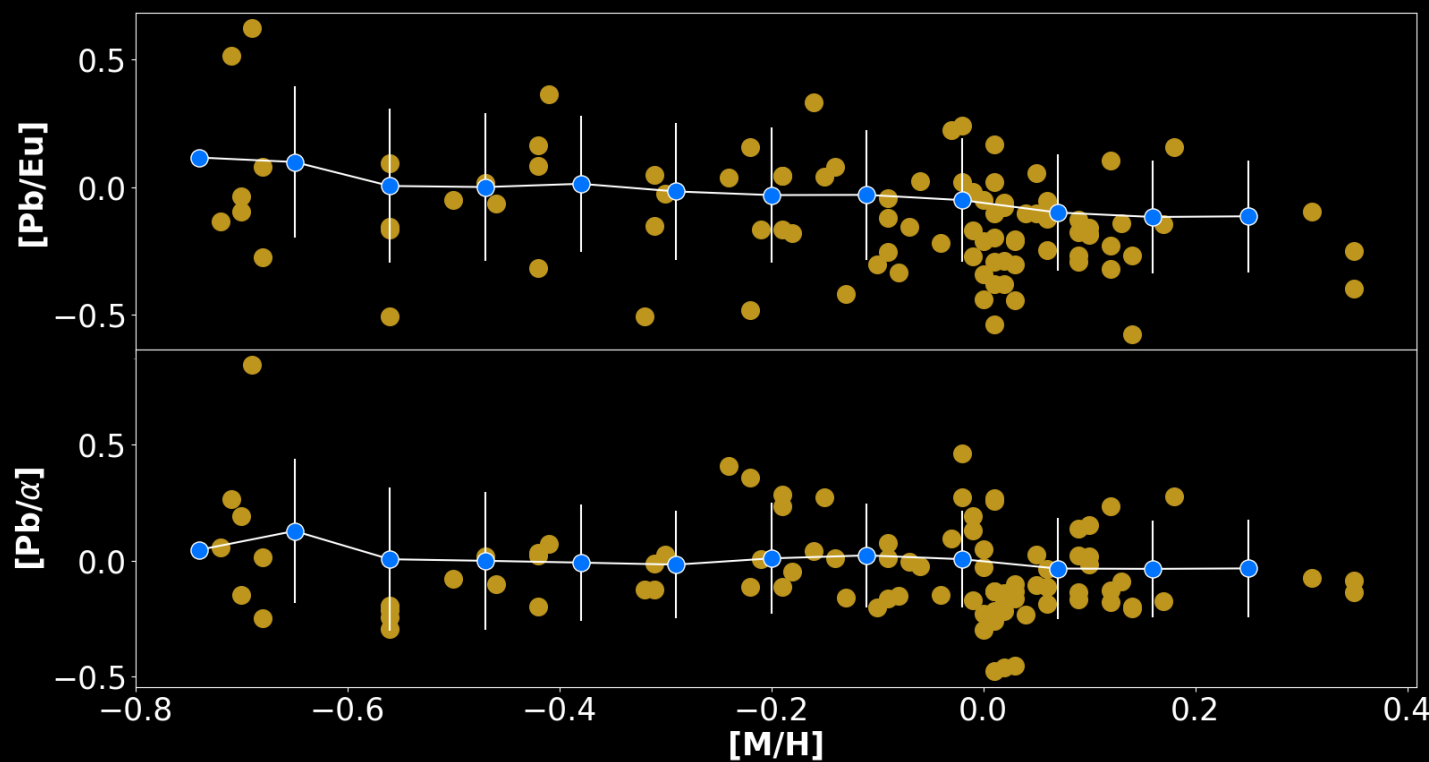
- $-0.7 < [\text{Pb}/\text{Fe}] \text{ (dex)} < +3.3$
- Certaines étoiles avec $[\text{Pb}/\text{Fe}] > 2.0 \text{ dex}$ et $[\text{M}/\text{H}] < -2.0 \text{ dex.}$
- Carbon Enhanced Metal-Poor (CEMP) stars **confirmées + nouveaux candidats**



IV. [Pb/Eu] vs [M/H]

Etude sur le disque Galactique (265 étoiles avec Pb, Eu et α)
→ $[\alpha/\text{Fe}]$ de Worley+12 et $[\text{Eu}/\text{Fe}]$ de Guiglion18 (Projet AMBRE)

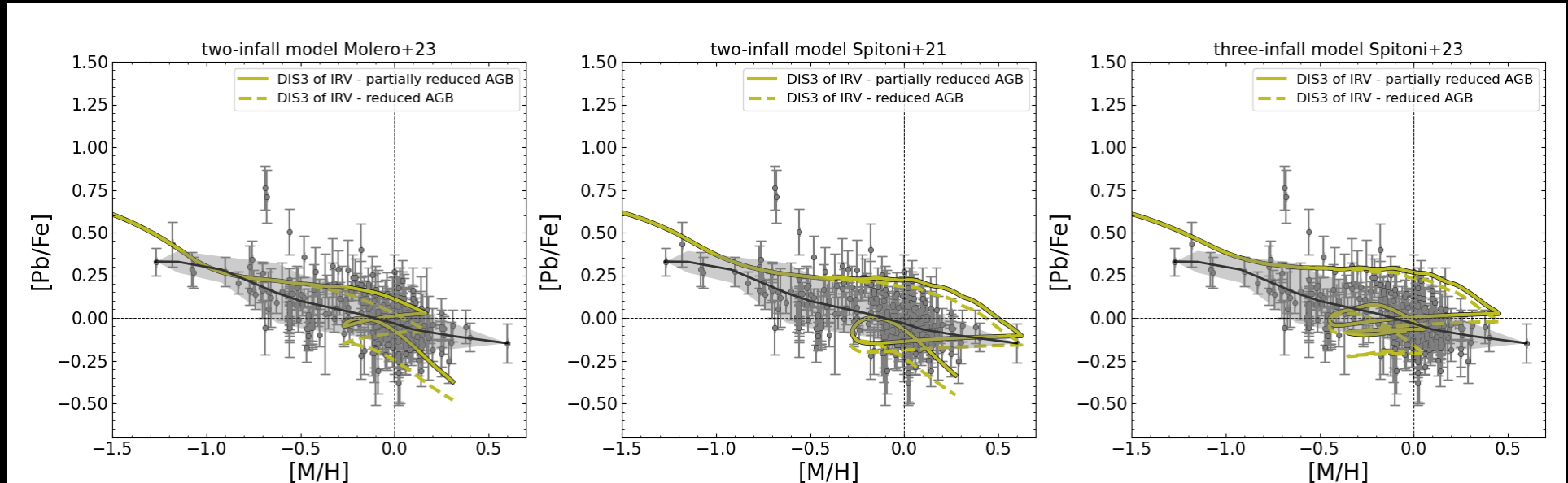
→ [Pb/Eu] et [Pb/ α] presque plat



IV. Comparaison avec les modèles chimiques

Meilleur accord:
2-infall model
[Spitoni et. al, 2021]

Réduction de la production de Pb par les AGB nécessaire



V. Conclusions

Les éléments s sont intéressants à étudier :

- Nucléosynthèse stellaire
- Evolution Chimique de la Galaxie

Principaux résultats

Nous investiguâmes les abondances de Ce et Nd pour 19 000 AGB :

Contursi+24a

- Abondances plus élevées pour les étoiles plus évoluées dans la phase AGB
- Corrélation entre Ce et Nd
- L'AGB dont la masse est comprise entre 1,5 et 2,5 Ms semble contribuer principalement aux abondances de Ce et de Nd
- Abondances de Ce de FRUITY plus proches de nos observations que des modèles de Monash

V. Conclusions

Les éléments s sont intéressants à étudier :

- Nucléosynthèse stellaire
- Evolution Chimique de la Galaxie

Principaux résultats

Nous investiguâmes le contenu en Ce dans la Voie Lactée pour ~ 7400 étoiles :

Contursi+23

- Tendance plate [Ce/Fe] vs [M/H] (pour $[M/H] > -0,75$ dex)
- Contribution plus tardive des étoiles AGB par rapport aux SN II révélée par [Ce/Ca] vs [Ca/H]
- Corrélation possible entre les abondances de Ce et la masse du système accréte

IV. GLOBAL Conclusions

Les éléments s sont intéressants à étudier :

- Nucléosynthèse stellaire
- Evolution Chimique de la Galaxie

Principaux résultats

Nous avons calculé et analysé les abondances de Pb avec le projet AMBRE:

Contursi, et al 2024b

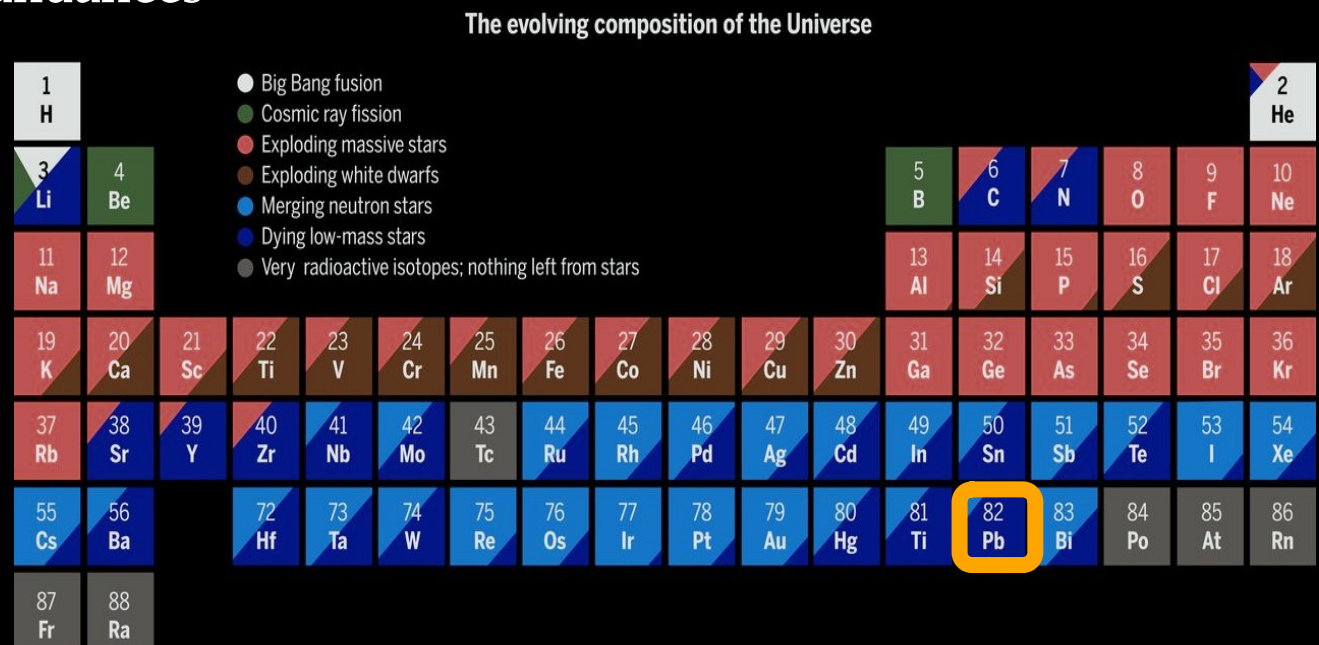
- 698 étoiles avec des abondances de Pb = LE PLUS GRAND CATALOGUE JAMAIS PUBLIÉ.
- Abondances de Pb dans 9 étoiles de référence Gaïa, AGB et CEMP
- Bonne comparaison avec les modèles d'évolution chimique (diminuer la contribution des AGB?)

VI. GLOBAL Conclusions

s- process elements are interesting elements to investigate:

- Stellar nucleosynthesis
- Galactic Chemical Evolution

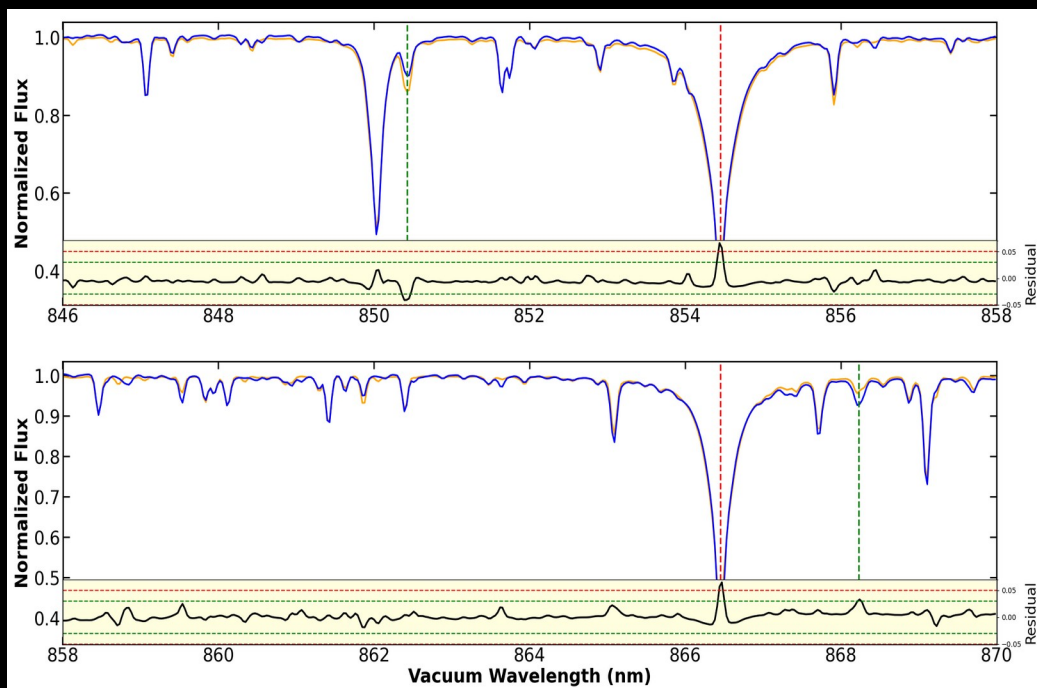
We used Ground-based data (**AMBRE** Project) and Space data (**Gaia/RVS**) to analyse **Ce**, **Nd** and **Pb** abundances



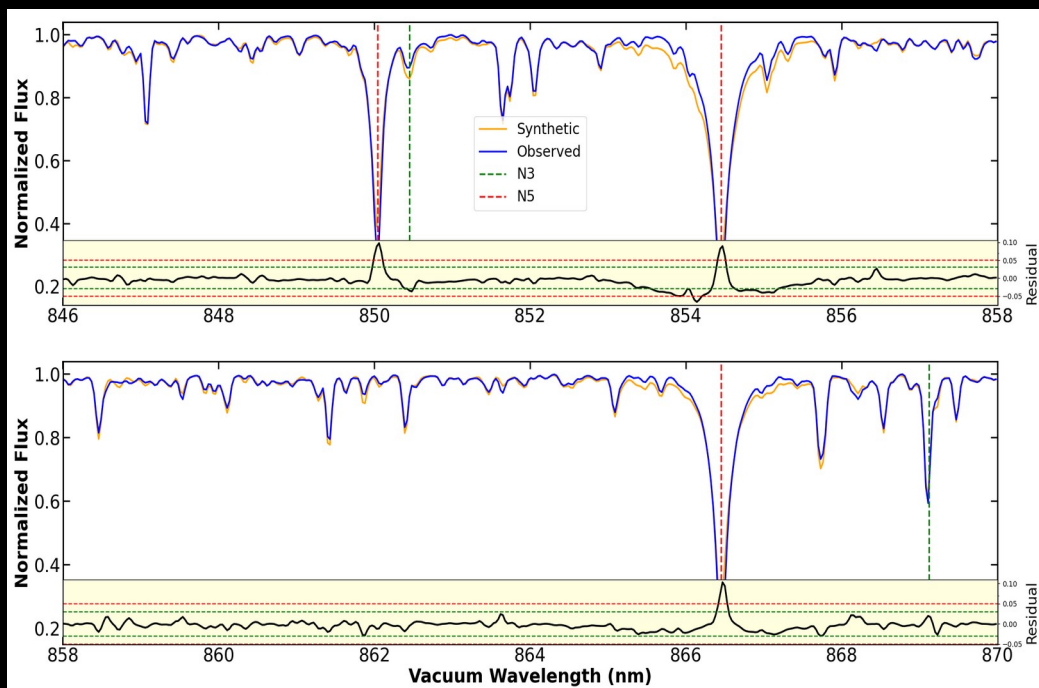
VI. GLOBAL Conclusions

Main results

→ We calibrated oscillator strength of 170 atomic lines to provide a line list for GSP-Spec analysis : Contursi+21



Sun

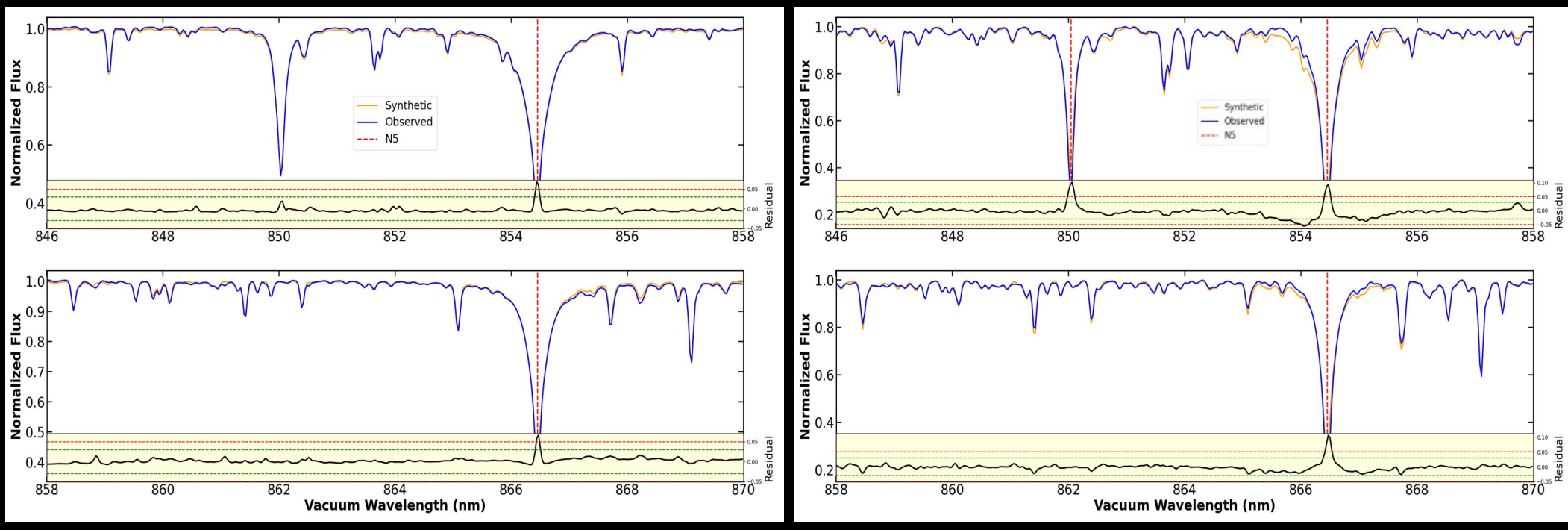


Arcturus

VI. GLOBAL Conclusions

Main results

→ We calibrated oscillator strength of 170 atomic lines to provide a line list for GSP-Spec analysis : Contursi+21



Sun

Arcturus

VI. GLOBAL Conclusions

s- process elements are interesting elements to investigate:

- Stellar nucleosynthesis
- Galactic Chemical Evolution

Main results

We investigate the Ce and Nd abundances in AGB stars for $\sim 19\,000$ stars :

Contursi+23b

- Higher abundances found for more evolved stars in the AGB
- Correlation found between Ce and Nd
- AGB with mass between 1.5 and 2.5 Ms seem to mainly contribute to Ce and Nd abundances
- FRUITY Ce abundances closer to our observations than Monash models

VI. GLOBAL Conclusions

s- process elements are interesting elements to investigate:

- Stellar nucleosynthesis
- **Galactic Chemical Evolution**

Main results

We investigate the Ce content of the Milky Way for ~ 7400 stars :

Contursi+23a

- Flat [Ce/Fe] vs [M/H] trend (for $[M/H] > -0.75$ dex)
- Later contribution of AGB stars compared to SN II revealed by [Ce/Ca] vs [Ca/H]
- Possible Correlation between Ce abundances and accreted system mass

VI. GLOBAL Conclusions

s- process elements are interesting elements to investigate:

- Stellar nucleosynthesis
- Galactic Chemical Evolution

Main results

We derived and analyzed Pb abundances with AMBRE project :

Contursi, in prep.

- 698 stars with Pb abundances = LARGEST CATALOGUE EVER PUBLISHED.
- Pb abundances in 9 Gaia Benchmark Stars
- Pb abundances in AGB and probably CEMP stars



VI. GLOBAL Conclusions

Important

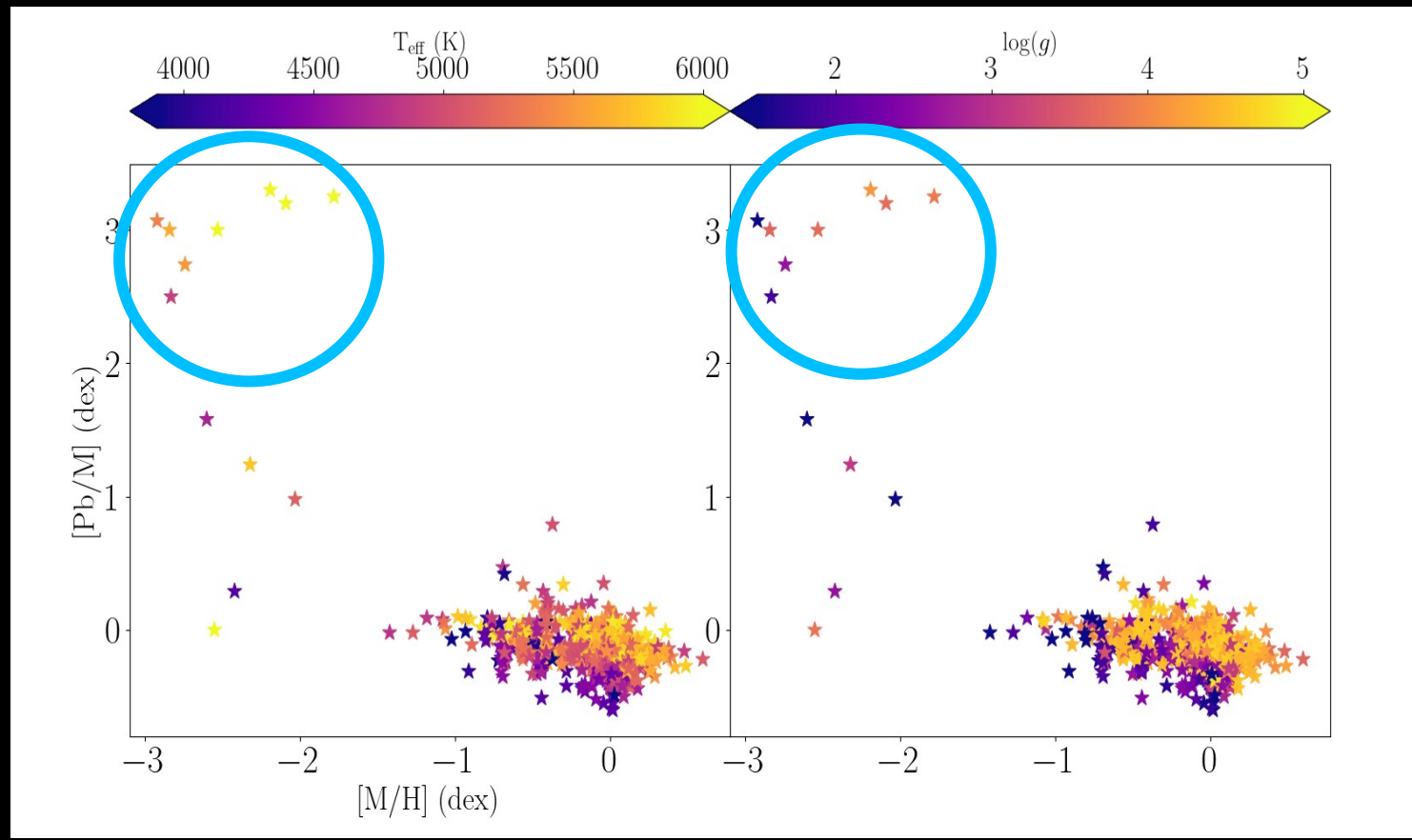
*Gaia/RVS is **SPACE spectroscopy** \neq **ground based spectroscopy***

- Continuous observations for years (34 months for DR3)
- Stable conditions (no atmosphere)
- Very good control and modeling of systematics
- Extremely homogeneous treatment
- High number statistics providing hundreds of thousand of high SNR (>150) data

**Parametrization quality comparable to ground-based surveys
with higher spectral resolution and wavelength coverage.**

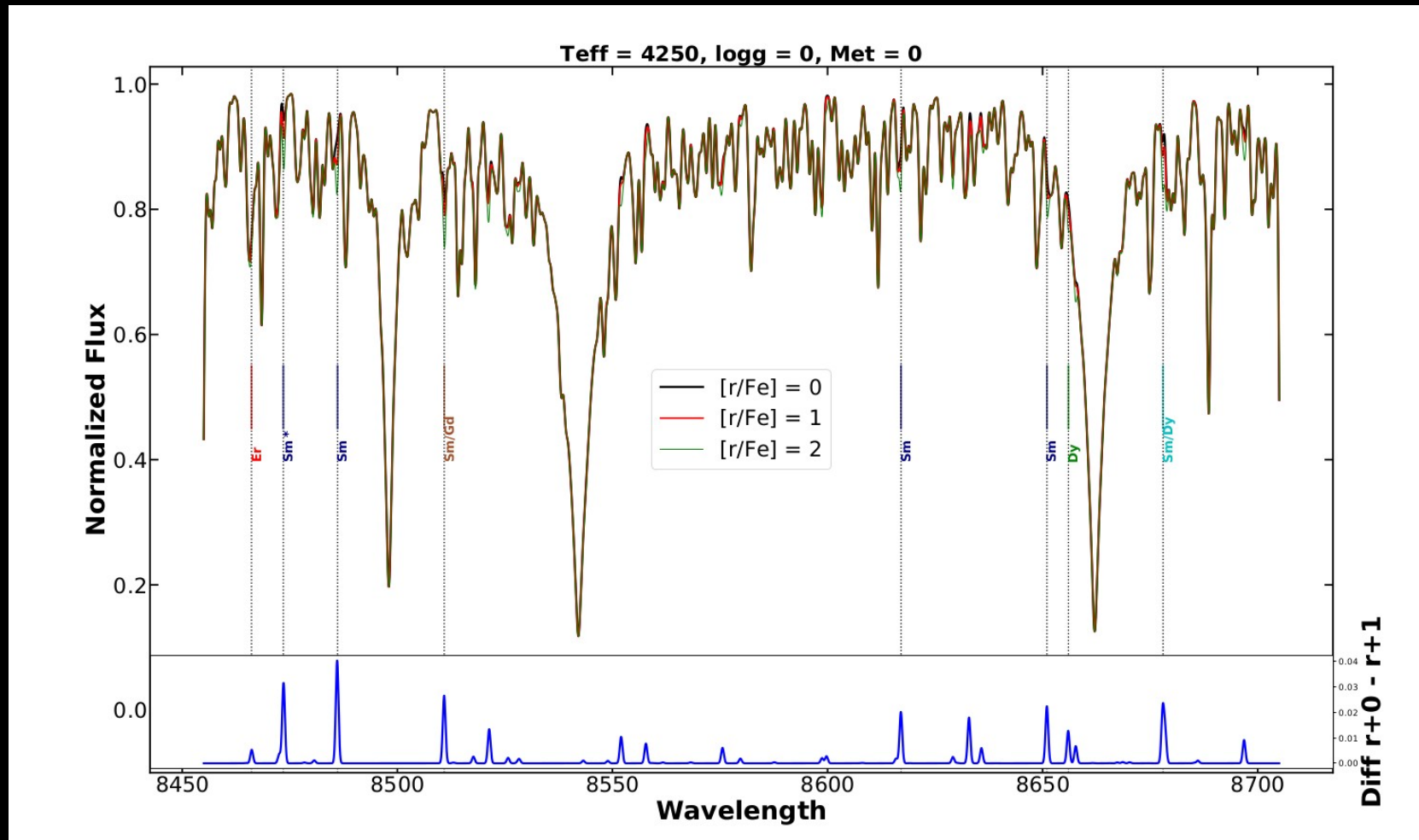
VI. Perspectives

- Study of [Pb/Fe] in Galactic disc, AGB production, CEMP ...
 - Contursi et al. In prep



VI. Perspectives

- Study of [Pb/Fe] in Galactic disc, AGB production, CEMP ...
- Include new elements in the Gaia DR4 analysis



VI. Perspectives

- Study of [Pb/Fe] in Galactic disc, AGB production, CEMP ...
- Include new elements in the Gaia DR4 analysis
- Derive heavy-element abundances with the new spectrograph CUBES @VLT (Cassegrain U-Band Efficient Spectrograph, 300 - 400 nm, $R = 20\,000$)
- Heavy elements in future surveys (WEAVE, 4MOST, ...) and Gaia DR4 (end of 2025) ...

I. Milky Way

- Disc diameter : 30 kpc. Total Mass : 10^{12} Msun [Wilkinson+99, Deason+12]
- Thick disc identified by stellar counts towards Galactic pole [Yoshii82, Gilmore83].

Thin disc:

- Small dispersion of velocities (< 20 km/s)
- Quasi-circular orbits and young stars

Thick disc:

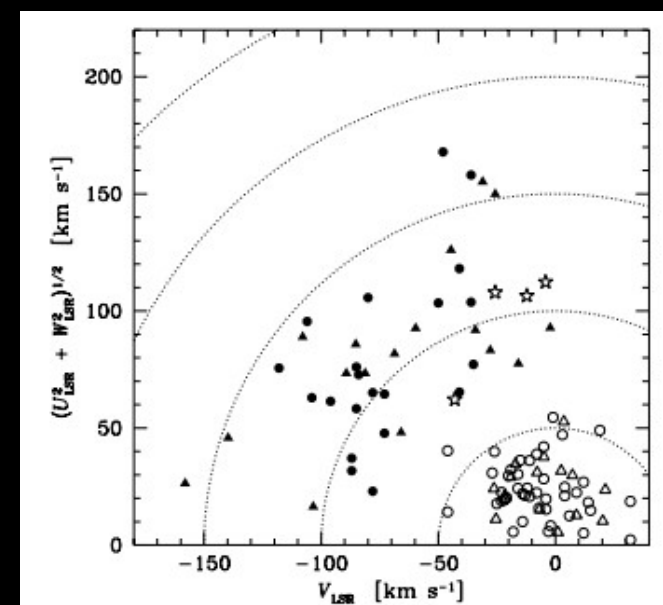
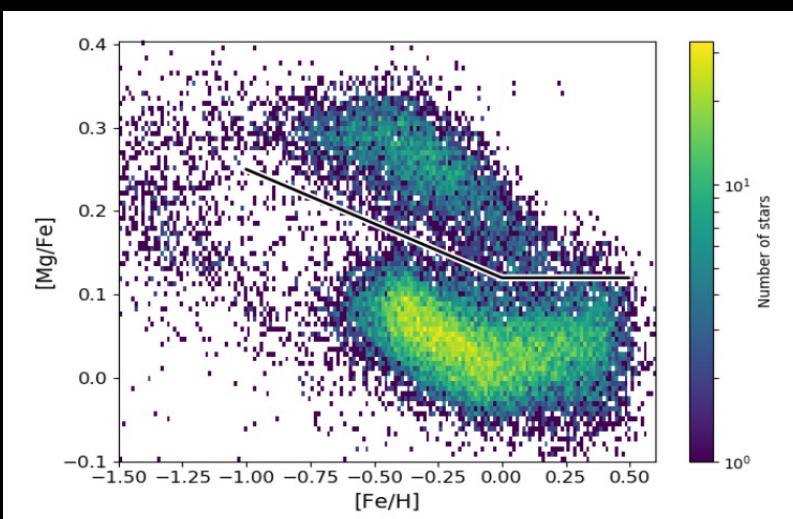
- Larger dispersion of velocities (~ 40 km/s)
- Different dynamics and chemistry ..

Bulge

- 25% of MW mass
- Rotation + dispersion + OC
- 2 stellar population (bar + accretion or thick disc)

Halo:

- 1% of MW mass. Old Stars
- Accreted stars + GC ...



I. Disc Formation

- [Haywood et al., 2013]: un changement de régime de formation stellaire serait à l'origine de cette discontinuité chimique.
 - [Snaith et al., 2015]: Formation stellaire, forte pendant les 4 premiers milliards d'années de formation du disque épais, se serait brusquement interrompue autour de 8 milliards d'années puis aurait progressivement repris pour former le disque mince.
 - [Nidever et al., 2014]: D'une part, les étoiles de la séquence du disque épais (riche en éléments α) partageraient une histoire de formation similaire, formées dans un milieu interstellaire turbulent et homogène, dominé par des molécules. D'autre part, les étoiles du disque mince (plus pauvres en $[\alpha/\text{Fe}]$) auraient été formées soit par accrétion de gaz couplée avec une chute du taux de formation stellaire, soit par une superposition de multiples populations caractérisées par différents taux de formation stellaire et différentes histoires d'enrichissement.
-
- La migration radiale d'étoiles du bulbe pour former le disque épais [Sellwood+02, Schönrich+09]. Cette migration radiale peut se décomposer en "blurring" (qui diffuse les orbites stellaires en conservant le moment angulaire mais en modifiant l'excentricité) et le "churning" (dû aux résonances de corotation avec la structure spirale de la Galaxie, et a pour effet de modifier le moment angulaire.)
 - Le chauffage d'un disque initial uniforme (gaz + étoiles + matière noire) perturbé par des inhomogénéités gravitationnelles [Bournaud et al., 2009].
 - Le chauffage d'un disque initial par une accrétion mineure provenant de Galaxies naines [Abadi et al., 2003]. Dans ce scénario, le disque épais se serait formé très rapidement (en moins de 500 millions d'années) et les dispersions des vitesses typiques pour des étoiles vieilles du disque épais seraient supérieures à 80 km/s. Les étoiles accrétables auraient une histoire chimique différente de celles formées in-situ.
 - Accrétion d'un satellite riche en gaz [Brook et al., 2004, 2007]. Le disque épais aurait été formé in situ suite à l'accrétion d'une Galaxie riche en gaz. Caractérisées par un disque de gaz incorporé dans un halo de matière noire, les deux Galaxies auraient fusionné suivant une rotation prograde. Le pic de formation stellaire à partir du gaz aurait été atteint il y a environ 9 milliards d'années. Ce scénario forme donc le disque épais à partir du gaz accréter et non des étoiles déposées sur des orbites coplanaires, tel que proposé par [Abadi et al., 2003]

I. X- process

Sources of Li, B and Be :

- Primordial nucleosynthesis [*Coc+04*]
- Cosmic rays fission (Spallation) [*Reeves+70*]
- HBB in AGBs also appears to be responsible for the production of ^7Be (becoming ^7Li by electron capture) [*Scalo+75, Sackmann+92*].
- ν -process [*Woosley+90*].

Difference between Li from stars and asteroids :

Li destroyed in star interiors [*Iben67*]

I. SN Ia + e- process

SNIa : Si lines but not H lines. SN Ib : He lines but no Si and H lines

SN Ic : No H, He and Si lines

Mass Transfer \Rightarrow Temperature increases (combustion of H and He) on the WD surface.
The white dwarf then tends towards the Chandrasekhar critical mass.
Center WD density increases \Rightarrow C burning (under degenerate conditions). Pressure cst.
Pressure increases \Rightarrow Thermonuclear explosion.

e- process : Iron peak linked to the high binding energy per nucleon and to a statistical equilibrium between photodisintegration and thermonuclear reactions (if the number of atomic nuclei and free protons and electrons are in equilibrium), which seems to be especially during Si burning [Hoyle46, Arcones+23]:



I. SN II + α - process

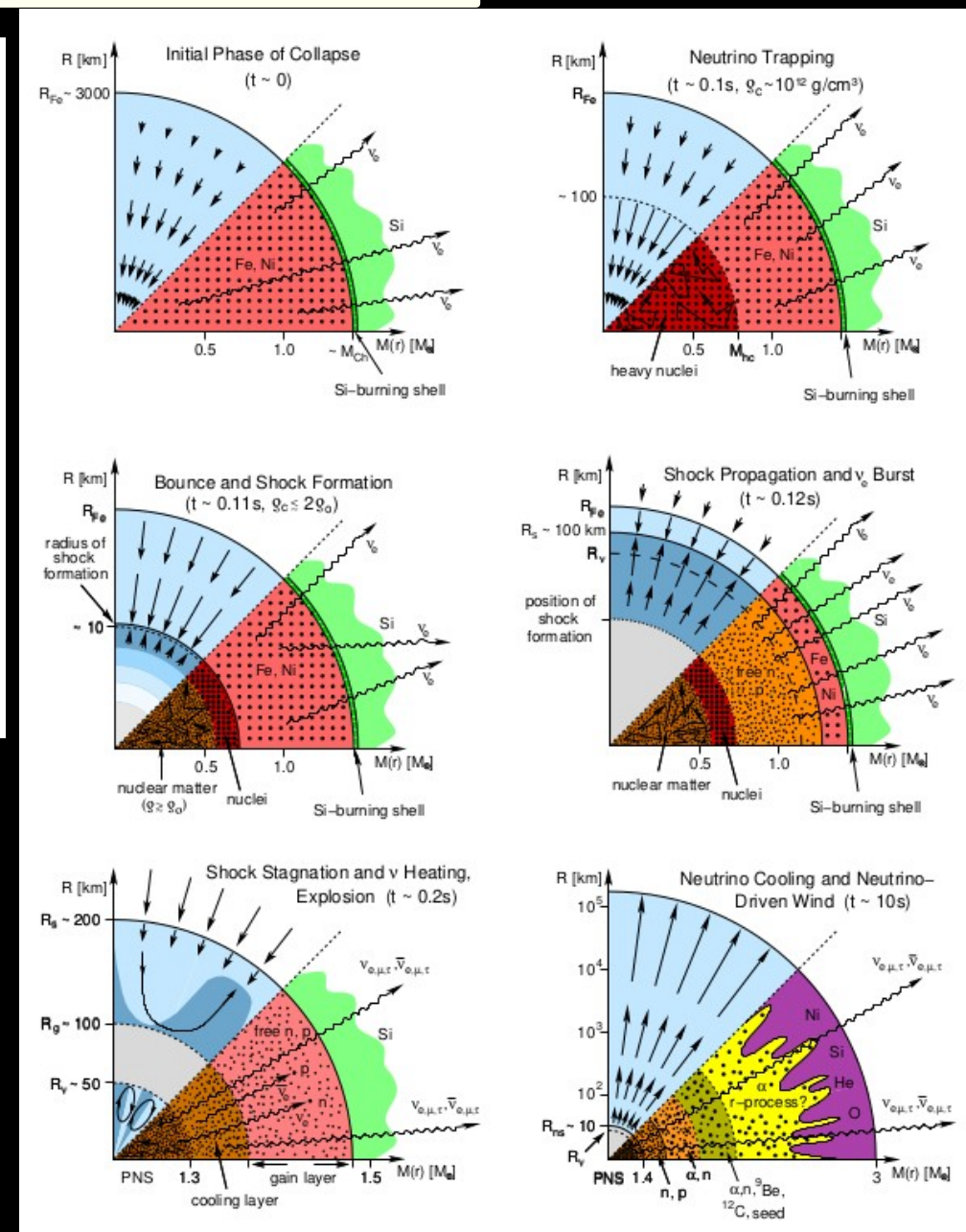
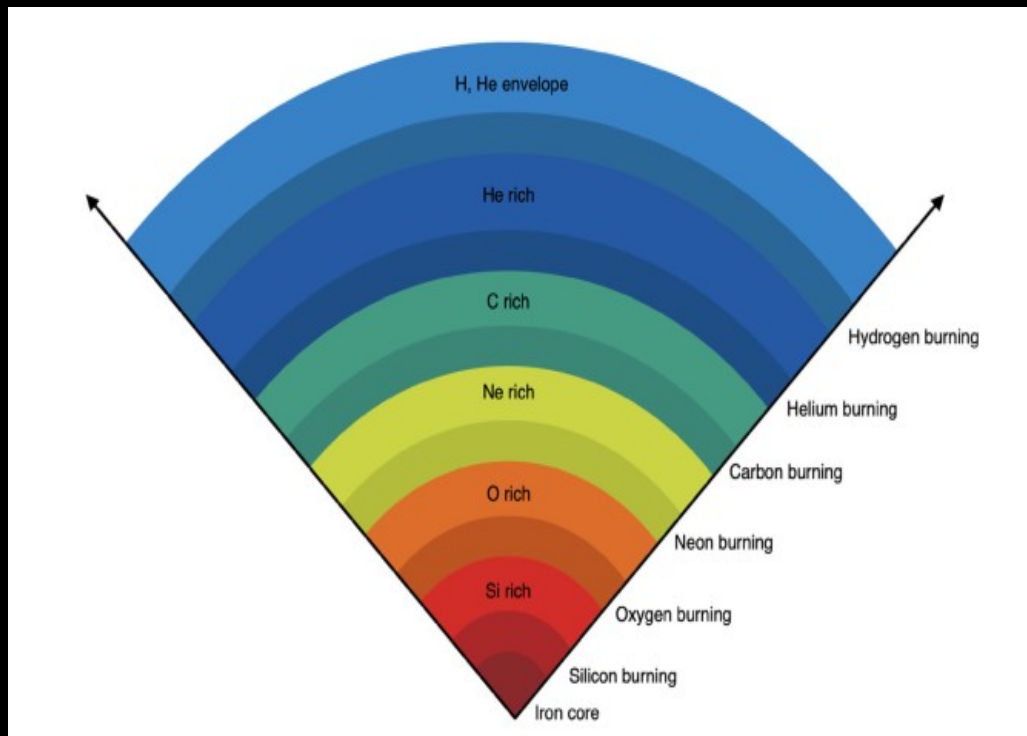
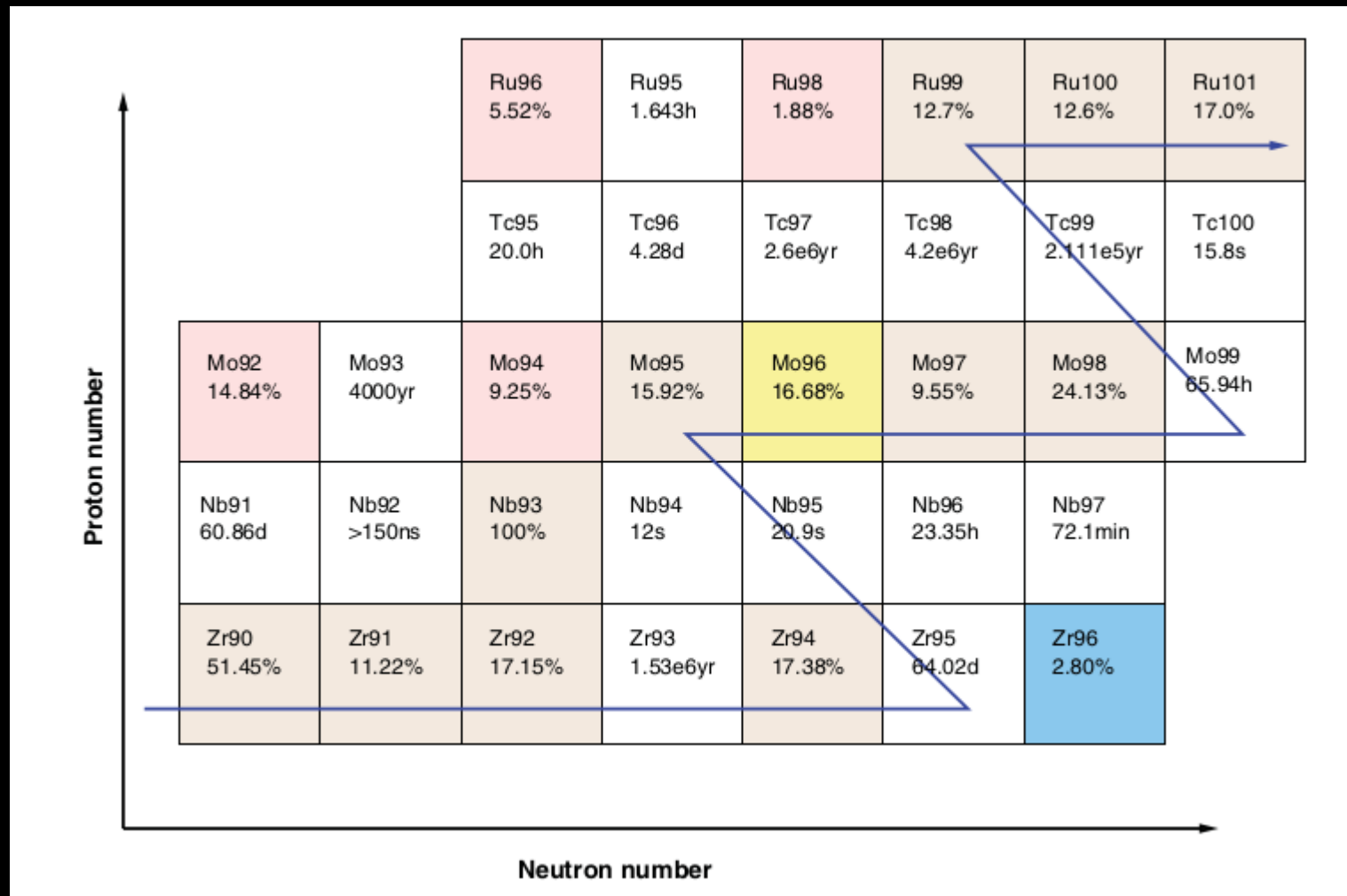


Photo-dissociation:



I. S- process

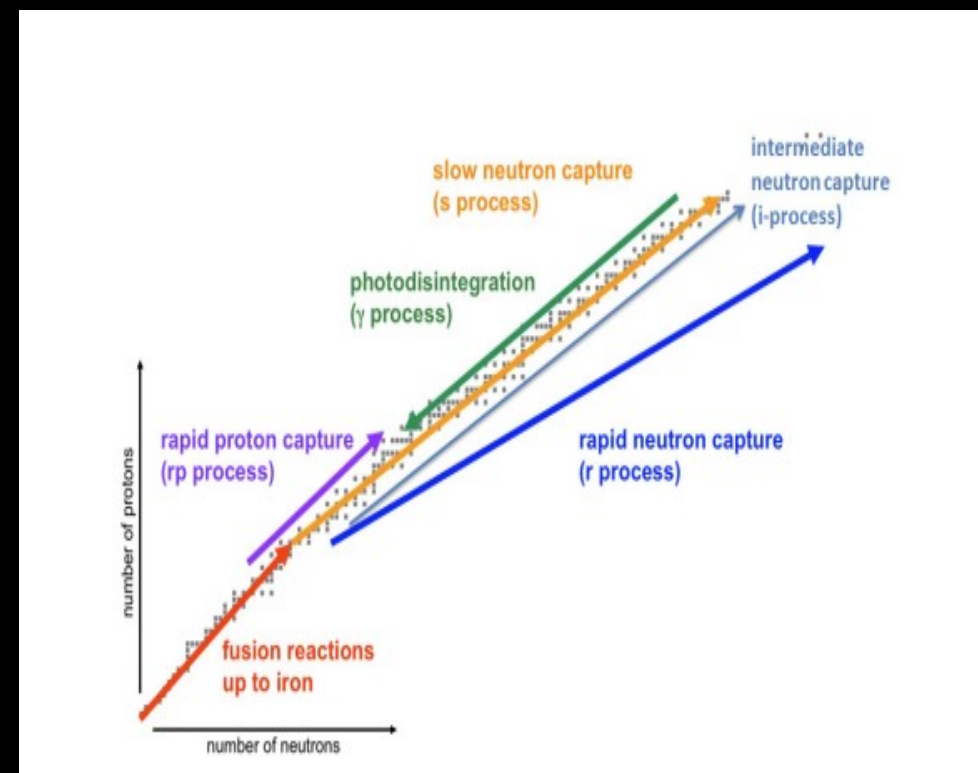
n-density : 10^{12} neutrons/cm³.



I. r- process

n-density : 10^{20} neutrons/cm³.

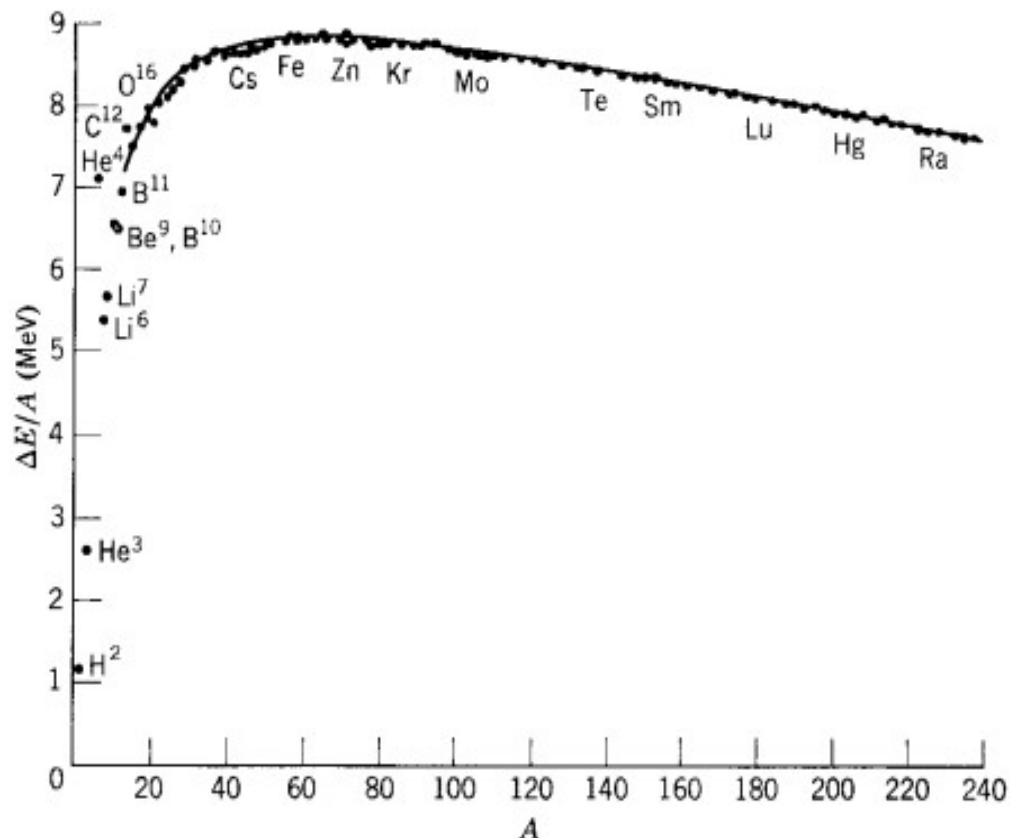
Several sources ? (large scattering
at low-metallicity)



I. Nucleosynthesis and Heavy Atoms

Atoms lighter than Fe
formed by nuclear fusion

Atoms higher than Fe mainly
by neutron capture through 2
main processes :
slow (s-) and rapid (r-)
[Burbidge & al. 57, Cameron 57]



I. p- and ν -process

$\sim 20\%$ p: Mo

$\sim 7\%$: Ru

→ SN II (H-rich layers [*Burbidge+57*])

→ Massive stars (O/Ne layers), SNII, SN Ia [*Arnould76, Choprin22b*]

→ decomposed in pn, vp and pn (neutrino winds)

I. i- process

- Impact for Xe, Yb, Ta and Pb
- Low-mass and low-met AGB [e.g. *Choplin22*] during PIE (overcome of the entropy barrier between H- and He-layers).
- He-flash in low-mass and low-met ?

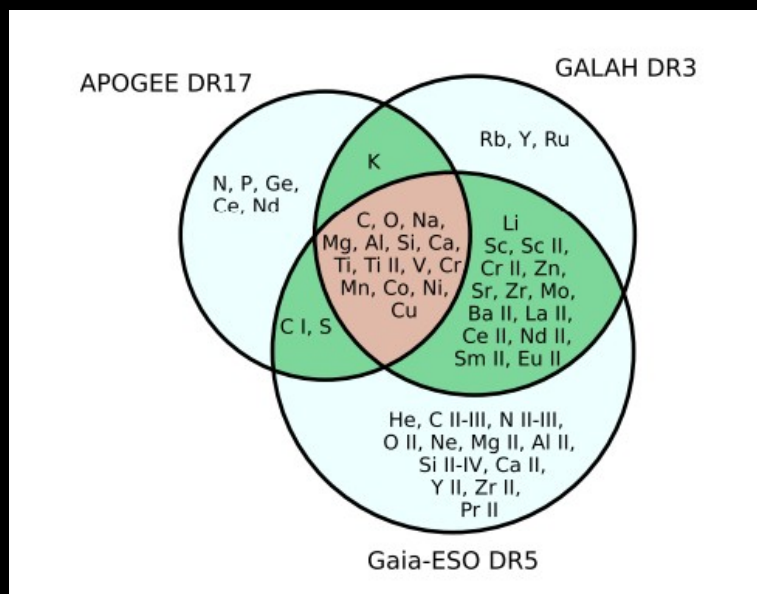
I. Spectro surveys results

1st study of Galactic Archaeology : Edvardsson93 (200 stars)

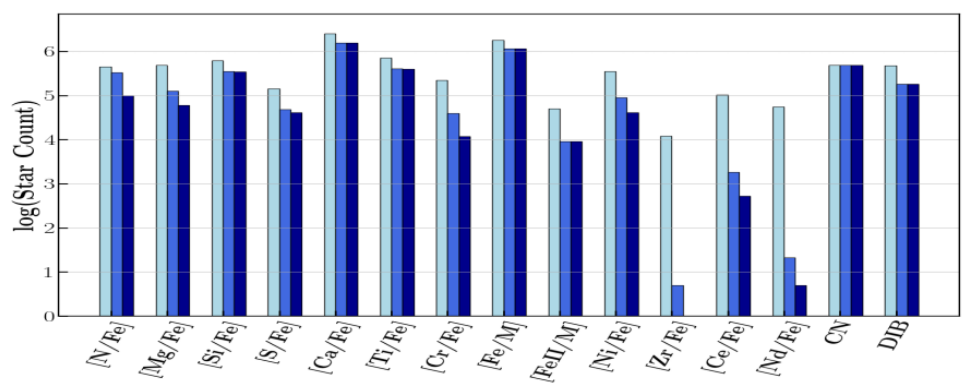
APOGEE : [García Pérez+13] : metal-poor stars in bulge ($[Fe/H] < 1.7$ dex).

[Martig+15]: young stars (< 6 millions d'années) αrich ($[\alpha/Fe] > 0.2$ dex), different to disc trend. Zasowski+19: constant knee in Mg abund with distance to galactic center: strong radial migration. Hayes+22: BAWLAS catalog (Ce, Nd ...)

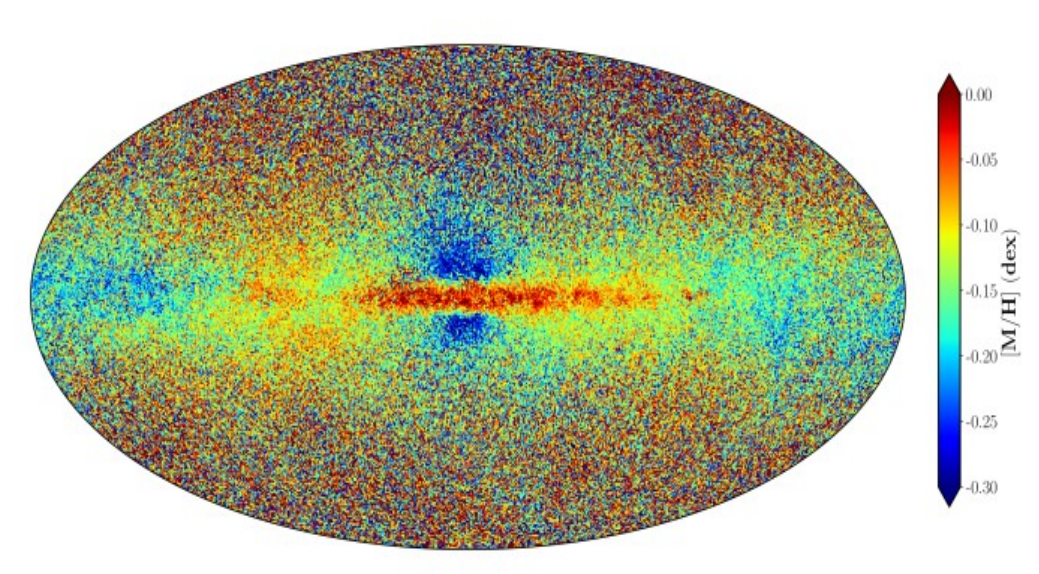
GALAH : 170 papers. Abundance tendance between thin and thick disc wrt met. and age [Buder+18]. Higher [Eu/Mg] abundance in accreted systems than in-situ [Matsuno+21]



I. Gaia DR3 main results



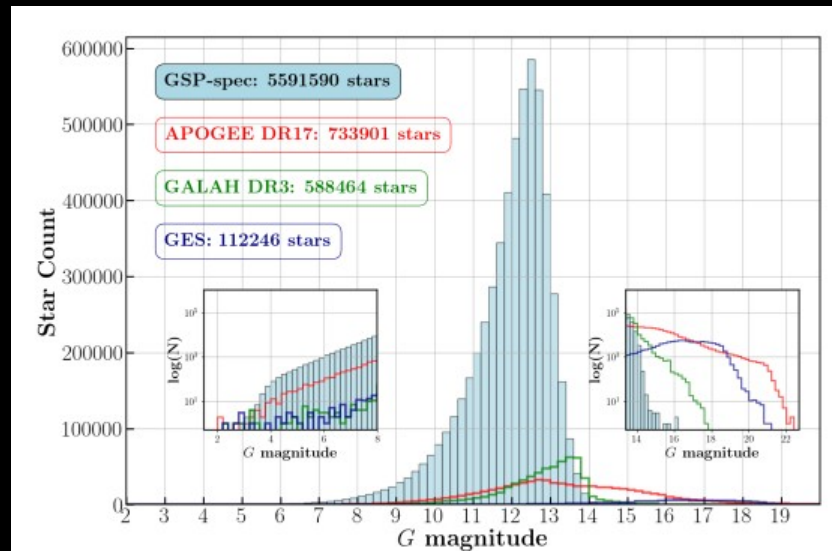
Main Gaia DR3 results :



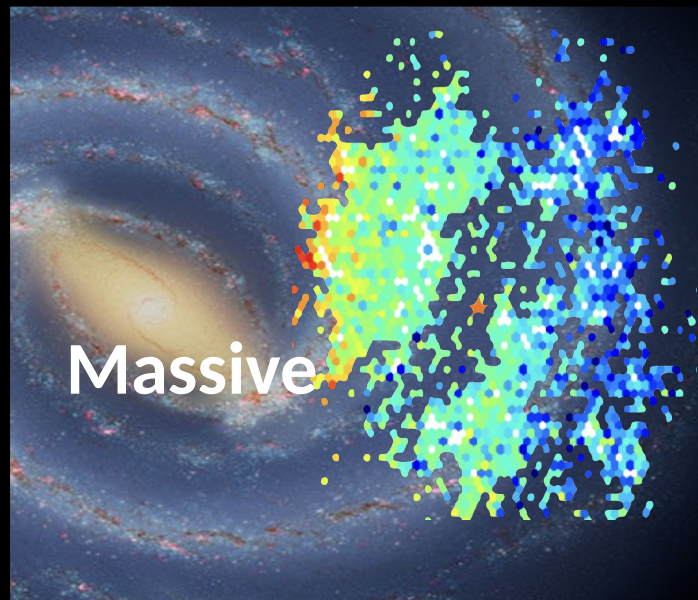
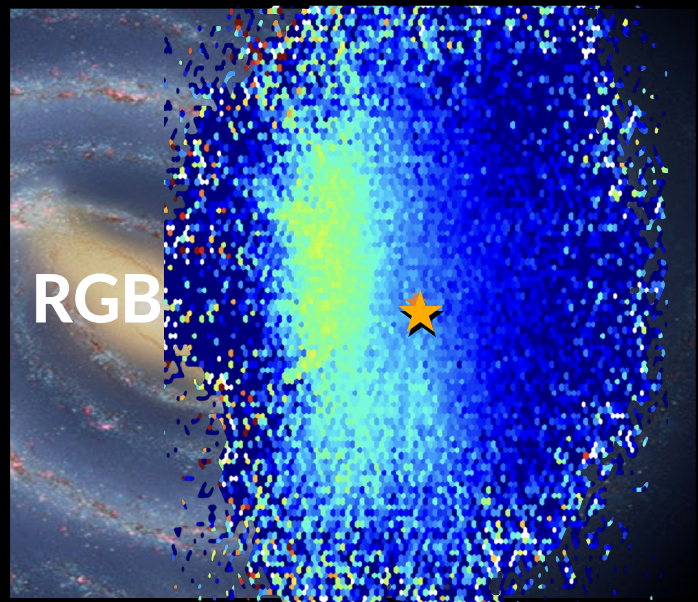
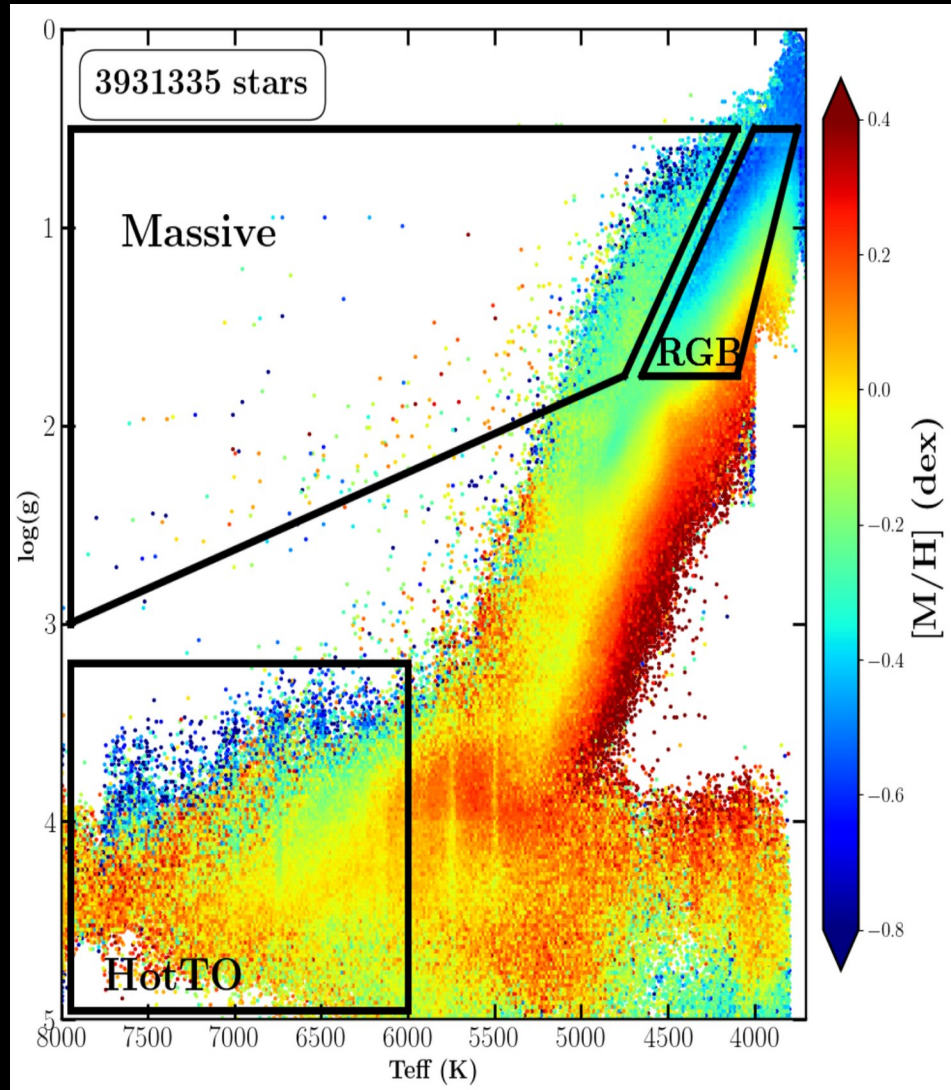
→ Young stellar population which trace stellar arms
[Recio-Blanco+23, Poggio+23]

→ Stars with chemical and dynamic data typical of the disc (rapid rotation and metallicities greater than -0.75 dex) detected at great distances from the plane, but this distance depends on the radius of the stars, revealing flaring of the disc.

→ Accreted systems stars

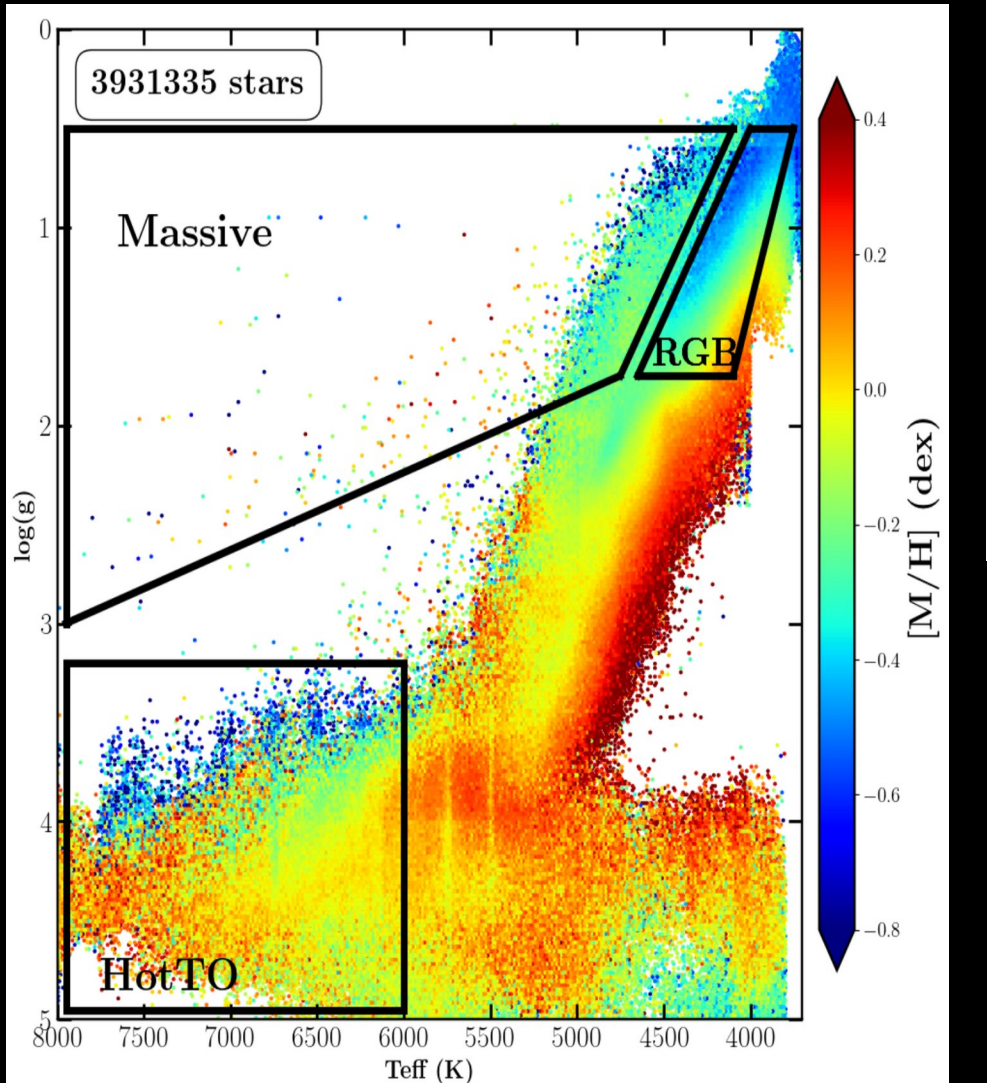


I. Massive stars population

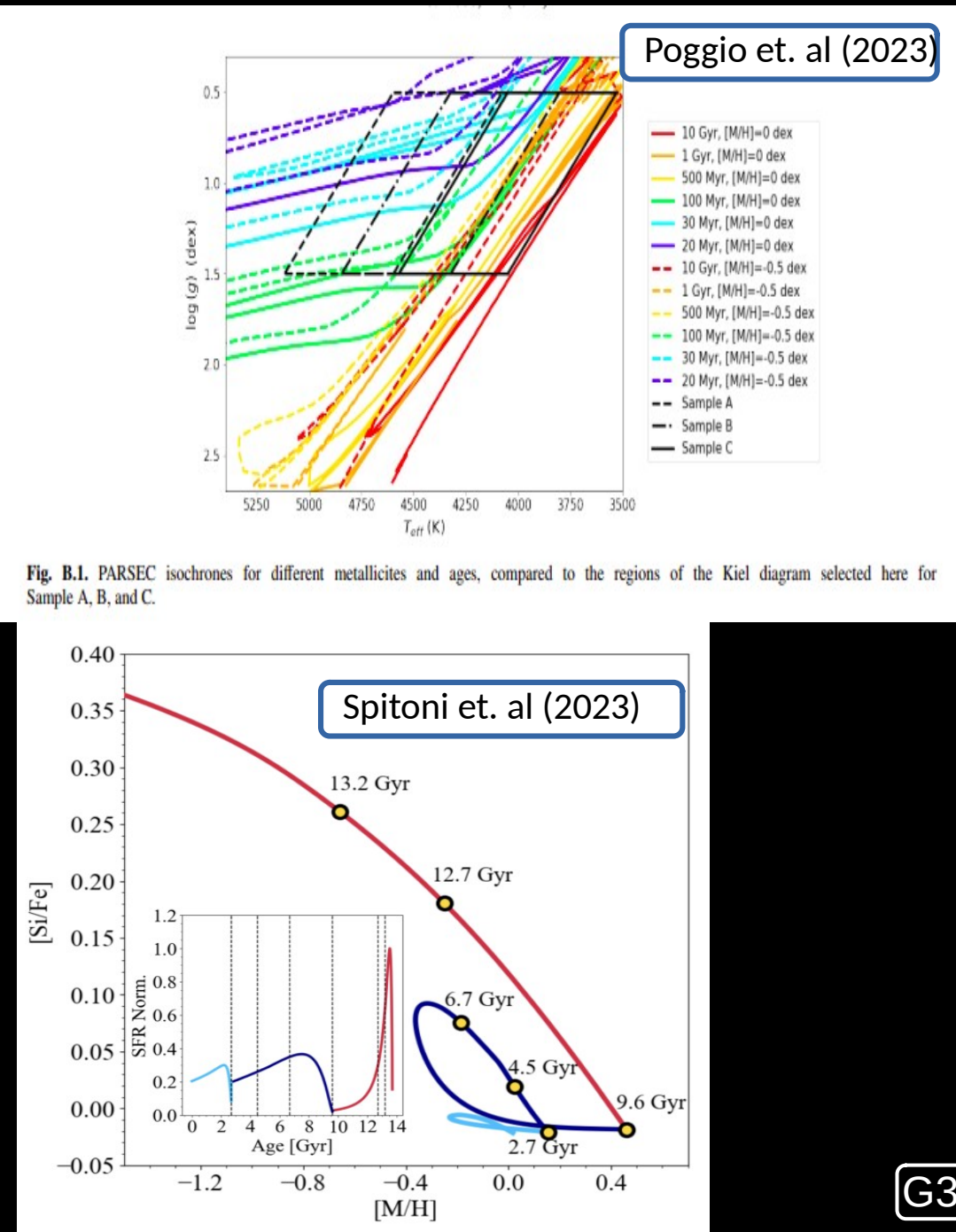


Gaia Collaboration, ARB et al. (2022)

I. Massive stars population

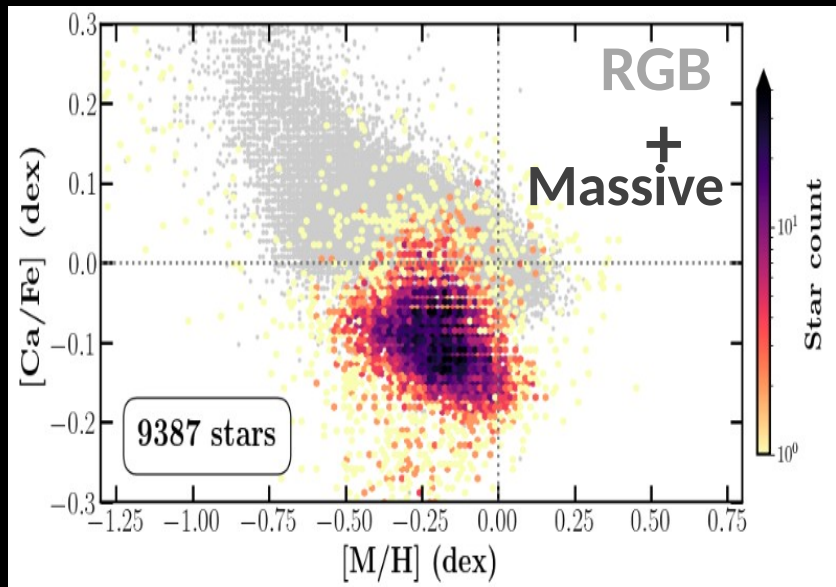
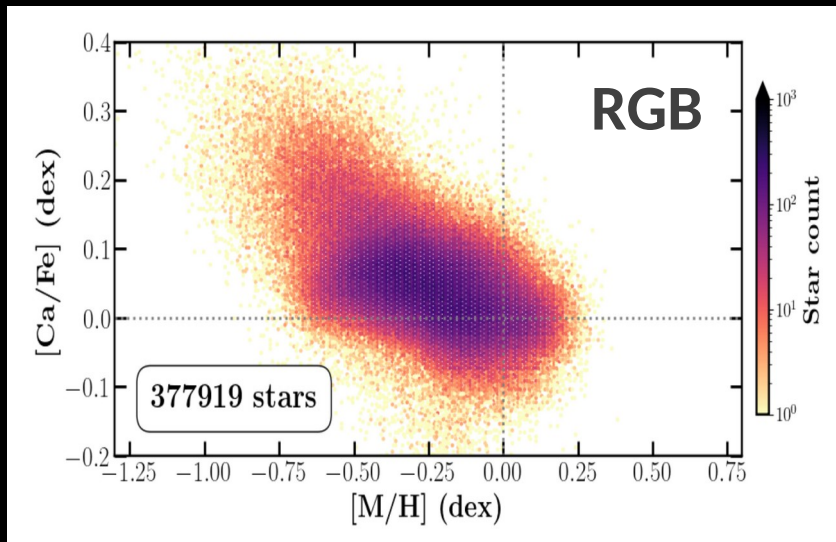


Gaia Collaboration, ARB et al. (2022)

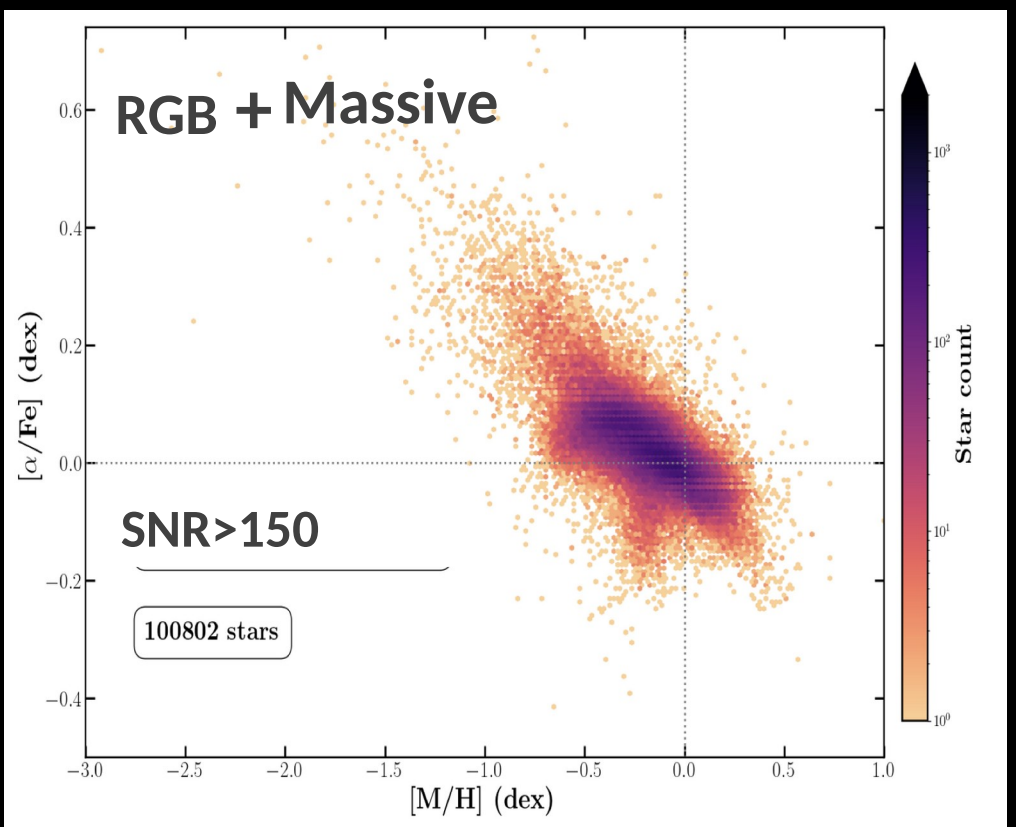


I. Massive stars population

[Ca/Fe]



[α /Fe]



I. Gaia DR3 lines



Elt	λ	λ_{ab}^-	λ_{ab}^+	λ_{norm}^-	λ_{norm}^+
N I	863.161	863.071	863.281	862.891	863.371
N I	868.579	868.489	868.699	868.309	868.939
Mg I	847.602	847.512	847.692	847.212	847.812
Si I	853.851	853.731	853.941	853.371	854.961
*Si I	855.916	855.856	856.036	855.376	856.156
Si I	868.872	868.782	868.992	868.602	869.232
*S I	867.258	866.988	867.378	866.898	867.998
*S I	869.701	869.551	869.821	869.281	869.971
Ca I	863.631	863.511	863.691	863.361	863.931
Ca II	849.856	849.706	849.976	849.586	850.276
Ca II	850.216	850.156	850.276	849.886	850.306
Ca II	854.264	854.114	854.384	853.544	854.864
Ca II	854.624	854.564	854.744	854.294	854.804
Ca II	866.272	866.152	866.332	866.002	866.572
Ca II	866.632	866.512	866.692	866.302	866.782
*Ti I	852.069	851.979	852.129	851.799	852.249
Ti I	857.209	857.119	857.269	856.999	857.359
Ti I	869.472	869.382	869.562	869.292	869.832
Cr I	855.118	855.058	855.208	854.878	855.478
Cr I	864.567	864.447	864.627	864.207	864.867
*Fe I	848.296	848.206	848.446	847.666	848.896
*Fe I	851.641	851.551	851.851	851.281	852.001
*Fe I	852.901	852.691	853.081	852.481	853.321
Fe I	857.416	857.296	857.506	856.876	858.166
Fe I	858.462	858.312	858.612	858.132	858.762
Fe I	862.397	862.277	862.517	862.127	862.697
Fe I	867.713	867.593	867.863	867.443	868.013
*Fe I	869.101	868.891	869.191	868.441	869.821
Fe II	858.794	858.764	858.824	858.254	859.274
Ni I	863.937	863.847	864.027	863.697	864.147
Zr II	852.748	852.658	852.838	852.388	853.018
*Ce II	851.375	851.285	851.465	851.015	851.555
Nd II	859.389	859.299	859.479	859.209	859.689

I. Gaia DR3 calibrations



Parameter	p_0	p_1	p_2	p_3	p_4
$\log(g)$	0.4496	-0.0036	-0.0224		
[M/H]	0.274	-0.1373	-0.0050	0.0048	
[M/H] _{OC}	-0.7541	1.8108	-1.1779	0.2809	-0.0222

To be used and adapted to your scientific goal

Element	p_0	p_1	p_2	p_3	p_4	Recommended interval	extrapol flag
As a function of $\log(g)$							
[α /Fe]	-0.5809	0.7018	-0.2402	0.0239	0.0000	1.01	4.85
[Ca/Fe]	-0.6250	0.7558	-0.2581	0.0256	0.0000	1.01	4.85
[Mg/Fe]	-0.7244	0.3779	-0.0421	-0.0038	0.0000	1.30	4.38
[S/Fe]	-17.6080	12.3239	-2.8595	0.2192	0.0000	3.38	4.81
[Si/Fe]	-0.3491	0.3757	-0.1051	0.0092	0.0000	1.28	4.85
[Ti/Fe]	-0.2656	0.4551	-0.1901	0.0209	0.0000	1.01	4.39
[Cr/Fe]	-0.0769	-0.1299	0.1009	-0.0200	0.0000	1.01	4.45
[Fe I/H]	0.3699	-0.0680	0.0028	-0.0004	0.0000	1.01	4.85
[Fe II/H]	35.5994	-27.9179	7.1822	-0.6086	0.0000	3.53	4.82
[Ni/Fe]	-0.2902	0.4066	-0.1313	0.0105	0.0000	1.41	4.81
[N/Fe]	0.0975	-0.0293	0.0238	-0.0071	0.0000	1.21	4.79
[α /Fe]	-0.2838	0.3713	-0.1236	0.0106	0.0002	0.84	4.44
[Ca/Fe]	-0.3128	0.3587	-0.0816	-0.0066	0.0020	0.84	4.98
As a function of $T_{\text{eff}}/5750$							
[α /Fe]	-6.6960	20.8770	-21.0976	6.8313	0.0000	4000	6830
[Ca/Fe]	-7.4577	23.2759	-23.6621	7.7657	0.0000	4000	6830
[S/Fe]	0.1930	-0.2234	0.0000	0.0000	0.0000	5700	6800

I. Spectres RVS

Avant d'être analysés par le module GSP-Spec une estimation de la vitesse radiale des spectres RVS [Katz et al., 2023] est déterminée par la DPAC/CU6 (CCF). A noter également que le vrai domaine spectral observé par le RVS s'étend de 845 à 872 nm mais que les spectres sont analysés uniquement entre 846 et 870 nm afin de minimiser les effets de bord.

De plus, avant analyse, les spectres sont normalisés avec un pseudo-continu local et sont ré-échantillonnés avec un pas initial de 0.01 par la DPAC/CU6 (conduisant à 2400 wlp) puis 0.03 nm par GSP-Spec $\sqrt{3}$, conduisant à des spectres RVS ayant 800 wlp permettant d'augmenter le S/N d'un facteur 3 (sans pour autant dégrader la résolution spectrale grâce au sur-échantillonnent du RVS).

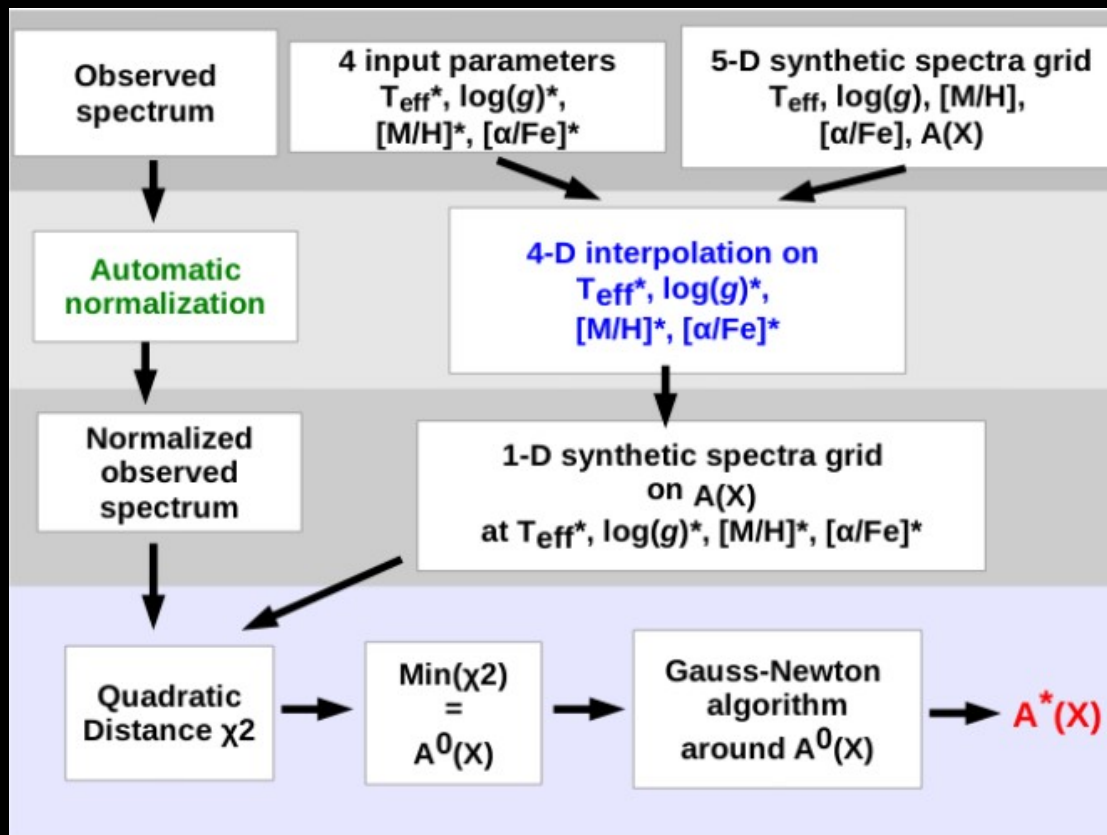
Les spectres synthétiques ont ensuite été convolués à la résolution spectrale du RVS (11 500) avec un pas en longueur d'onde de 0.03 nm en utilisant les outils développés par la DPAC/CU6 [Sartoretti+18].

I. GSP-Spec atm. Param.

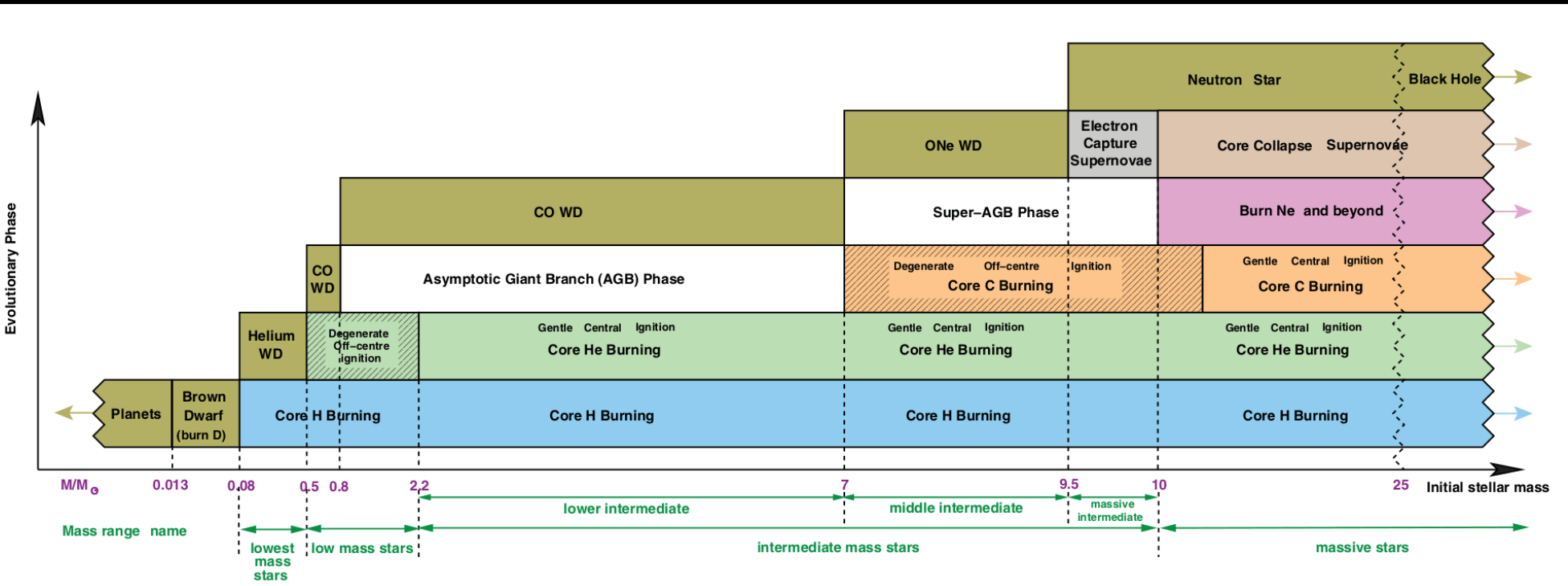
- 4D Grid composed by 13 848 spectra
- MatisseGauguin procedure initialized by DEGAS [Bijaoui+10] code (decision three).
- MATISSE code [Recio-Blanco+06] : observed spectrum projected on vectors (take into account sensitivity of each wavelength flux). The MATISSE projection is first applied at the DEGAS solution in a local environment of ± 500 K in Teff , ± 0.5 dex in log(g), ± 0.25 dex in [M/H] and ± 0.20 dex in [α/Fe] (corresponding to the parameter space region of each training function). This produces a second solution around which MATISSE is applied again. This iterative procedure is repeated until convergence.
- GAUGUIN code [Bijaoui12] gives exact solution (Gauss-Newton algo) by first giving the most negative gradient as a function of the difference between observed and synthetic spectra. Once direction found, the gradient is iteratively computed until convergence.
- Solution used to normalized spectra: For this purpose, the observed spectrum (O) is compared to an interpolated synthetic one from the 4-D reference grid (S) having the same atmospheric parameters. First, the most appropriate wavelength points of the residuals ($\text{Res} = S / O$) are selected using an iterative procedure implementing a linear fit to Res followed by a σ – clipping. Then, the residual trend is fitted with a third degree polynomial. Finally, the refined normalised spectrum is obtained after dividing the observed spectrum by a linear function resulting by the fit of the residuals. [Santos-Peral+20].

I. GSP-Spec abundances

- 1D spectra (from 5D grid) compared to observed one.
- Second normalization around the line
- minimum of quadratique distance computed $\Rightarrow A^0(X)$
- Final abundance obtained iteratively



I. Stellar life

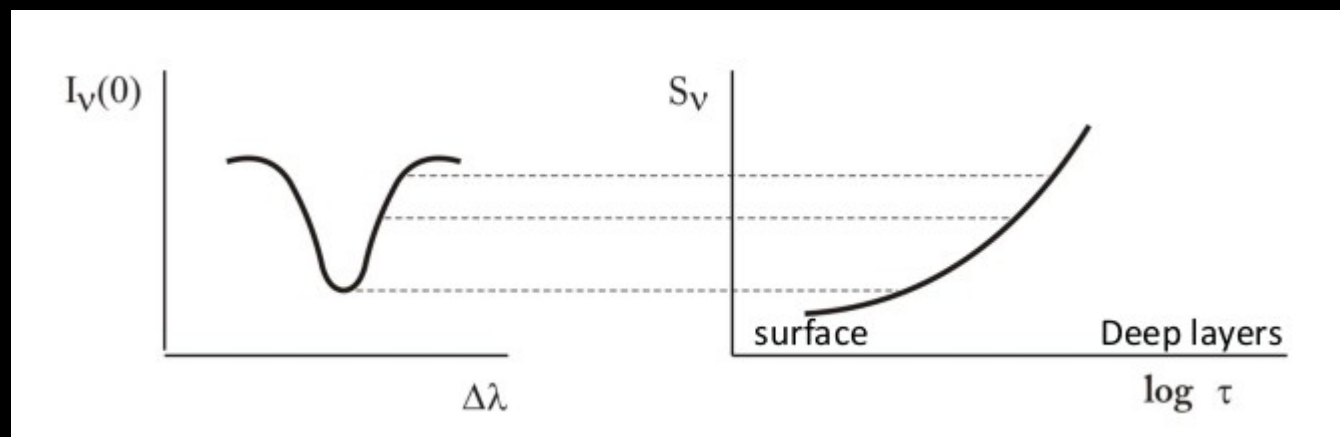


FDU : thermohaline mixing (thermal diffusion + chemical mixing) + PIE (metal poor stars = low entropy barrier between H and He- rich layers)

Second Dredge-Up (SDU) for intermediate-mass stars : overcome of the entropy barrier.

I. line depth

Les raies faibles possèdent une opacité bien plus faible que l'opacité du continu. Elles sont dites optiquement fines. Le flux au centre des raies est plus faible qu'au niveau du continu puisque le rayonnement proche du centre de la raie provient de régions moins profondes que pour le continu. L'opacité est plus forte au niveau du cœur qu'au niveau des ailes de la raie. Le rayonnement des différentes parties de la raie provient de différentes profondeurs dans l'atmosphère stellaire.



I. Teff anf log(g)

Teff methods :

- Bolometric flux
- Calibration from (B-V)
- Line-depth
- **Indipendence between Exitation potential and Teff (Boltzmann law)**

logg methods :

- $g = GM/R^2$
- Balmer Jump
- Wings of some large lines
- **Fe I = Fe II (Ionisation balance)**
- Asteroseismology

I. Automatic methods

Optmisation : GAUGUIN

Projection : Matisse

Classification : DEGAS

II. Gaia Benchmark Stars

- 34 GBS to calibrate surveys [Blanco-Cuaresma+14] with known angular diameters (from interferometry), bolometric flux (from energy spectral distrib.) and distances (parallaxes)
- Obs from NARVAL, HARPS, UVES
- Derivation of atm. Params. by 8 different methods

II. Reference Stars

Well known atmospheric parameters and individual chemical abundances ($^{12}\text{C}/^{13}\text{C}$, C, N, O, α -elts ..)

Contursi & al., 2021

Table 1. Atmospheric parameters and chemical abundances for our reference stars.

Star	Cool giants		Cool dwarfs		Hot dwarf	
	Arcturus	μ Leo	61 Cyg A	ϵ Eri	Sun	Procyon
T_{eff} (K)	4286	4474	4374	5076	5771	6554
$\log(g)$ (g in cm s^{-2})	1.60	2.51	4.63	4.61	4.44	4.00
[Fe/H] (dex)	-0.55	0.22	-0.36	-0.12	0.00	-0.04
[α /Fe] (dex)	0.22	0.12	0.02	-0.01	0.00	-0.07
V_{micro} (km s^{-1})	1.95 ^(a)	1.95 ^(a)	1.07 ^(b)	1.14 ^(b)	0.87 ^(c)	1.69 ^(d)
V_{macro} (km s^{-1})	4.30 ^(a)	2.58 ^(a)	1.83 ^(c)	2.91 ^(c)	3.57 ^(c)	4.60 ^(d)
$V_{\sin i}$ (km s^{-1})	3.80 ^(a)	5.06 ^(a)	0.70 ^(e)	2.40 ^(c)	1.60 ^(c)	2.80 ^(d)
[C/Fe] (dex)	0.43 ^(f)	-0.18 ^(g)	0.60 ^(h)	-0.06 ^(h)	0.00	-0.05 ^(h)
[N/Fe] (dex)	0.00	0.37 ^(g)	0.00	0.00	0.00	0.00
[O/Fe] (dex)	0.50 ^(f)	-0.13 ^(g)	0.47 ^(h)	-0.17 ^(h)	0.00	0.14 ^(h)
[Ca/Fe] (dex)	0.12	0.03	-0.03	0.04	0.00	0.03
$^{12}\text{C}/^{13}\text{C}$	6.30 ⁽ⁱ⁾	20.0 ⁽ⁱ⁾	89.9	89.9	89.9	89.9

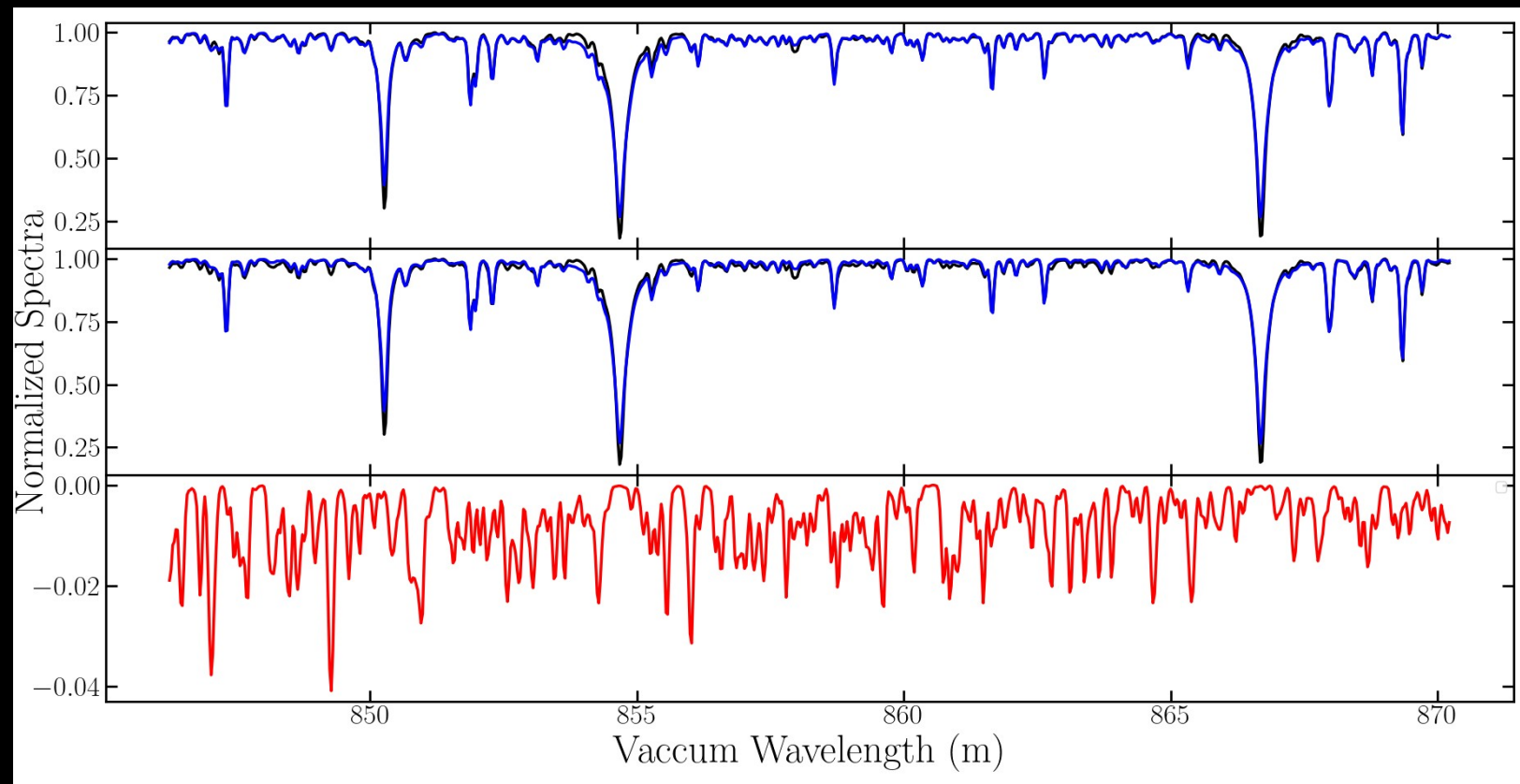
References. The data come from Jofré et al. (2018) or are assumed solar-scaled abundances except the following: ^(a)Hekker & Meléndez (2007), ^(b)Jofré et al. (2015), ^(c)Valenti & Fischer (2005), ^(d)Bruntt et al. (2010), ^(e)Benz & Mayor (1984), ^(f)Ramírez & Allende Prieto (2011), ^(g)Gratton & Sneden (1990), ^(h)Luck (2017), and ⁽ⁱ⁾Smith et al. (2013).

Observed spectra from Wallace+11 for Sun (FTS, $R \sim 670\ 000$),
Hinkle+00 ($R \sim 150\ 000$) for Arcturus,
PEPSI spectra ($R \sim 270\ 000$, 2x8.4 Large Binocular Telescope) otherwise.

II. C for the Ref. Stars

Arcturus: C, N, O from Ramirez+11 (C I lines).

[C/Fe] higher of 0,4 dex from Smith+13 (molecular C)



II. GES Linelist

- GES line list based on VALD database: 1300 atomic and molecular lines from 475 nm to 685 nm and 850-895 nm. Optimized for FGK stars.
- Consider hfs, isotopic split.
- Kurucz data used if no data found.
- One "flag" for fit quality for Sun and Arcturus.
- Second "flag" for log(gf) quality
- Y if recommended line, N if not, U if unknown

II. Cool giant comparison

Contursi et al. (2021)

Table 2. Quality-fit parameters (QFP) computed from the comparison between the synthetic and observed spectra at $R = 11\,500$ (800 *wlp*) for the GES line list, the complete GSP-Spec line list (GL), or rejecting the core of the calcium triplet lines (GL_{noCaT}).

Star	Cool giants		Cool dwarfs			Hot dwarf
	Arcturus GES/GES _{noCaT}	μ Leo GES/GES _{noCaT}	61 Cyg A GES/GES _{noCaT}	ϵ Eri GES/GES _{noCaT}	Sun GES/GES _{noCaT}	Procyon GES/GES _{noCaT}
χ^2	0.23/0.04	0.31/0.19	0.08/0.05	0.21/0.05	0.07/0.03	0.17/0.04
N_5	17/0	18/7	0/0	11/0	4/0	6/0
N_3	42/0	59/46	1/0	10/3	7/1	43/4
N_1	210/123	390/286	306/196	273/146	96/50	176/84

[Fe/H]: Arcturus :-0.55, μ Leo : +0.22

Better fit for Arcturus than for μ Leo mainly due to metallicity

II. Cool dwarf comparison

Contursi et al. (2021)

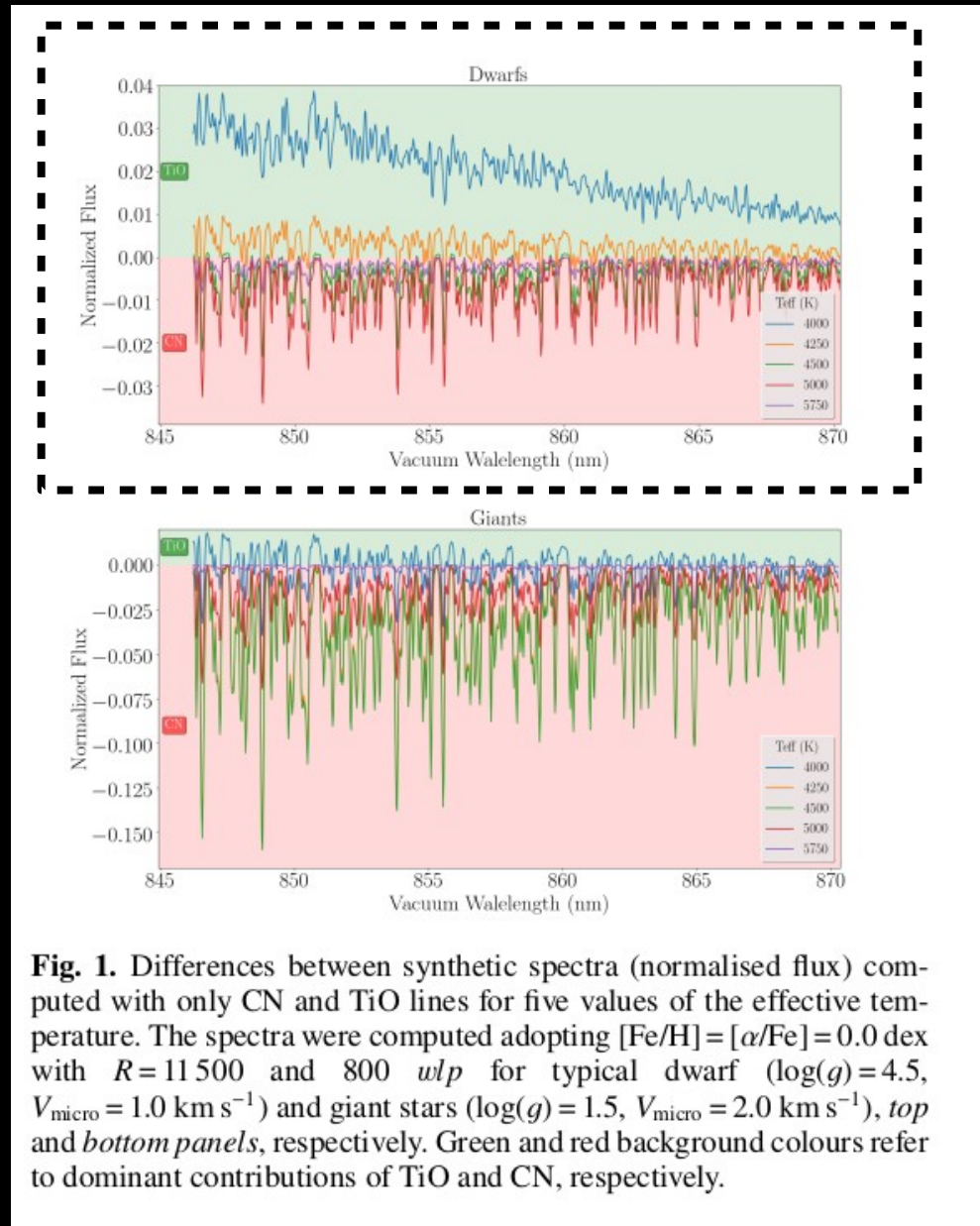
Table 2. Quality-fit parameters (QFP) computed from the comparison between the synthetic and observed spectra at $R = 11\,500$ (800 *wlp*) for the GES line list, the complete GSP-Spec line list (GL), or rejecting the core of the calcium triplet lines (GL_{noCaT}).

Star	Cool giants		Cool dwarfs			Hot dwarf
	Arcturus GES/GES _{noCaT}	μ Leo GES/GES _{noCaT}	61 Cyg A GES/GES _{noCaT}	ϵ Eri GES/GES _{noCaT}	Sun GES/GES _{noCaT}	Procyon GES/GES _{noCaT}
χ^2	0.23/0.04	0.31/0.19	0.08/0.05	0.21/0.05	0.07/0.03	0.17/0.04
N_5	17/0	18/7	0/0	11/0	4/0	6/0
N_3	42/0	59/46	1/0	10/3	7/1	43/4
N_1	210/123	390/286	306/196	273/146	96/50	176/84

1. Better agreement than giants especially in terms of N3 and N5
2. ϵ Eri exhibits worse fit because ...

II. Cool dwarf comparison

- TiO dominant if $T_{\text{eff}} < 4000\text{K}$
- CN contribution reaches a maximum around 5000K (T_{eff} of ϵ Eri's)
- Better fit for ϵ Eri if C abundance decreased by 0.2 dex



II. Cool dwarf comparison

Contursi et al. (2021)

Table 2. Quality-fit parameters (QFP) computed from the comparison between the synthetic and observed spectra at $R = 11\,500$ (800 *wlp*) for the GES line list, the complete GSP-Spec line list (GL), or rejecting the core of the calcium triplet lines (GL_{noCaT}).

Star	Cool giants		Cool dwarfs			Hot dwarf Procyon GES/GES_{noCaT}
	Arcturus GES/GES_{noCaT}	μ Leo GES/GES_{noCaT}	61 Cyg A GES/GES_{noCaT}	ϵ Eri GES/GES_{noCaT}	Sun GES/GES_{noCaT}	
χ^2	0.23/0.04	0.31/0.19	0.08/0.05	0.21/0.05	0.07/0.03	0.17/0.04
N_5	17/0	18/7	0/0	11/0	4/0	6/0
N_3	42/0	59/46	1/0	10/3	7/1	43/4
N_1	210/123	390/286	306/196	273/146	96/50	176/84

1. Better agreement than giants especially in terms of N_3 and N_5
2. ϵ Eri exhibits worse fit because molecules ...
3. 61 Cyg A better than Sun because smaller metallicity and better fit of Ca triplet.

II. Dwarf comparison

Contursi et al. (2021)

Table 2. Quality-fit parameters (QFP) computed from the comparison between the synthetic and observed spectra at $R = 11\,500$ (800 *wlp*) for the GES line list, the complete GSP-Spec line list (GL), or rejecting the core of the calcium triplet lines (GL_{noCaT}).

Star	Cool giants		Cool dwarfs			Hot dwarf
	Arcturus GES/GES _{noCaT}	μ Leo GES/GES _{noCaT}	61 Cyg A GES/GES _{noCaT}	ϵ Eri GES/GES _{noCaT}	Sun GES/GES _{noCaT}	Procyon GES/GES _{noCaT}
χ^2	0.23/0.04	0.31/0.19	0.08/0.05	0.21/0.05	0.07/0.03	0.17/0.04
N_5	17/0	18/7	0/0	11/0	4/0	6/0
N_3	42/0	59/46	1/0	10/3	7/1	43/4
N_1	210/123	390/286	306/196	273/146	96/50	176/84

Teff (K): Procyon :6554, Sun : 5771, 61CygA : 4374, ϵ Eri : 5076

→ Higher temperature = less lines = easier to have better fit (because difficulty in obtaining accurate atomic measurements).

→ Almost as good as other dwarfs without Ca triplet

II. Dwarf vs Giant

Contursi et al. (2021)

Table 2. Quality-fit parameters (QFP) computed from the comparison between the synthetic and observed spectra at $R = 11\,500$ (800 *wlp*) for the GES line list, the complete GSP-Spec line list (GL), or rejecting the core of the calcium triplet lines (GL_{noCaT}).

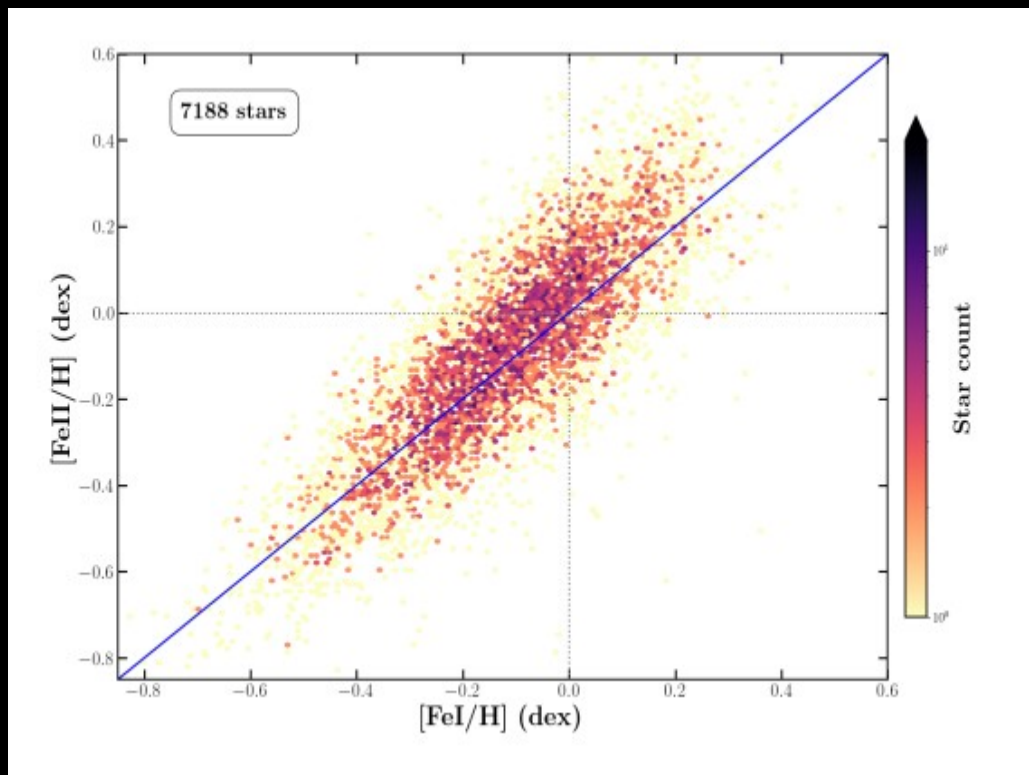
Star	Cool giants		Cool dwarfs		Hot dwarf	
	Arcturus GES/GES _{noCaT}	μ Leo GES/GES _{noCaT}	61 Cyg A GES/GES _{noCaT}	ϵ Eri GES/GES _{noCaT}	Sun GES/GES _{noCaT}	Procyon GES/GES _{noCaT}
χ^2	0.23/0.04	0.31/0.19	0.08/0.05	0.21/0.05	0.07/0.03	0.17/0.04
N_5	17/0	18/7	0/0	11/0	4/0	6/0
N_3	42/0	59/46	1/0	10/3	7/1	43/4
N_1	210/123	390/286	306/196	273/146	96/50	176/84

Tefflogg/metallicity: Arcturus : 4286/1.60/-0.55 61CygA : 4374/4.63/-0.36

- Larger mismatches in Arcturus than 61CygA (N_3 , N_5) caused by Ca triplet fit.
- Better fit if lower C abundance in 61CygA.

II. Fe II line

- Unidentified line in Hot Star Spectra
- Fe II line tuned by 8.786 dex.
- Fe II confirmed by GSP-Spec data

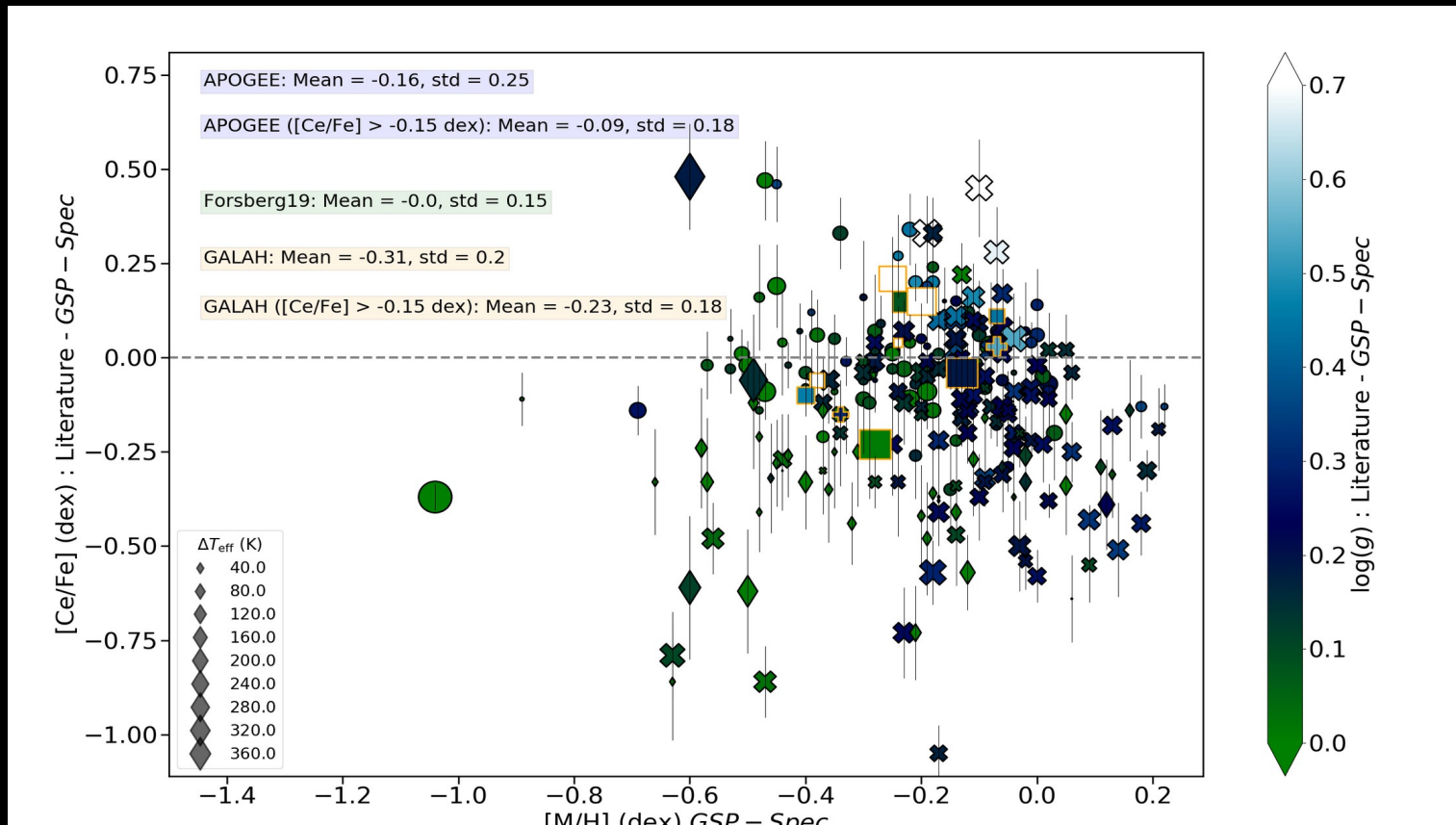


III. GSP Spec flags

Parametrization flags == 0 (Best stellar parametrization)

- CeUpLim ≤ 2 (Indicator of Line-depth compared to noise level)
- CeUncer ≤ 1 (Reliability of abundance uncertainty based on atm. params and S/N)

III. Selection of Low-Uncertainty Sample

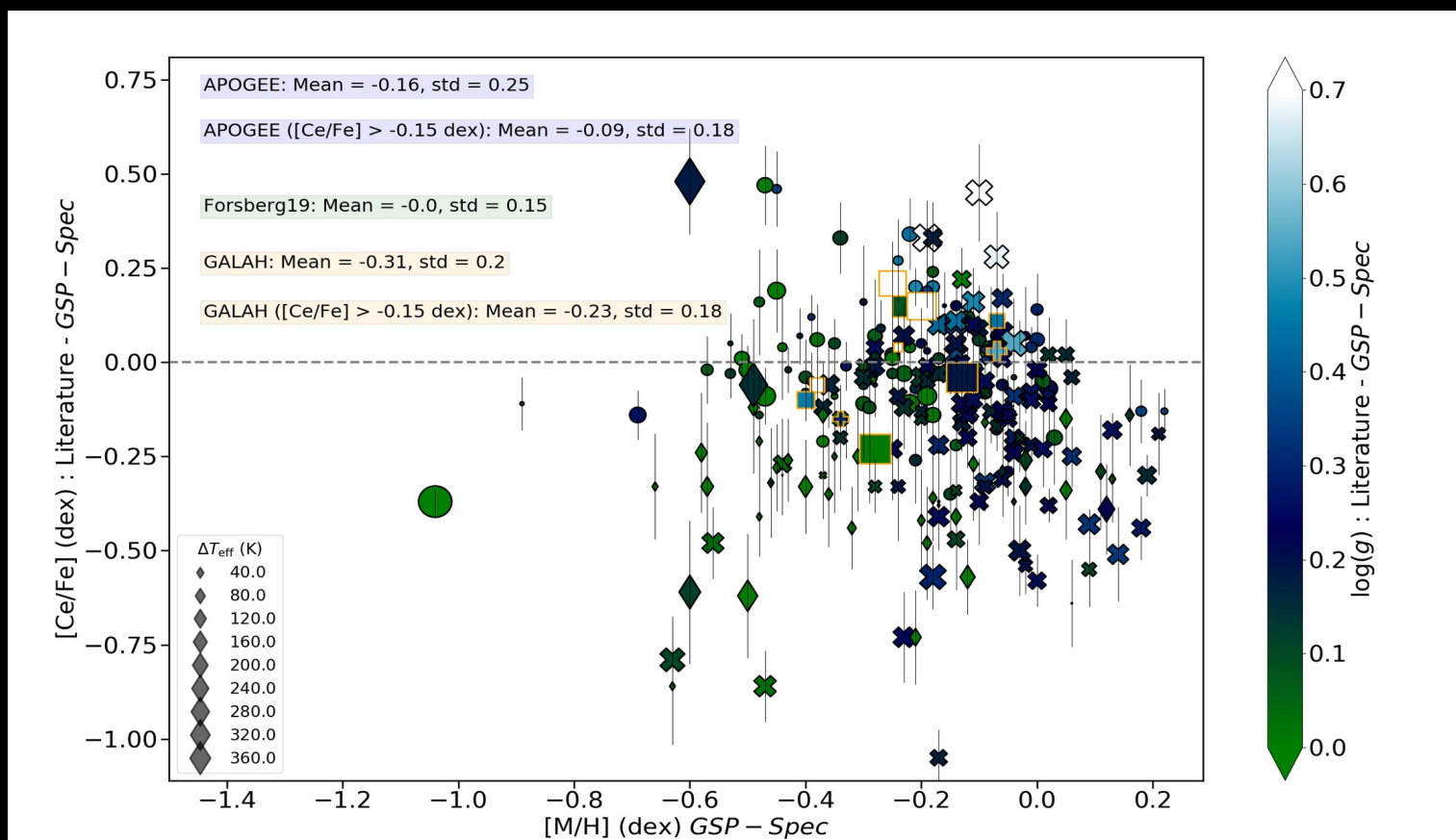


Contursi et. al, 2022.

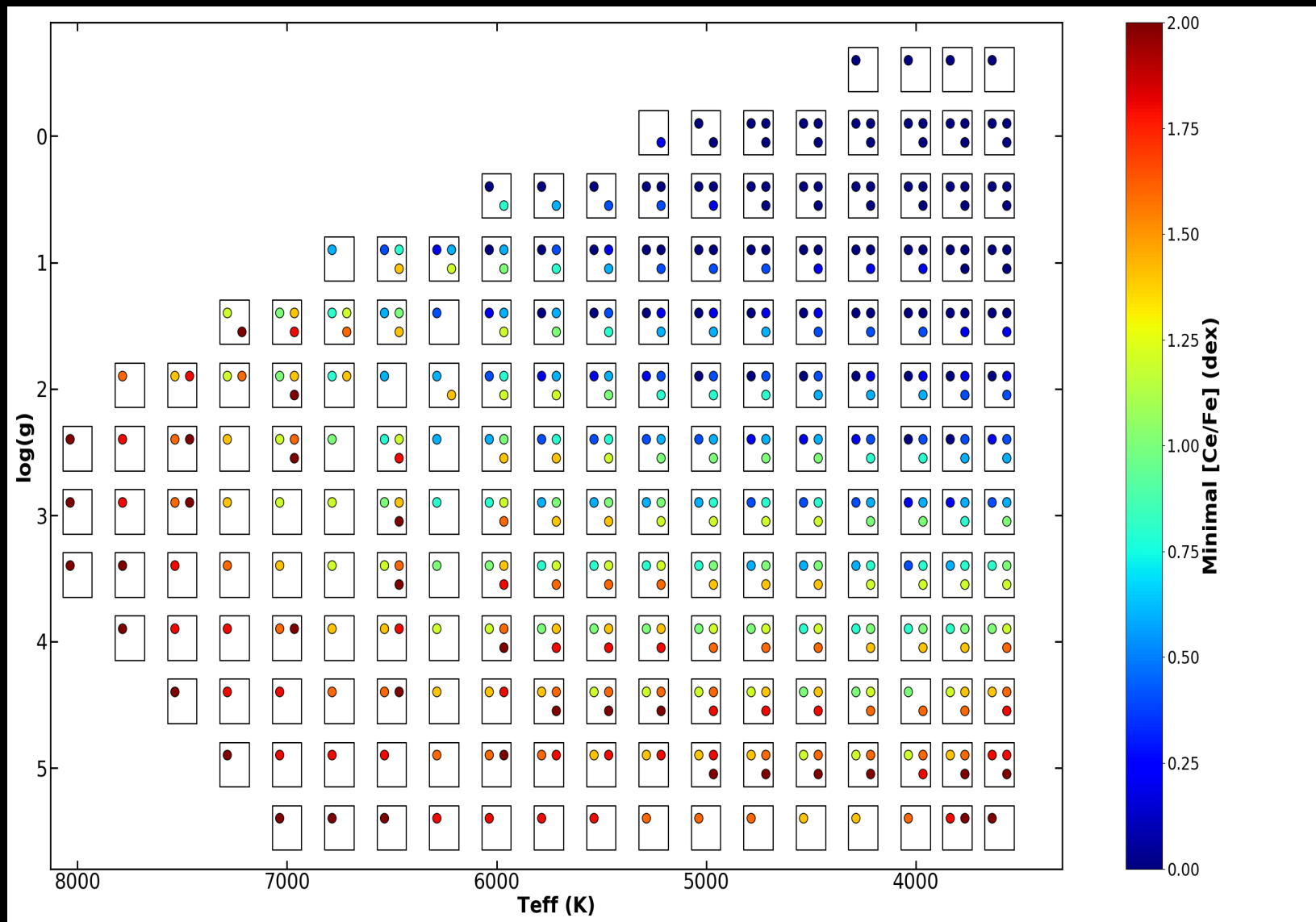
III. Selection of Low-Uncertainty Sample

Considered flags :

- Parametrization flags == 0 (Best stellar parametrization)
- CeUpLim ≤ 2 (Indicator of Line-depth compared to noise level)
- CeUncer ≤ 1 (Reliability of abundance uncertainty based on atm.params and S/N)
- vbroad ≤ 13 km/s and $\Delta[\text{Ce}/\text{Fe}] \leq 0.2$ dex



III. Ce detection



III. Orbits computation

Palicio et. al, 2023

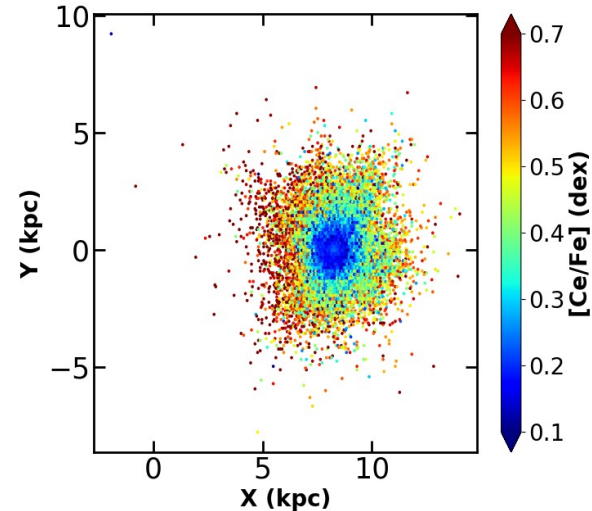
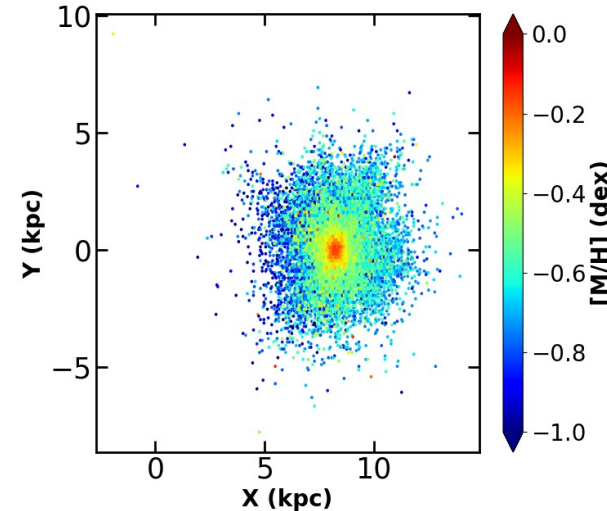
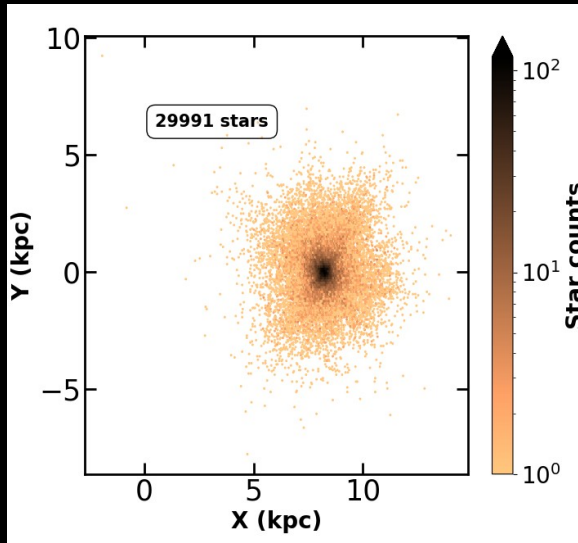
- Sun's Galactocentric position $(R, Z)_\odot = (8.249, 0.0208)$ kpc
(Gravity Collaboration et al. 2021)
- Galactocentric cylindrical velocities
 $(V_R, V_\phi, V_Z)_\odot = (-9.5, 250.7, 8.56)$ km/s (*Reid & Brunthaler 2020*)
- Gaia's α, δ , line-of-sight velocity and *Bailer-Jones et al. (2021)*
geometric distances for each target.
- The orbital parameters (actions, Zmax ...) computed using :
 - Stäckel fudge method *Binney (2012)*
 - Rescaled version of the *McMillan (2017)* **axisymmetric** Galactic potential.

Galactocentric distance of the Sun is $R_\odot = 8.249$ kpc
Circular velocity of the Local Standard of Rest is set to 238.5 km/s
(*Gravity Collaboration et al. 2021*).

III. Ce Galactic general properties

(X,Y) plane : Majority of stars in solar neighborhood

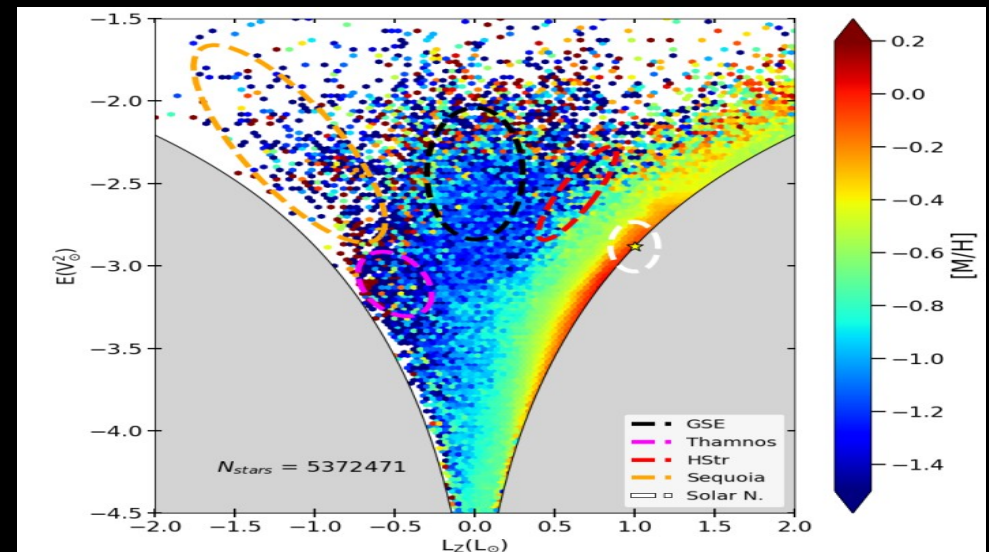
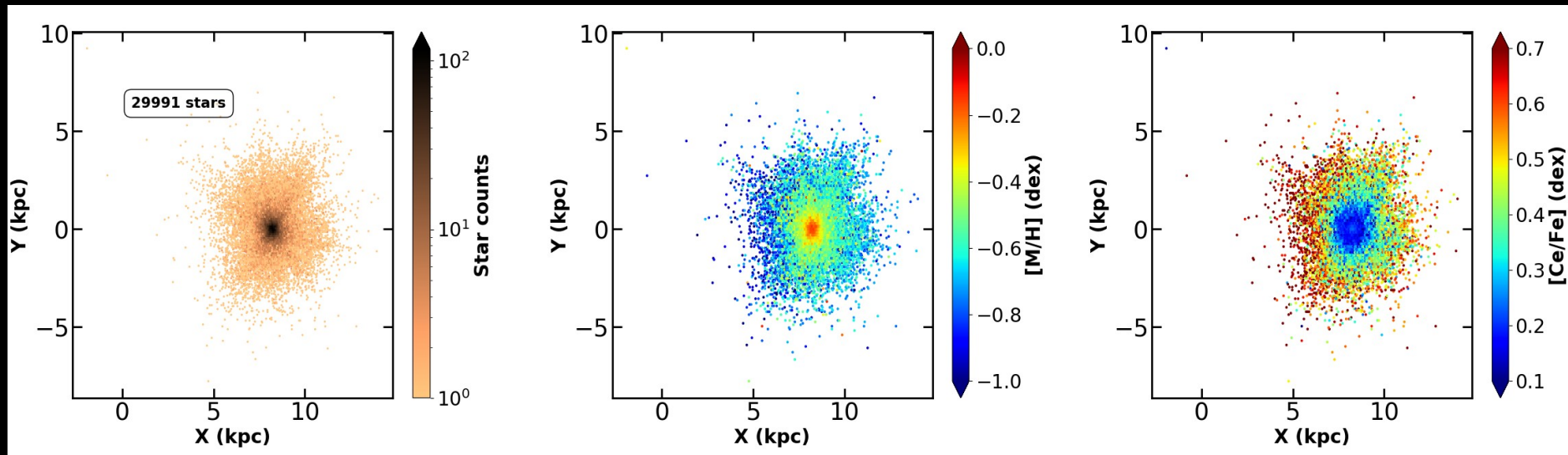
Contursi et. al, 2023



III. Ce Galactic general properties

(X,Y) plane : Majority of stars in solar neighborhood

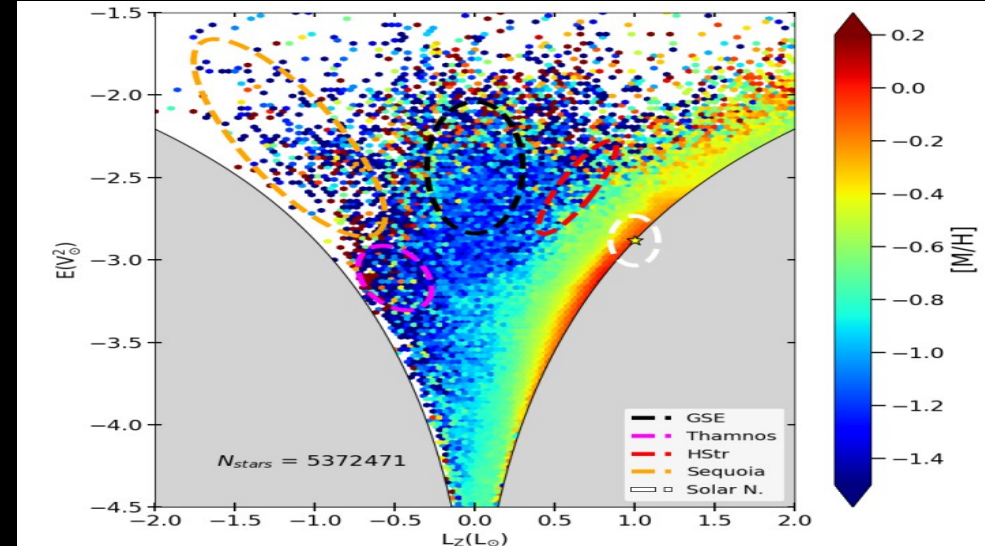
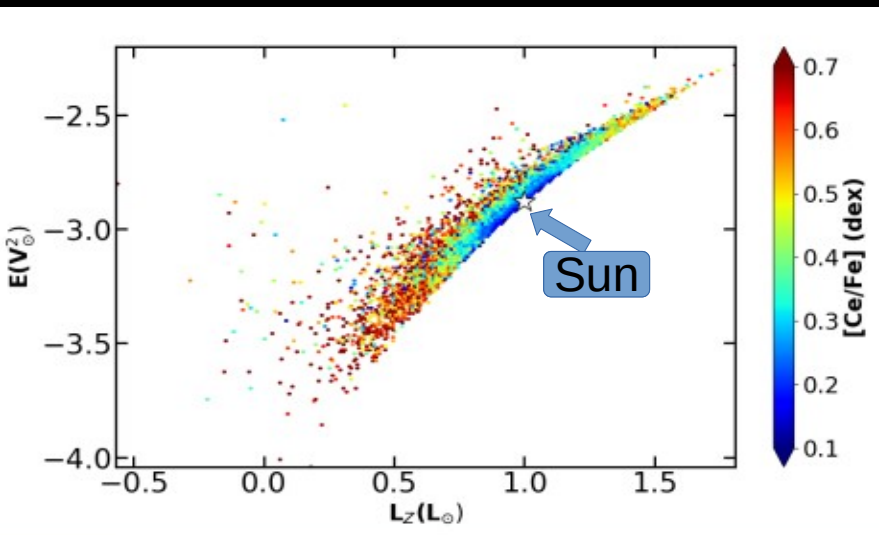
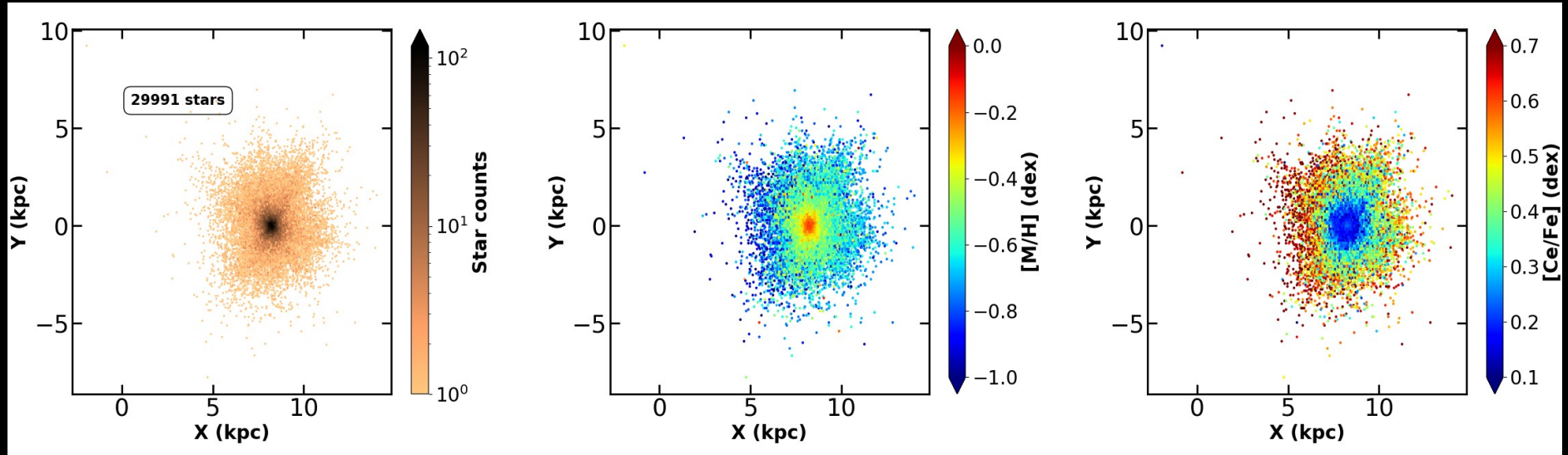
Contursi et. al, 2023



III. Ce Galactic general properties

(X,Y) plane : Majority of stars in solar neighborhood
→ Stars in accreted systems

Contursi et. al, 2023

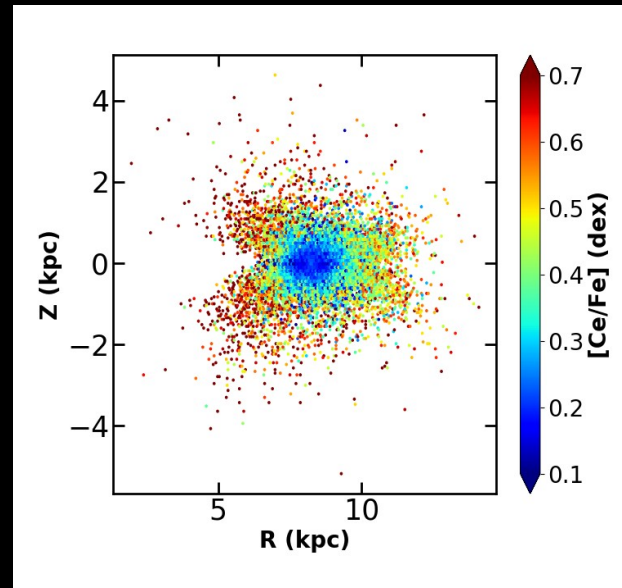
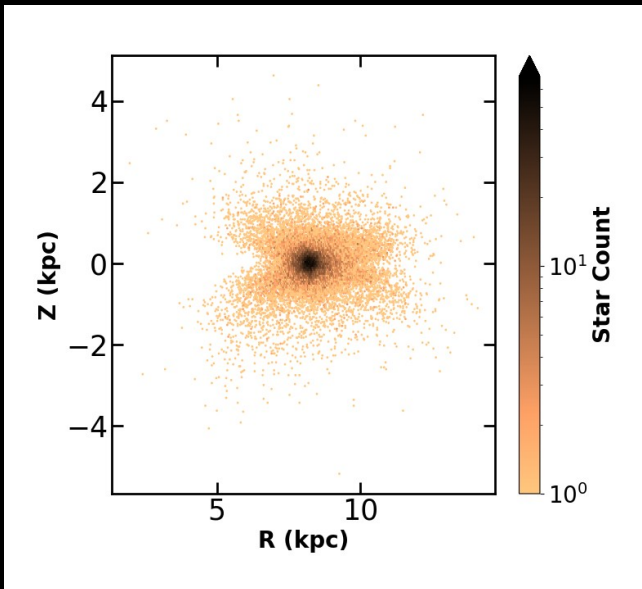


III. Ce Galactic general properties

(R,Z) plane : Majority of **disc** stars

Some stars (Ce-rich) not in thin disc

Contursi et. al, 2023

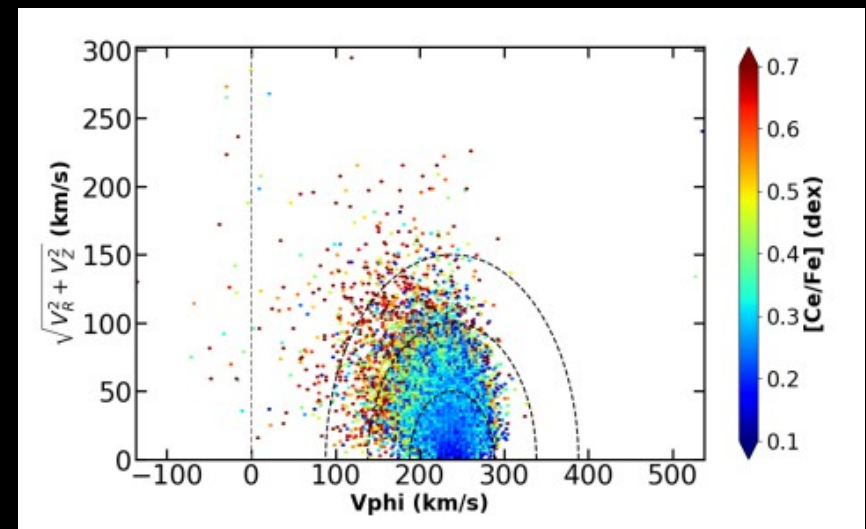
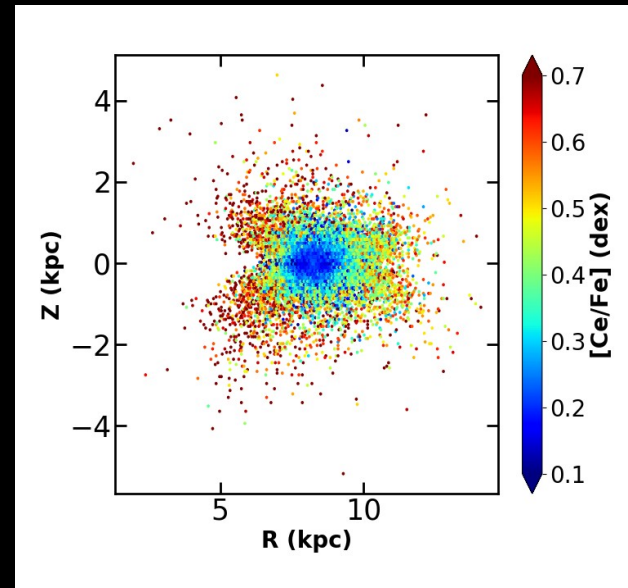
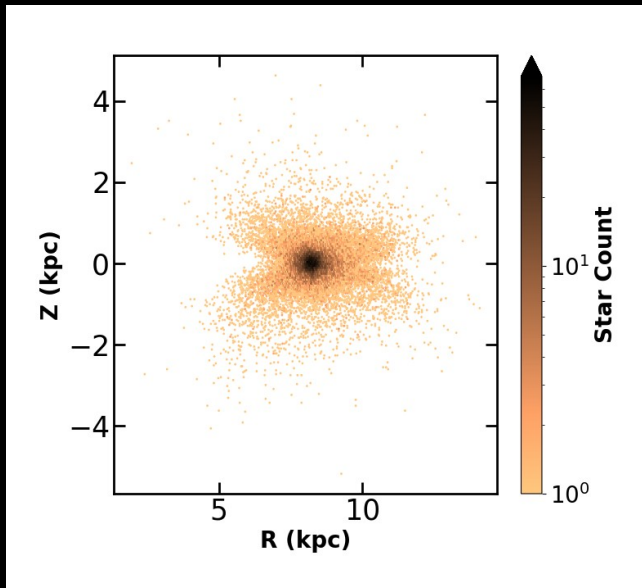


III. Ce Galactic general properties

(R,Z) plane : Majority of disc stars

Some stars (Ce-rich) not in thin disc

Contursi et. al, 2023

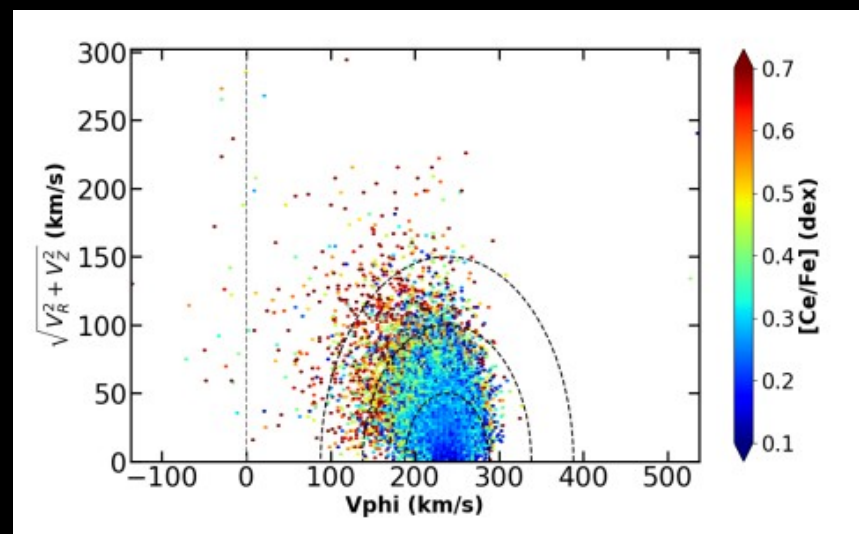
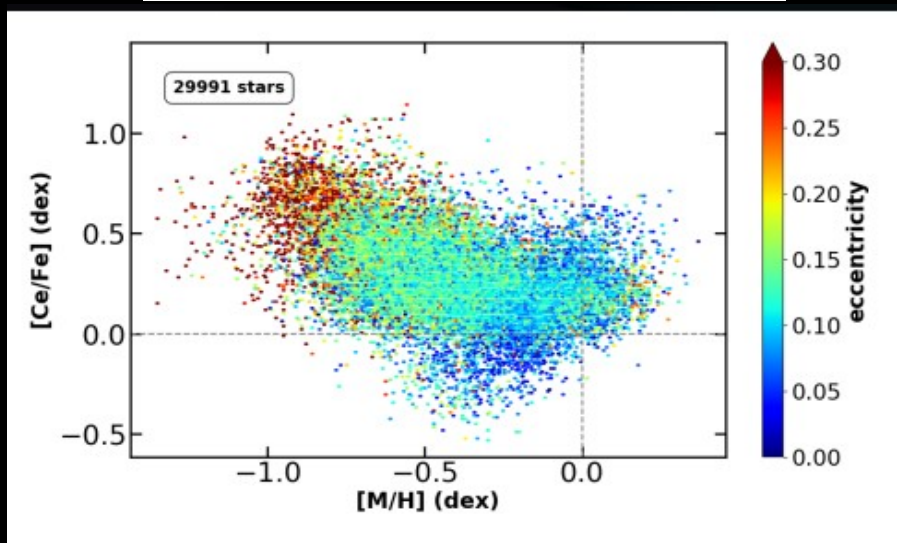
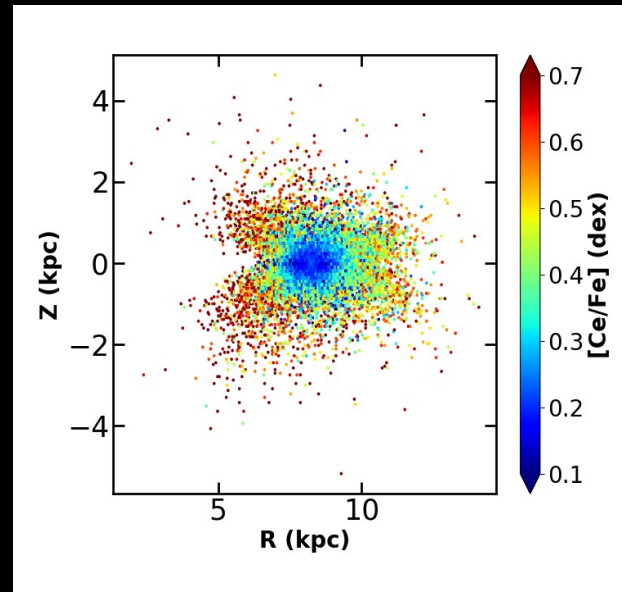
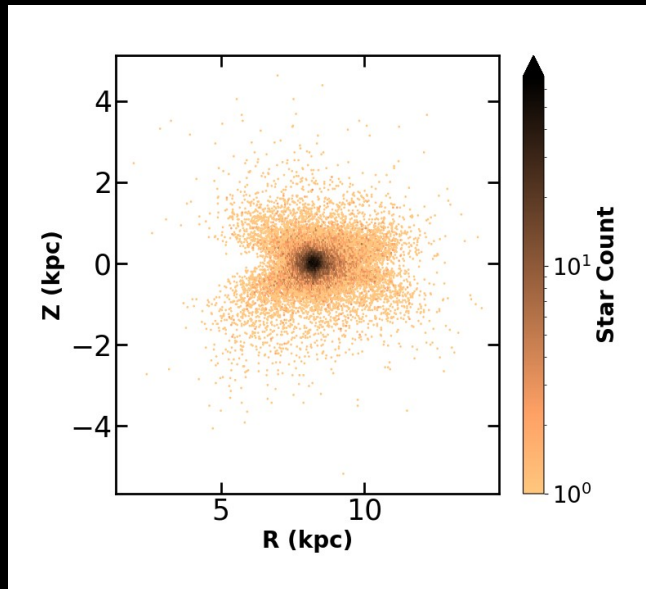


III. Ce Galactic general properties

(R,Z) plane : Majority of disc stars

Some stars (Ce-rich) not in thin disc

Contursi et. al, 2023

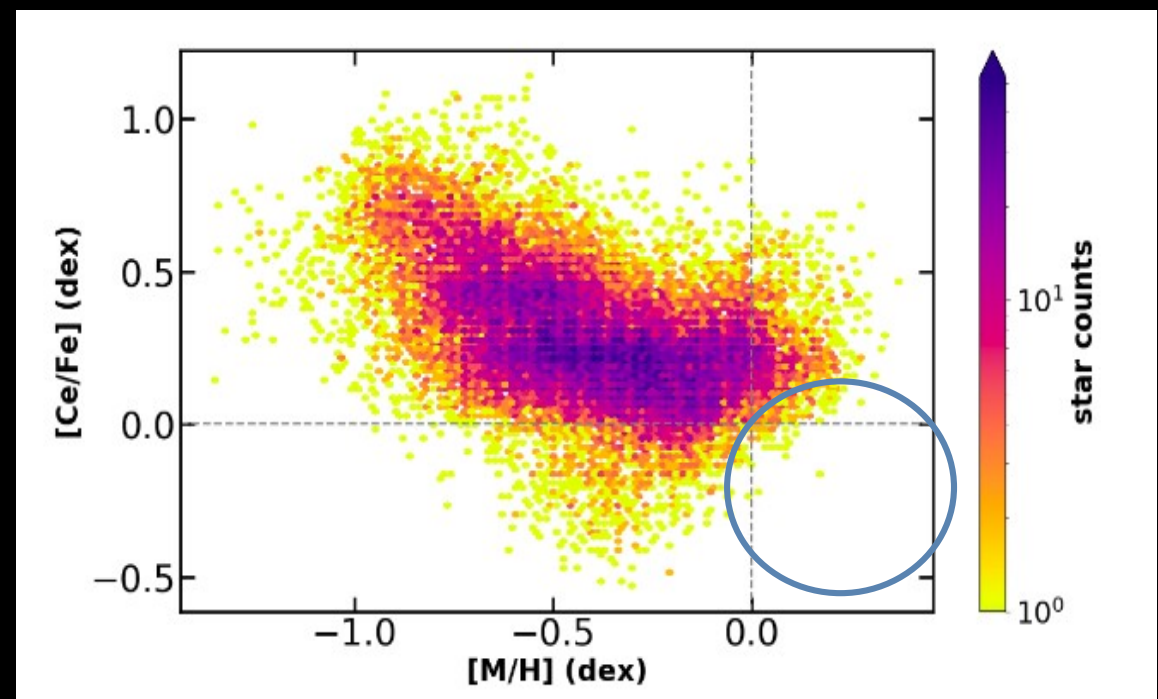


III. High-quality unbiased sample

Metal-rich cerium poor,

stars difficult to detect

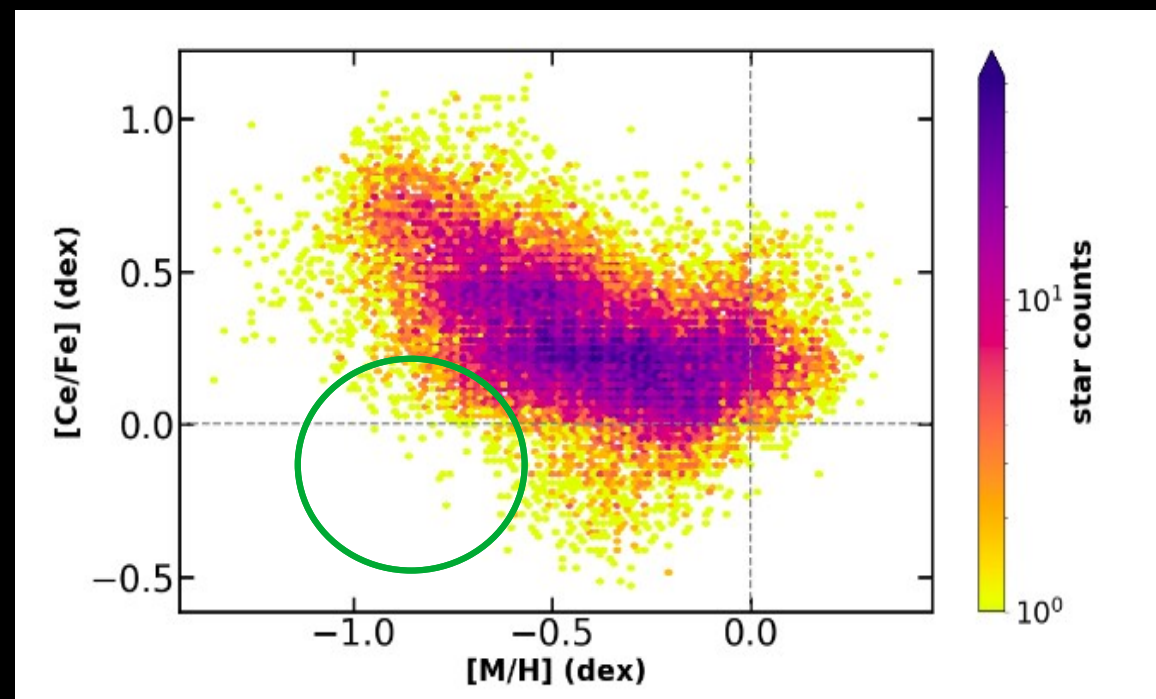
Contursi et. al, 2023



III. High-quality unbiased sample

metal-poor cerium poor
stars difficult to detect

Contursi et. al, 2023



III. High-quality unbiased sample

Metal-rich cerium poor,
metal-poor cerium poor
stars difficult to detect

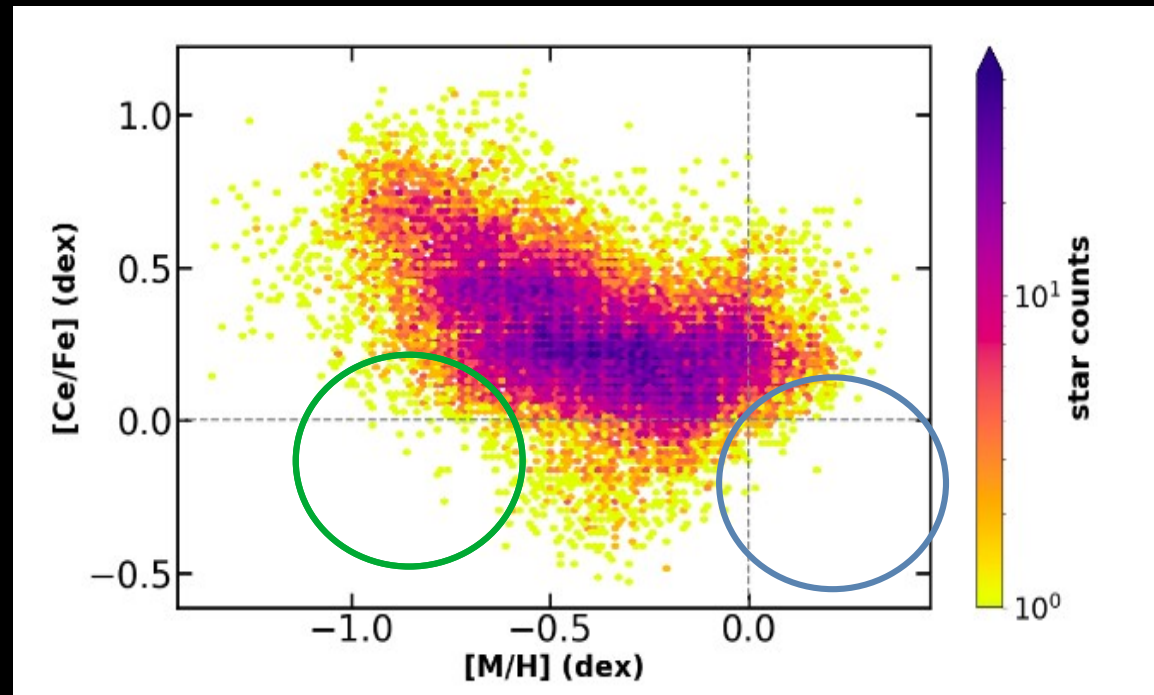
→ Define an unbiased
sample (7397 stars) :

$$3800 < T_{\text{eff}} \text{ (K)} < 4800$$

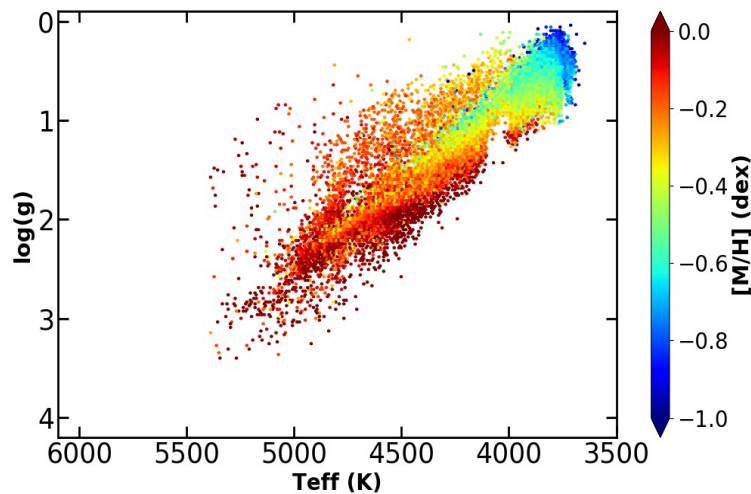
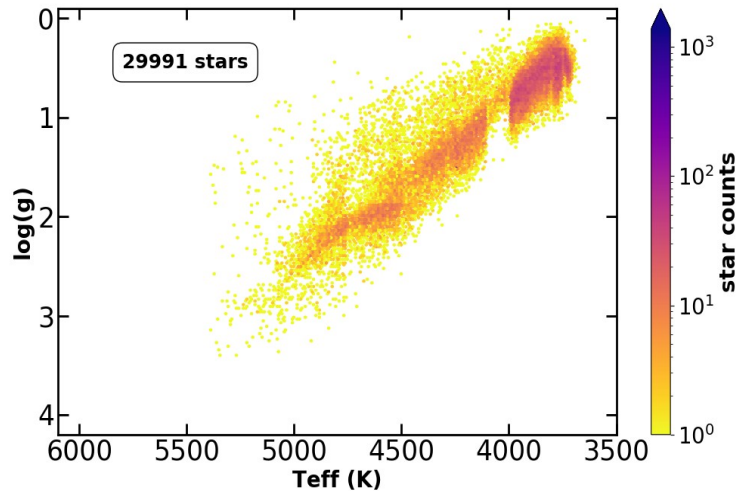
$$\Delta[\text{Ce}/\text{Fe}] < 0.1 \text{ dex}$$

$$SNR > 300$$

Contursi et. al, 2023



III. Kiel diagram of Ce Low-Uncertainty Sample



III. [Ce/Ca] in literature

$\delta[\text{Ce}/\text{Ca}]/\delta[\text{Ca}/\text{H}] = 0.087^{\pm 0.013}$, similarly to high-Ia population of Griffith+21 (low-Mg abundances = thin disc).

[Ce/Ca] decreases in Griffith+21 (for $[\text{Ca}/\text{H}] > 0,1$ dex) because of their constant [Mg/Fe]. Ca abundances decreases and more compatible with models.

III. Decreasing horizontal gradient

Negative Radial gradient of [Ce/H] :

$$\delta[\text{Ce}/\text{H}]/\delta R = -0.028^{\pm 0.017} \text{ dex.kpc}^{-1}$$

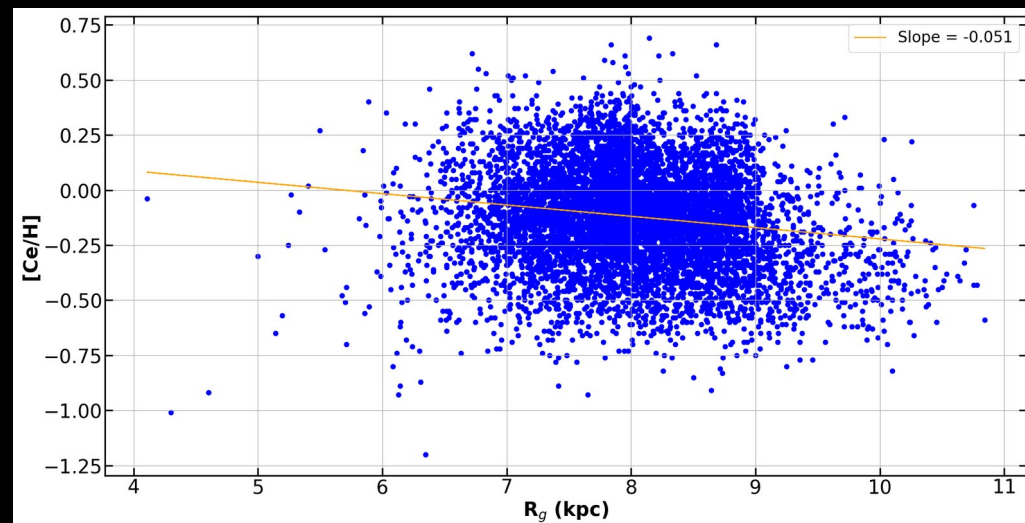
Similar to $\delta[\text{Ce}/\text{H}]/\delta R = -0.024^{\pm 0.003}$
 dex.kpc^{-1} from Cepheids of da Silva +16.

Agreement with decreasing metallicity
gradient of the disc (Recio-Blanco +22)

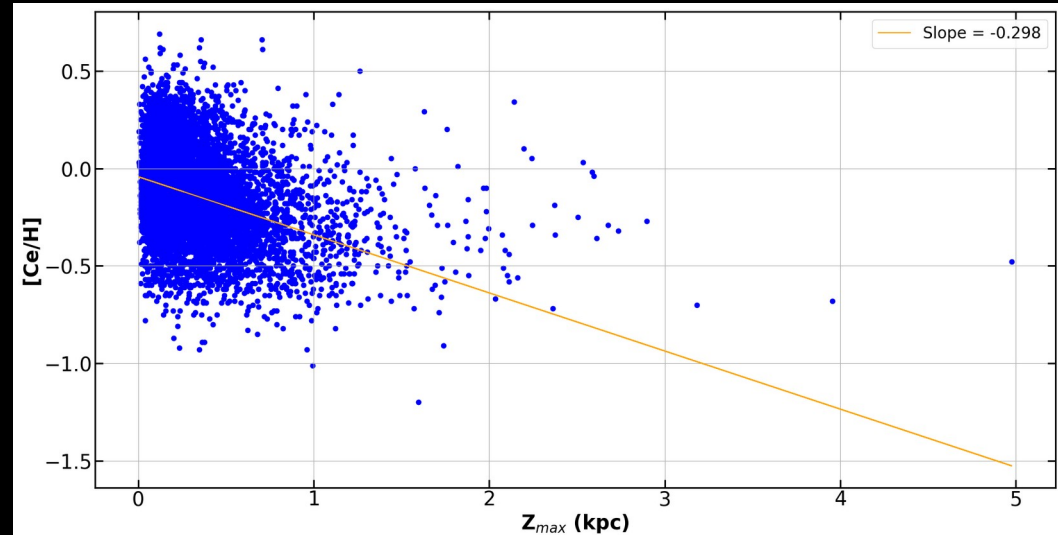
→ Decreasing number of generation of
AGB departing from Galactic plane

Radial Gradient in [Ce/Fe]:

$$\delta[\text{Ce}/\text{Fe}]/\delta R = -0.001^{\pm 0.004} \text{ dex.kpc}^{-1}$$



III. Decreasing vertical gradient



Negative Vertical Gradients in [Ce/H]:

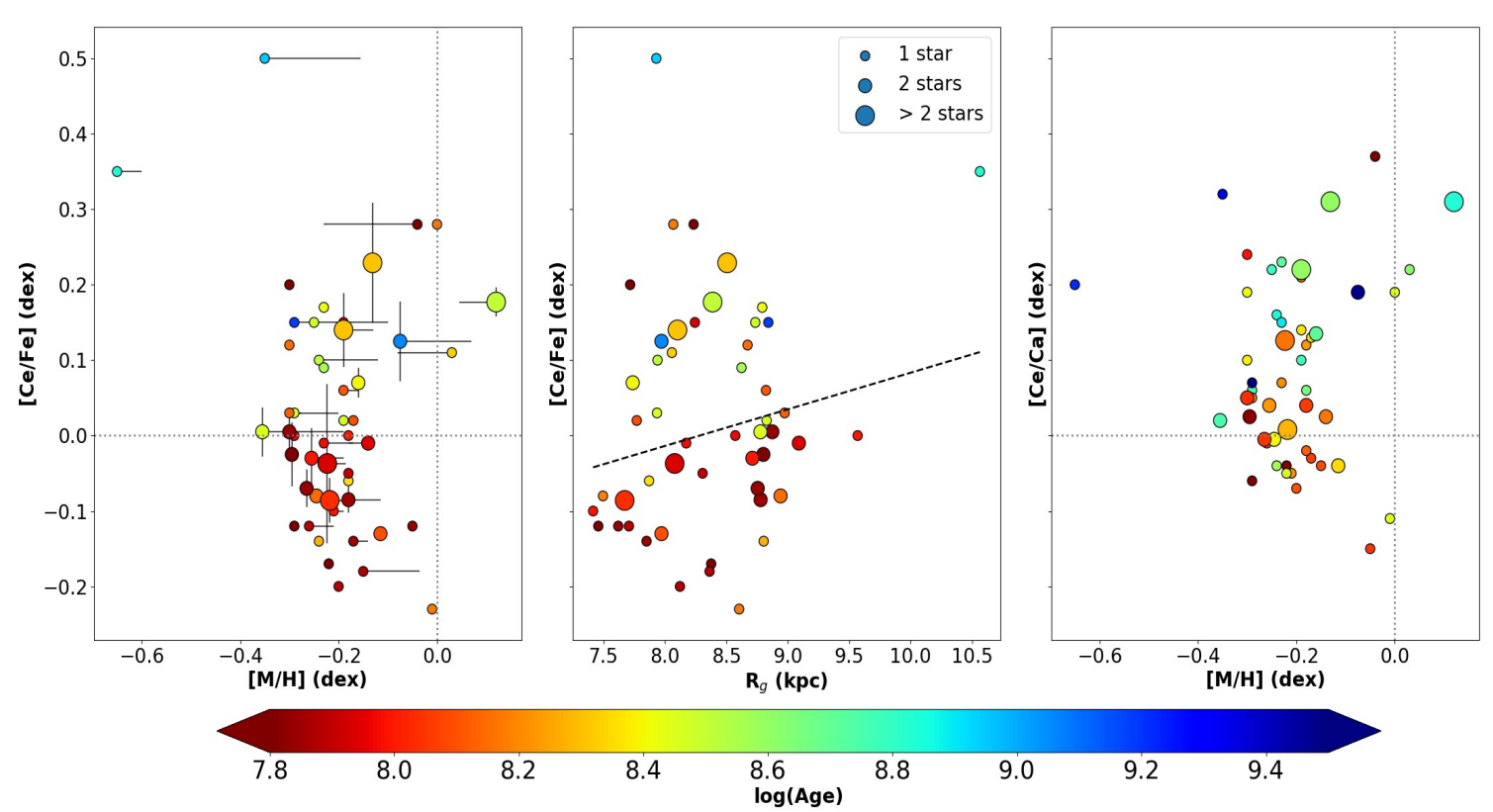
$$\delta[\text{Ce}/\text{H}]/\delta Z_{\max} = -0.297^{\pm 0.021} \text{ dex.kpc}^{-1}$$

Vertical Gradient in [Ce/Fe]:

$$\delta[\text{Ce}/\text{Fe}]/\delta Z_{\max} = 0.086^{\pm 0.011} \text{ dex.kpc}^{-1}$$

Compatible with $\delta[\text{La}/\text{Fe}]/\delta Z_{\max} = 0.030^{\pm 0.025} \text{ dex.kpc}^{-1}$ from Tautvaišiene +21

III. Ce in Open Clusters



82 stars in 53 different OC found

The GSP-Spec $[\text{M}/\text{H}]$ and $[\text{Ce}/\text{Fe}]$ in agreement with litterature.

Older OCs appear more enriched in Ce contrarely to what found in litterature.

Biases in Young stars ?

$[\text{Ce}/\text{Fe}]$ horizontal gradient compatible with field stars and literature [Sales-Silva+22]

No clear trend between $[\text{Ce}/\text{Ca}]$ and $[\text{M}/\text{H}]$

III. Chemical evolution models

Ingredients :

- Initial conditions: chemical composition of the primordial gas and the nature of the system (closed or open, infall or outflow).
- SFR from the gas and their mass spectrum. Depends on IMF
- Stellar yields (Elements are produced in stars and released into the interstellar medium)
- Gas flows (infall, outflow, radial flow).

Approaches :

- Parallel approach : Simultaneous formation of MW components
- Infall models ...

III. Three infall model

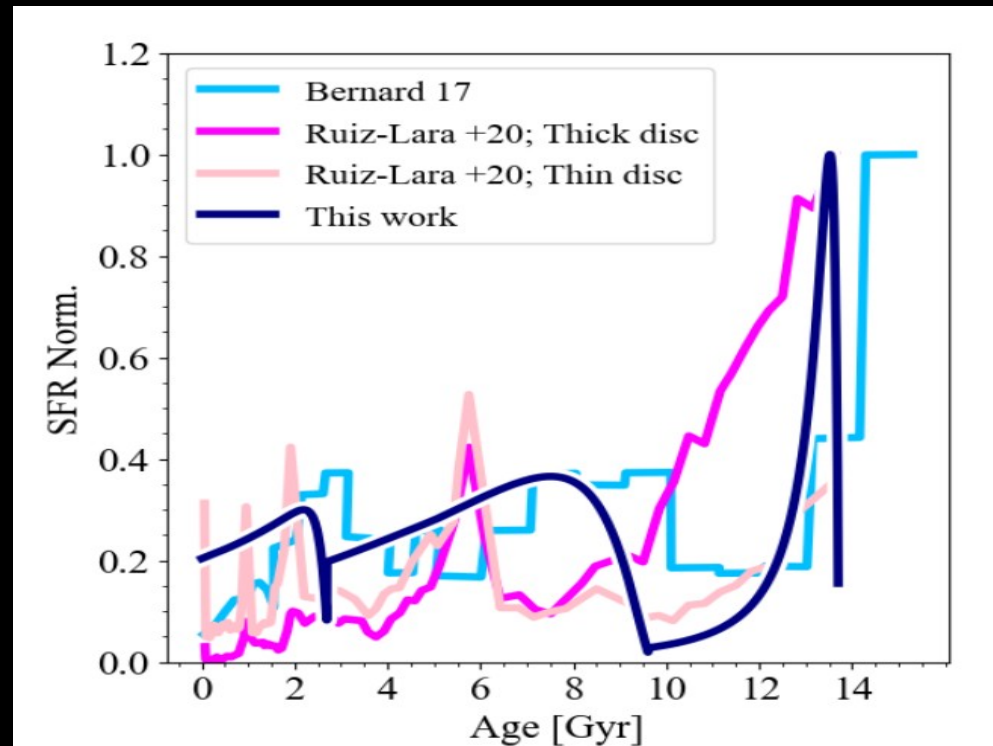
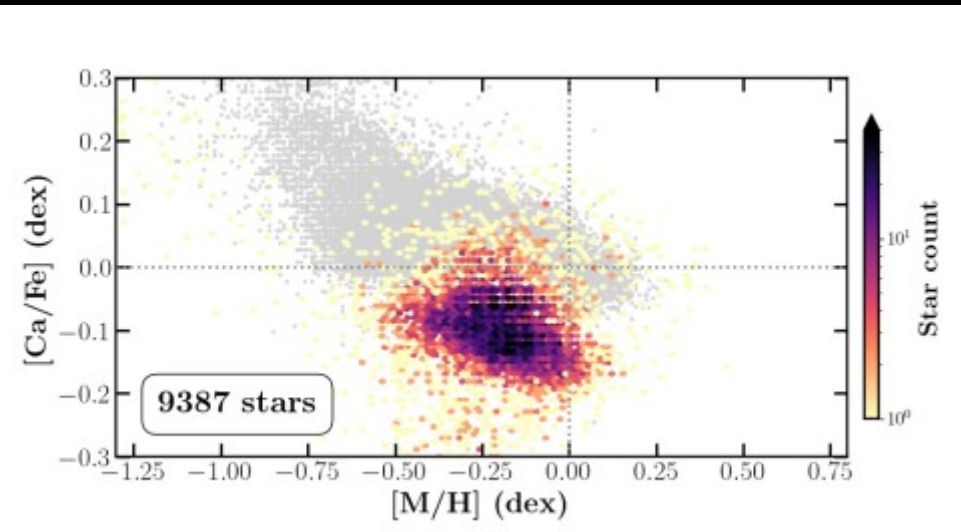
$$I_i(t) = \chi_{1,i} A e^{-t/\tau_1} + \theta(t - t_{max}) \chi_{2,i} B e^{-(t-t_{max})/\tau_2} + \theta(t - t_{max2}) \chi_{3,i} C e^{-(t-t_{max2})/\tau_2}$$

τ_1 , τ_2 et τ_3 : time scales of gas accretion

θ : Heaviside function

$\chi_{1,i}$, $\chi_{2,i}$ et $\chi_{3,i}$: abundances per unit mass of the element i

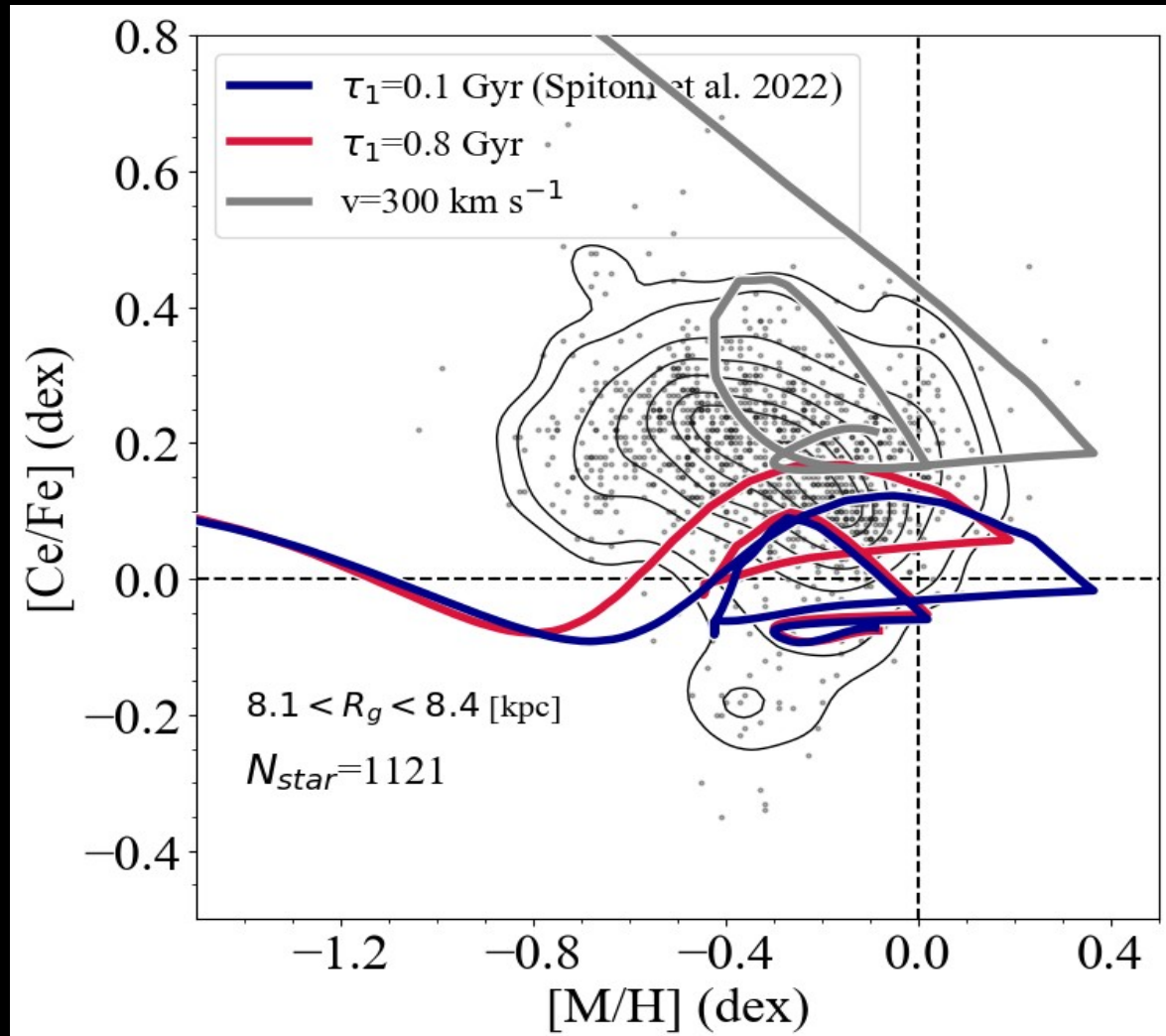
t_{max} et t_{max2} : Galactic times associated to infalls



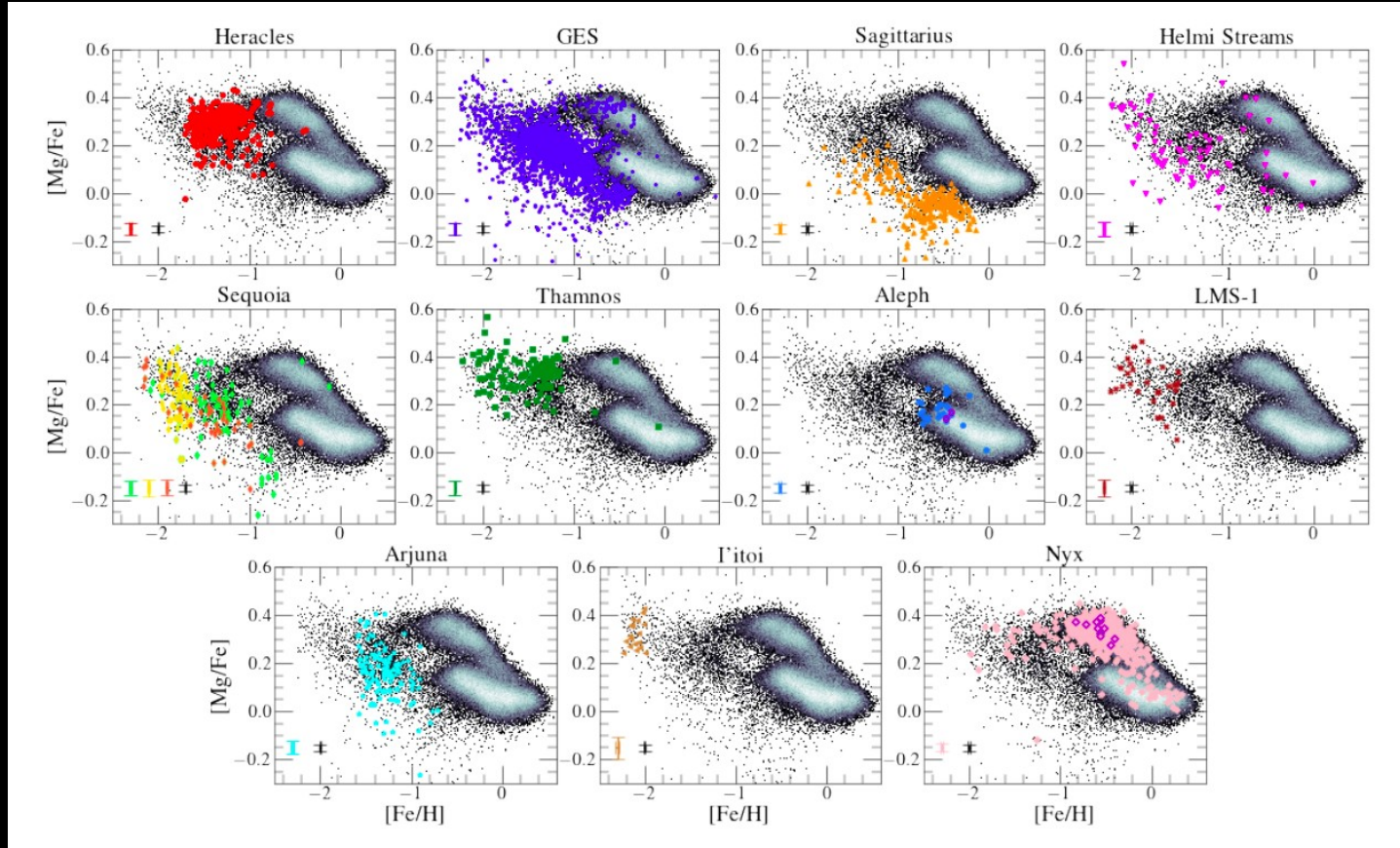
III. Three infall model

Extreme case :
Rotating massive stars
(*Limongi+18*) where all stars
have a rotation of 300 km/s.

Contursi et. al, 2023



III. Ce and Nd in accreted systems



Horta+23

III. Ce and Nd in accreted systems

Aguado+21 rapportent une abondance moyenne de barium pour GSE inférieure à notre rapport [Ce/Fe] d'environ 0.7 dex.

Matsuno+21 ont trouvé certaines étoiles de GSE enrichies en Ba et en La, en accord avec nos abondances en cérium (avec des abondances variant de -0.2 à 1.1 dex et des moyennes de [Ba/Fe] et [La/Fe] proches de 0.4 et 0.2 dex).

COMMENT sont calculées les masses Recio

Matsuno+22 : [Y/Fe] and [Ba/Fe] in GES > Sequoia

<i>Gaia DR3 Id</i>	System	<i>S/N</i>	T_{eff} (K)	$\log(g)$	[M/H] (dex)	[Ca/Fe] (dex)	[Nd/Fe] (dex)	[Ce/Fe] (dex)
2410346779070638720	GES	68	4846	2.02	-0.98	0.16	1.12 ± 0.24	-
1591836174070974592	Helmi	101	3806	0.95	-0.73	0.37	0.73 ± 0.21	0.57 ± 0.20
5282079908816150912	Sequoia	407	4407	1.32	-1.53	0.47	0.25 ± 0.19	0.36 ± 0.20
1294315577499064576	Thamnos	657	4309	1.51	-1.01	0.27	0.17 ± 0.19	0.56 ± 0.08

III. Ce in s- process rich GC: M4

4 stars of M4 found

→ [M/H] of these stars similar to [M/H] of M4
(Caretta+09, Yong+08)

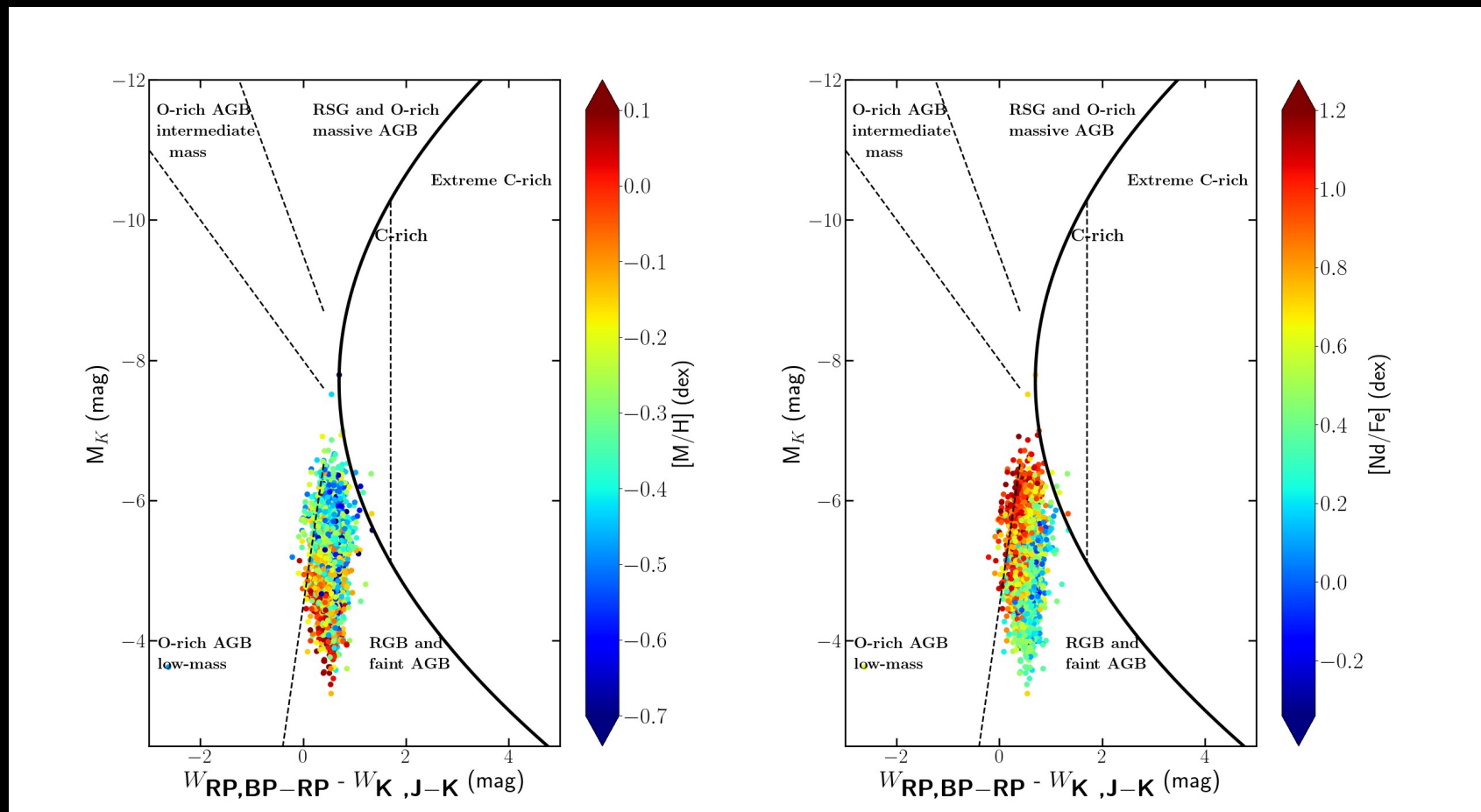
→ Teff, log(g) and [Ce/Fe] also fully compatible with *Yong+08*. (mean difference in [Ce/Fe] = -0.05 dex)

Mean [Ce/Fe] = 0.46 ± 0.07 dex. Enhanced compared to M5

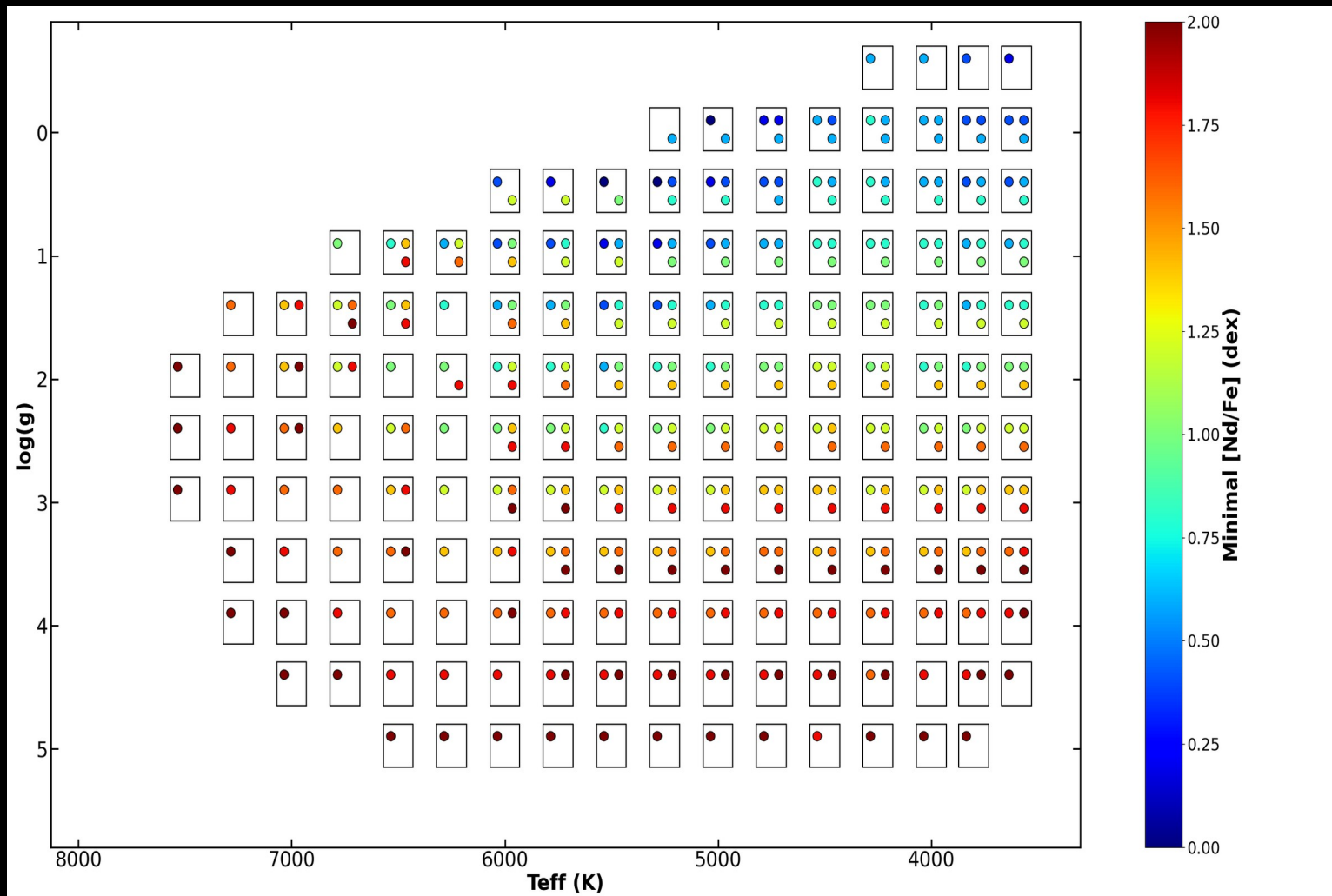
→ Contribution source of s- different hence different chemical origin.

IV. AGB Nature

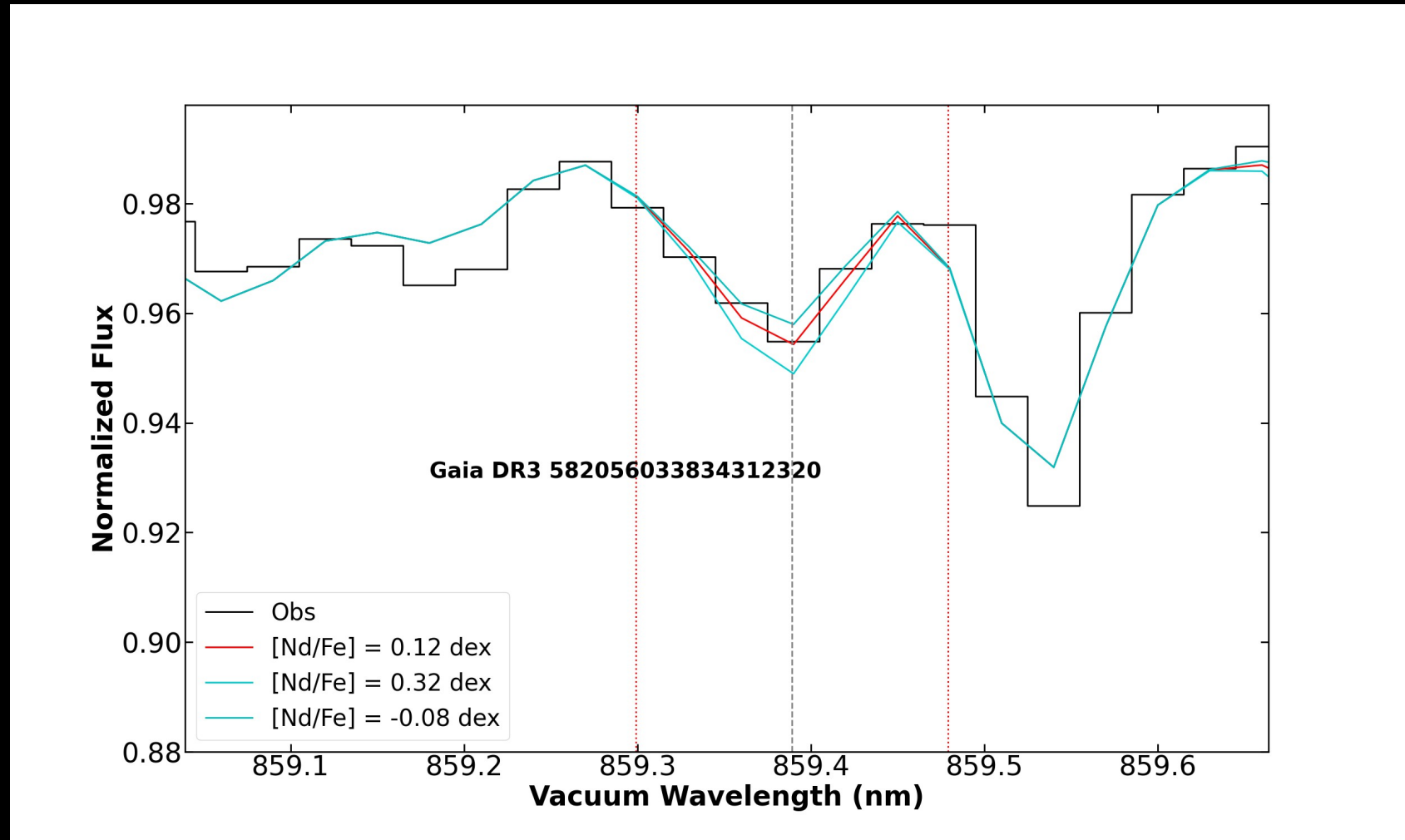
- Over the 19 544 AGB with Ce/Nd, 445 LPV
- No sign of Carbon enhancement from cnew_gspsspec ~ 0 (for 13873 stars) nor C-rich flag from Lebzelter+23



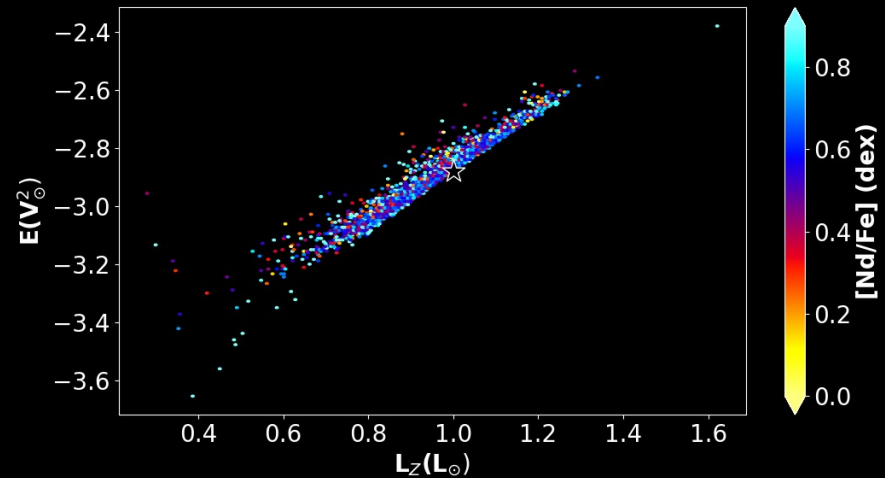
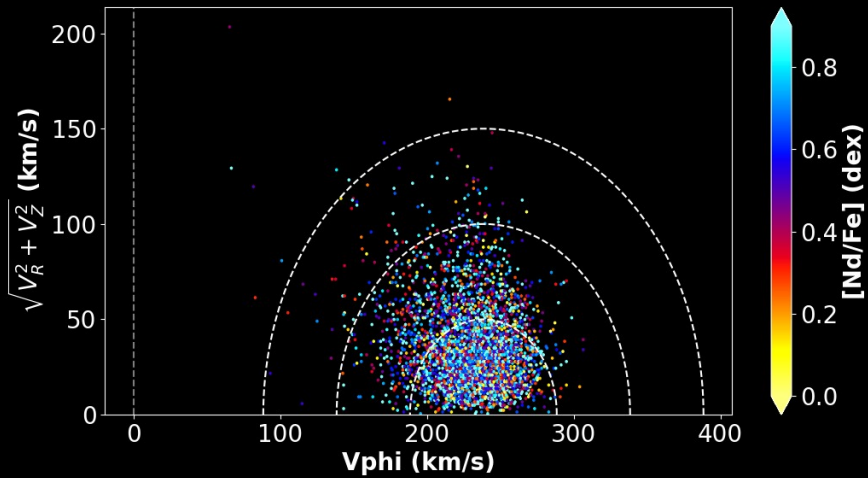
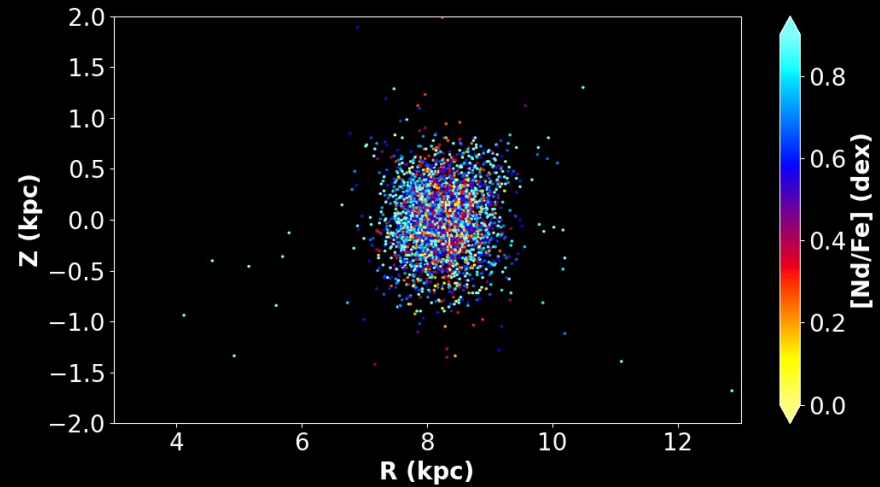
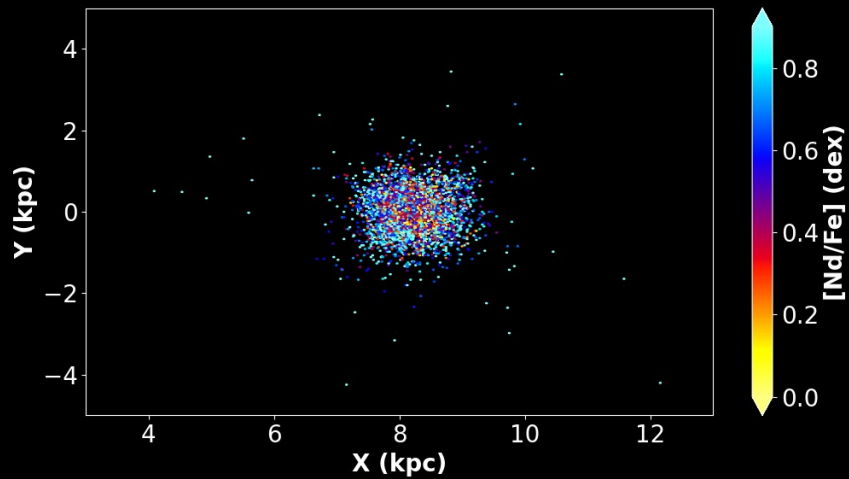
IV. Nd line detection



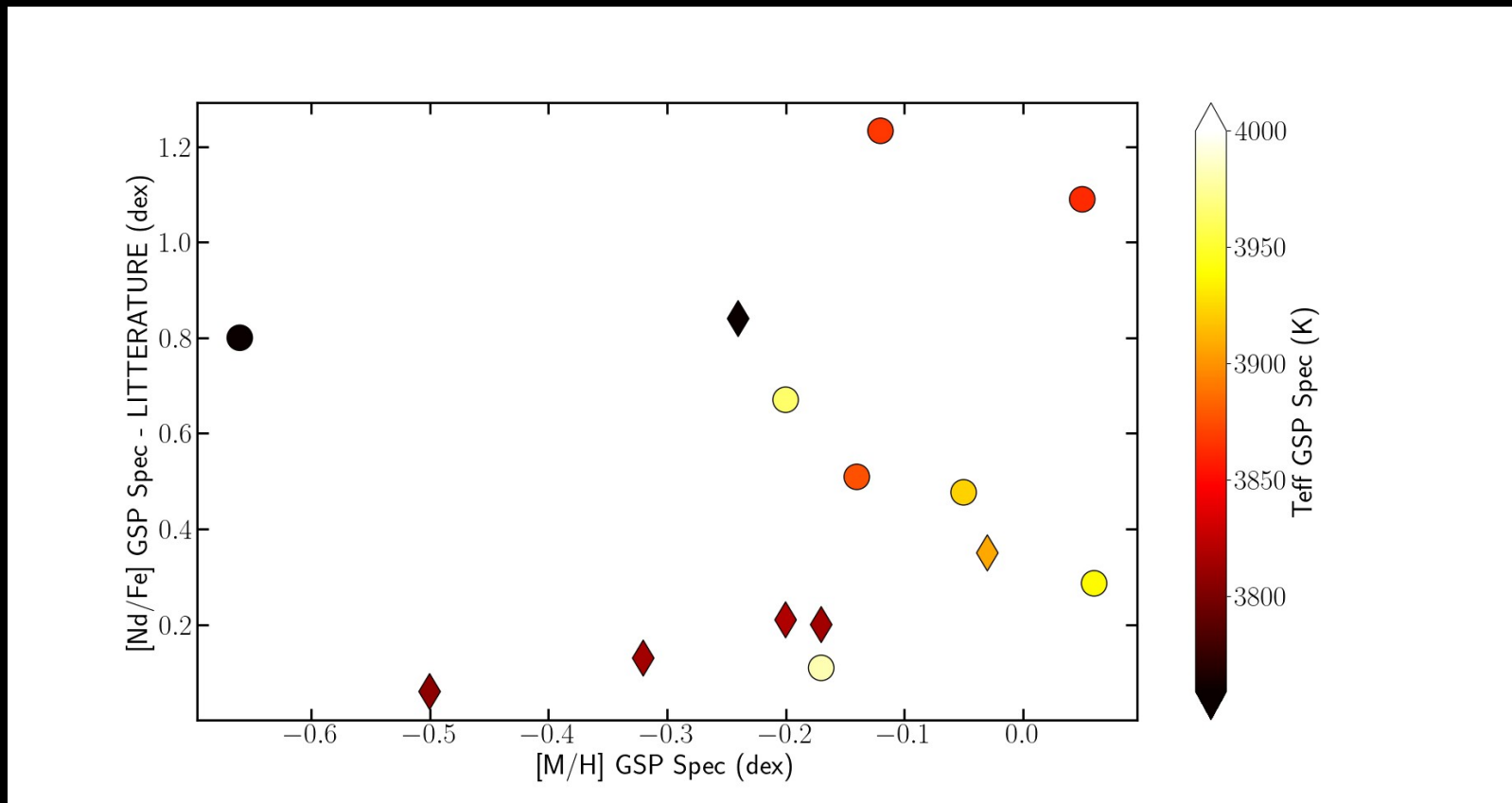
IV. Nd line



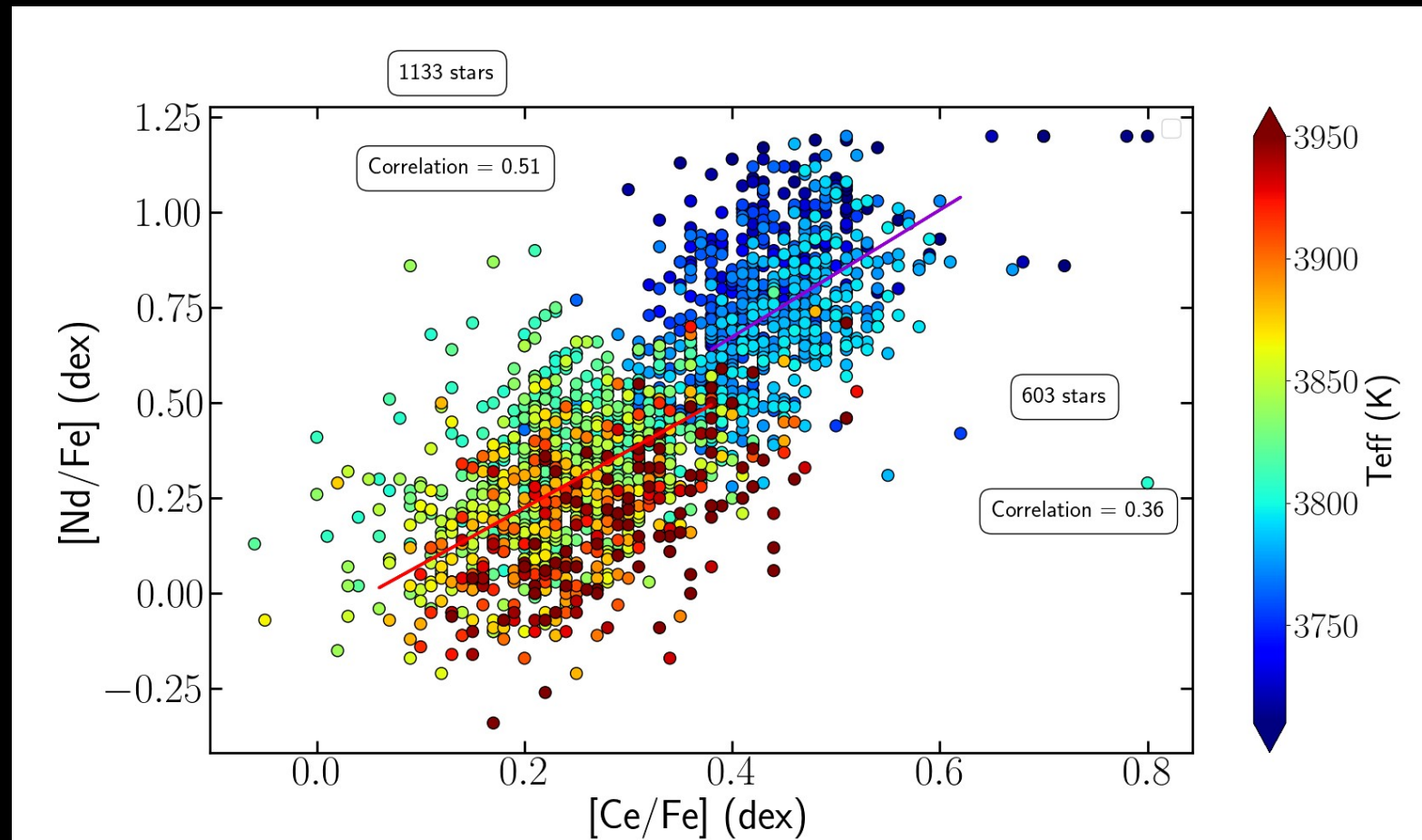
IV. Nd Galactic general properties



IV. Nd calibration

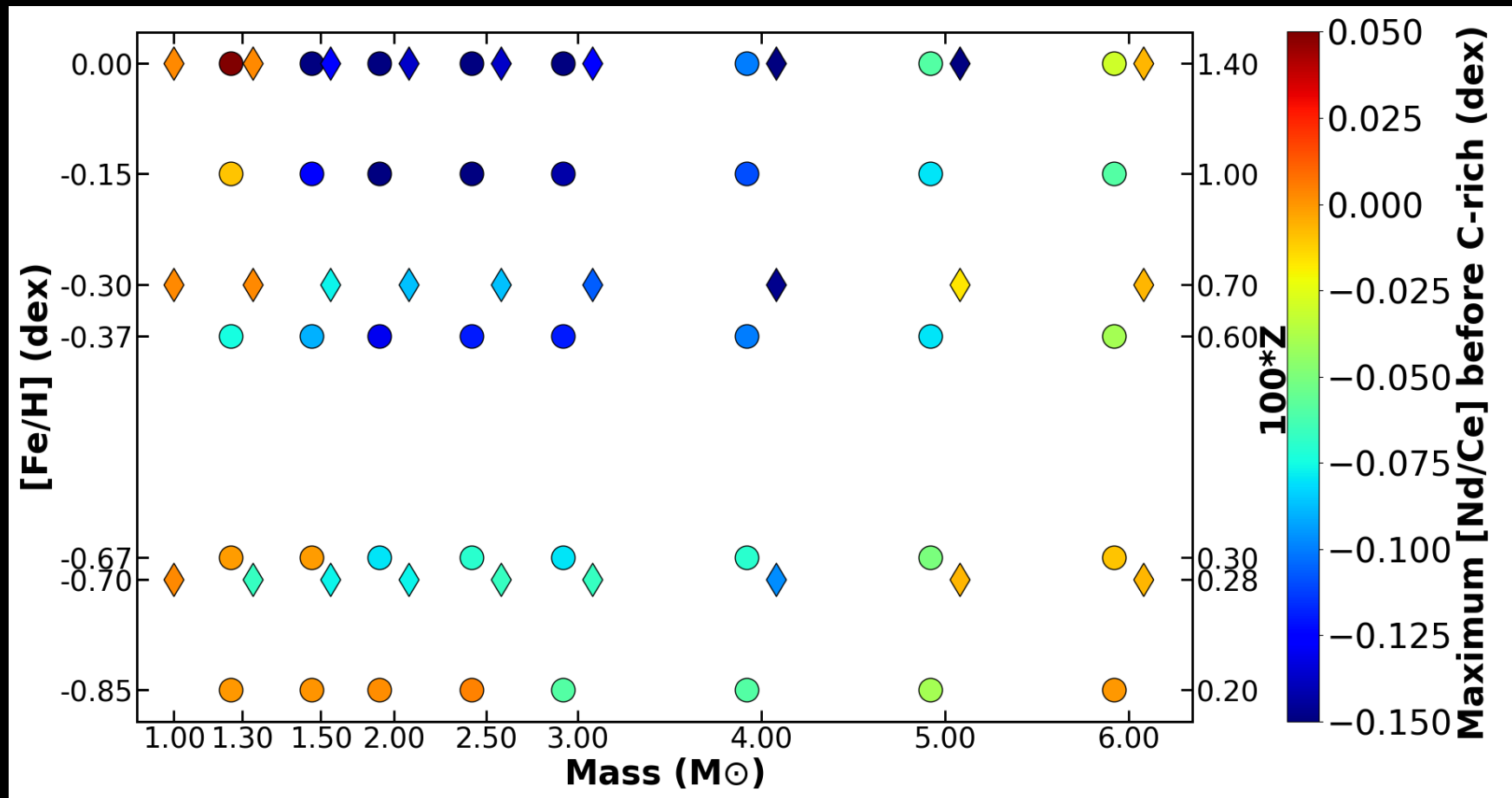


IV. Ce/Nd correlation



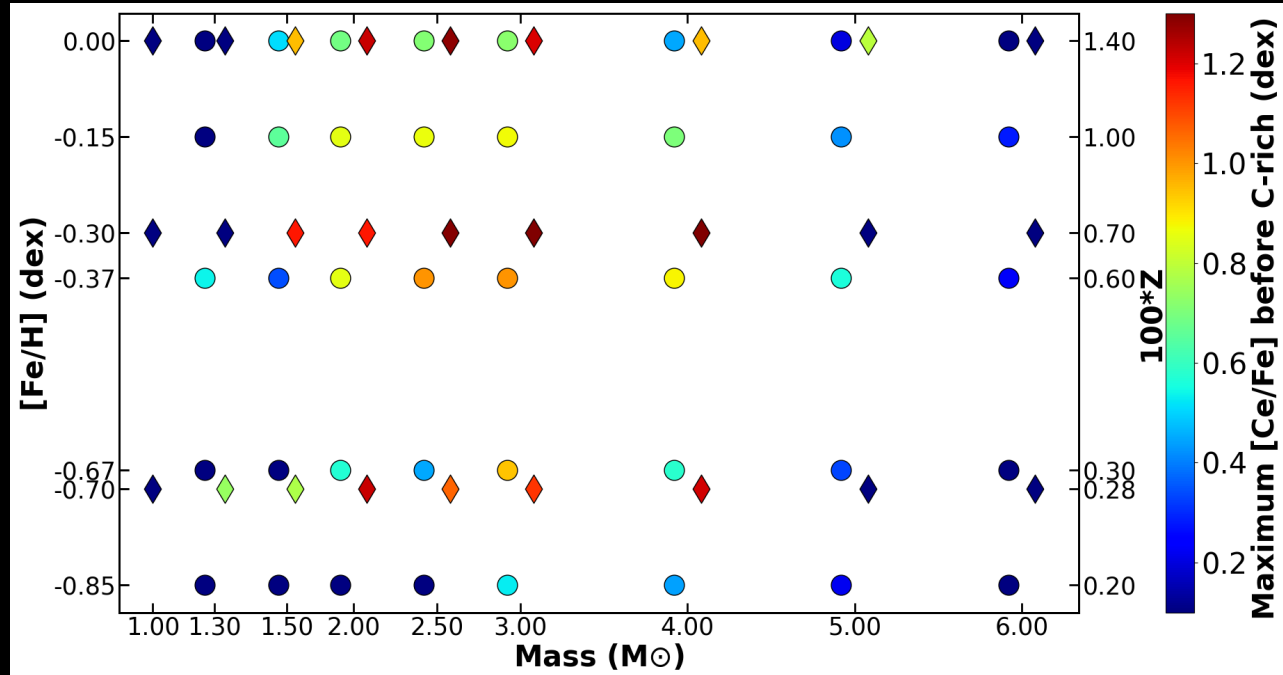
IV. [Nd/Ce] in AGB

Same production whatever mass and met.



IV. [Ce/Fe] in massive AGB

- $^{22}\text{Ne}(\alpha, \text{n})^{25}\text{Mg}$ source activated (hotter temperatures at base of convective zone) and more efficient during last TPs.
- Smaller neutron exposure → reduction of second peak s-.
- Decrease of TDU efficiency (H-exhausted mass is higher → greater compression of H layers and thinner but hotter H-shell → Less time to ignite 3α reaction → shorter interpulse episode → less efficient TDU)



IV. FRUITY vs Monash

More C in He intershell in FRUITY because 3a reaction.

FRUITY : Reimer93 for e-AGB + Vassiliadis93 then
Shrink of ^{13}C pocket in tip AGB ==> less s-

IV. s- in AGB

[Ce/Y] should decrease with increasing [Fe/H] due to neutron exposure in the ^{13}C pocket proportional to the $^{13}\text{C}/^{56}\text{Fe}$ ratio. The number of iron seeds is proportional to metallicity, whereas ^{13}C is not because of its primary origin [Busso+01].

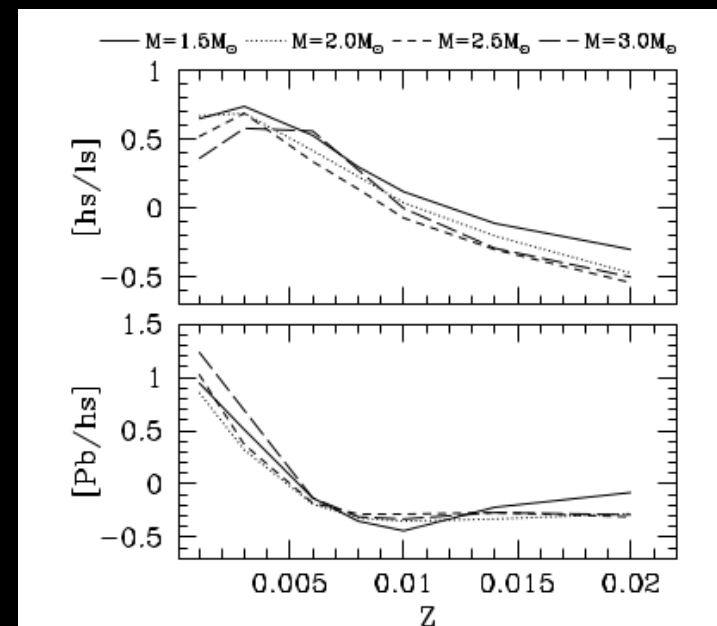
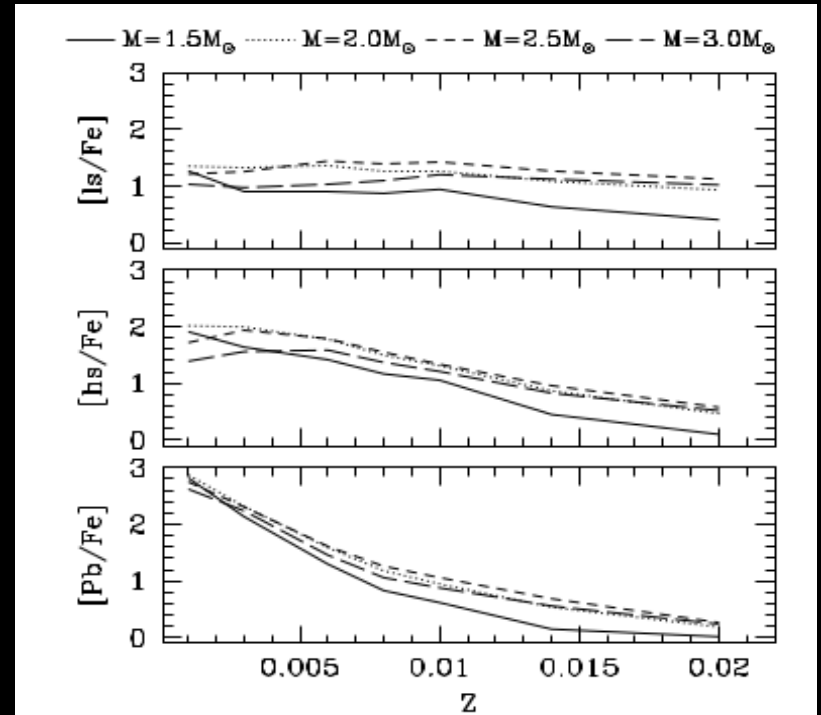
[Rb/Zr] > 0 \rightarrow $^{22}\text{Ne}(\alpha, n) ^{25}\text{Mg} \rightarrow$ Massive AGB

Solar met : ls, hs > Pb

IV. s- in AGB

[Ce/Y] should decrease with increasing [Fe/H] due to neutron exposure in the ^{13}C pocket proportional to the $^{13}\text{C}/^{56}\text{Fe}$ ratio. The number of iron seeds is proportional to metallicity, whereas ^{13}C is not because of its primary origin [Busso+01].

$[\text{Rb/Zr}] > 0 \rightarrow ^{22}\text{Ne}(\alpha, \text{n}) ^{25}\text{Mg}$
 → Massive AGB



V. AMBRE project studies

AMBRE (Archéologie avec Matisse Basée sur les aRchives de l'ESO) project aim is to give homogeneous atmospheric parameters and chemical abundances to the community. It is based on $\sim 326\ 000$ ESO archived spectra (from UVES, FEROS, GIRAFFE).

Several previous analysis made :

- Iron pic elements : Mikolaitis et al., 2017.
- Li abundances : Guiglion et al., 2016, Prantzos et al., 2017
- r- process abundances (Eu, Gd and Dy) : Guiglion et al., 2018
- Sulfur abundances : Perdigon et al., 2021
- Mg abundances : Santos-Peral et al., 2020
- Pb abundances : Contursi et.al, in prep.

V. Pb studies in litterature

- Van Eck+01, +03: Pb-enhanced stars at low-met
- Jonsell+06, Lucatello+03, Sivarani+04, Ivans+05, Barbuy+11: Studies on HE0024-2523, CS29497-030, CS29497-030, HE 0338-3945, CS 31082-001, resp.
- Aoki+02: metal-poor stars ($-2.7 < [\text{Fe}/\text{H}] < -1.9$ dex). [Pb/Ba] dispersion
- Allen+06: 26 Ba-stars
- Roederer+09 : 27 metal-poor stars ($-3.1 < [\text{Fe}/\text{H}] < -1.4$ dex) enriched in heavy elts.
- Roederer+14 : 313 metal-poor stars with Pb abund.
- Mashonkina+12 : NLTE corrections for some Pb lines
- Roederer+20 and Peterson+21: Pb in 3 and 4 stars (resp.) from UV spectra

Gaia NIR

- Red Dwarfs (RD), cool White Dwarfs (WD), Brown Dwarfs (BD) and free-floating planets
- IMF of central regions
- Characterize/parametrized WD pop.
- High-precision astrometry in the NIR
- ...